Report No. FAA-RD-77-105

12

CERTIFICATION STUDY OF A DERIVATIVE MODEL OF A SMALL JET TRANSPORT AIRPLANE USING A PILOTED RESEARCH SIMULATOR

RAYMOND D. FORREST
SYSTEMS RESEARCH AND DEVELOPMENT SERVICE
FEDERAL AVIATION ADMINISTRATION
AMES RESEARCH CENTER
MOFFETT FIELD, CA. 94035

JUNE 1977
FINAL REPORT

U.S. DEPARTMENT OF TRANSPORTATION
FEDERAL AVIATION ADMINISTRATION
Systems Research & Development Service
Washington, D.C. 20590

The contents of this report reflect the views of the performing organization, which is responsible for the facts and accuracy of the data presented herein. The contents do not necessarily reflect the official views or policy of the Department of Transporation. This report does not constitute a standard, specification or regulation.

NOTICE

The U.S. Government does not endorse products or manufacturers. Trade or manufacturers names appear herein solely because they are considered essential to the object of this report.

NOTICE

This document is disseminated under the sponsorship of the Department of Transportation in the interest of information exchange. The U.S. Government assumes no liability for its contents or use thereof.

Technical Report Documentation Page

1. Report No.	2. Government Accession No.	3. Recipient's Catalog No.
FAA-RD-77-105		

4. Title and Subtitle	5. Report Date
Certification Study of a Derivative Model of a Small Jet Transport Airplane Using a Piloted Research Simulator.	June 1977
	6. Performing Organization Code
	8. Performing Organization Report No.

7. Author(s)	
Raymond D. Forrest	

9. Performing Organization Name and Address	10. Work Unit No. (TRAIS)
Federal Aviation Administration Flight Simulation Branch, ARD-540 P.O. Box 25 Moffett Field, CA 94035	182-530 015
	11. Contract or Grant No.
	13. Type of Report and Period Covered

12. Sponsoring Agency Name and Address	14. Sponsoring Agency Code
U.S. Department of Transportation Federal Aviation Administration Systems Research and Development Service Washington, DC 20590	ARD-500

15. Supplementary Notes

16. Abstract

The Flight Simulator for Advanced Aircraft (FSAA) at Ames Research Center was used to evaluate the flying qualities of a small jet transport and those of a derivative model of that airplane. The objective was to define technical criteria that piloted simulations must meet to enable their increased use for demonstrating compliance with transport category aircraft airworthiness requirements. Flying-qualities data were obtained for numerous test configurations and conditions using conventional certification flight test procedures. These data correlated well with the basic airplane data from the manufacturer's certification test report. Analysis of the simulator data showed valid results in critical test cases, such as the demonstration of static longitudinal stability and minimum control speed, with confidence that all influencing and limiting factors were identified. An important aspect was the accurate simulation of the control force-feel qualities of the reversible flight control system. The simulator was judged to have duplicated actual flight results with a high degree of confidence. It is concluded that it is technically feasible to pursue the increased use of simulation in conducting derivative airplane certification evaluations of the scope reported in this report.

17. Key Words		18. Distribution Statement
Certification	Reversible flight controls	Document is available to the U.S. public through the National Technical Information Service, Springfield, Virginia 22161.
Simulation	Airworthiness	
Flying qualities	Business jet transport	
Minimum Control Speed		
Stability and control		

19. Security Classif. (of this report)	20. Security Classif. (of this page)	21. No. of Pages	22. Price
Unclassified	Unclassified	85	

Form DOT F 1700.7 (8-72) Reproduction of completed page authorized

METRIC CONVERSION FACTORS

Approximate Conversions to Metric Measures

Symbol	When You Know	Multiply by	To Find	Symbol
	LENGTH			
in	inches	*2.5	centimeters	cm
ft	feet	30	centimeters	cm
yd	yards	0.9	meters	m
mi	miles	1.6	kilometers	km
	AREA			
in^2	square inches	6.5	square centimeters	cm^2
ft^2	square feet	0.09	square meters	m^2
yd^2	square yards	0.8	square meters	m^2
mi^2	square miles	2.6	square kilometers	km^2
	acres	0.4	hectares	ha
	MASS (weight)			
oz	ounces	28	grams	g
lb	pounds	0.45	kilograms	kg
	short tons (2000 lb)	0.9	tonnes	t
	VOLUME			
tsp	teaspoons	5	milliliters	ml
Tbsp	tablespoons	15	milliliters	ml
fl oz	fluid ounces	30	milliliters	ml
c	cups	0.24	liters	l
pt	pints	0.47	liters	l
qt	quarts	0.95	liters	l
gal	gallons	3.8	liters	l
ft^3	cubic feet	0.03	cubic meters	m^3
yd^3	cubic yards	0.76	cubic meters	m^3
	TEMPERATURE (exact)			
°F	Fahrenheit temperature	5/9 (after subtracting 32)	Celsius temperature	°C

*1 in = 2.54 (exactly). For other exact conversions and more detailed tables, see NBS Misc. Publ. 286, Units of Weights and Measures, Price $2.25, SD Catalog No. C13.10:286.

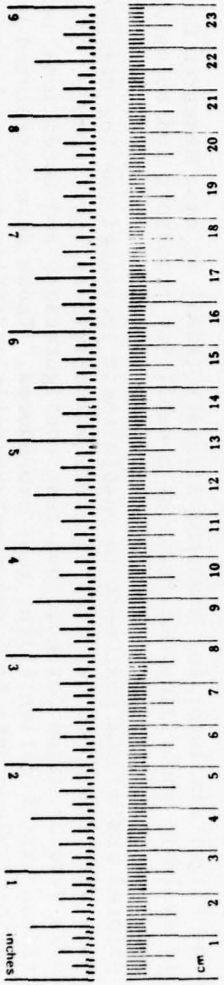

Approximate Conversions from Metric Measures

Symbol	When You Know	Multiply by	To Find	Symbol
	LENGTH			
mm	millimeters	0.04	inches	in
cm	centimeters	0.4	inches	in
m	meters	3.3	feet	ft
m	meters	1.1	yards	yd
km	kilometers	0.6	miles	mi
	AREA			
cm^2	square centimeters	0.16	square inches	in^2
m^2	square meters	1.2	square yards	yd^2
km^2	square kilometers	0.4	square miles	mi^2
ha	hectares (10,000 m^2)	2.5	acres	
	MASS (weight)			
g	grams	0.035	ounces	oz
kg	kilograms	2.2	pounds	lb
t	tonnes (1000 kg)	1.1	short tons	
	VOLUME			
ml	milliliters	0.03	fluid ounces	fl oz
l	liters	2.1	pints	pt
l	liters	1.06	quarts	qt
l	liters	0.26	gallons	gal
m^3	cubic meters	35	cubic feet	ft^3
m^3	cubic meters	1.3	cubic yards	yd^3
	TEMPERATURE (exact)			
°C	Celsius temperature	9/5 (then add 32)	Fahrenheit temperature	°F

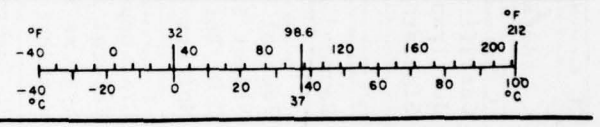

TABLE OF CONTENTS

	Page
SYMBOLS AND ABBREVIATIONS	iv
SUMMARY	1
INTRODUCTION	1
SIMULATION	2
Description of the Simulator	2
Modeling	4
CERTIFICATION TEST PROGRAM	5
Evaluation Pilots	6
Test Procedure	6
Data Acquisition	6
Test Conditions	7
DISCUSSION AND RESULTS	7
Nonpiloted Verification of Models	7
Flight Control Systems	9
Longitudinal Stability and Control	12
Minimum Control Speed	15
General Discussion	23
CONCLUDING REMARKS	25
APPENDIX A - CONTROL LOADER SYSTEM CHARACTERISTICS	27
APPENDIX B - AIRPLANE AERODYNAMIC MODEL EQUATIONS	29
APPENDIX C - FLIGHT CONTROL SYSTEM MODEL EQUATIONS	33
REFERENCES	37
TABLES	39
FIGURES	50

SYMBOLS AND ABBREVIATIONS

a_x, a_y, a_z	accelerations in body axes (positive forward, right and down, respectively), m/sec^2 (ft/sec^2)
b	wing span, m (ft)
C_D	drag coefficient, $\frac{\text{drag force}}{\bar{q}S}$
C_{h_e}	elevator hinge moment coefficient, $\frac{\text{elevator hinge moment}}{\bar{q}S_e\bar{c}_e}$
C_L	lift coefficient, $\frac{\text{lift force}}{\bar{q}S}$
C_ℓ	rolling-moment coefficient, $\frac{\text{rolling moment}}{\bar{q}Sb}$
C_m	pitching-moment coefficient, $\frac{\text{pitching moment}}{\bar{q}S\bar{c}}$
C_n	yawing-moment coefficient, $\frac{\text{yawing moment}}{\bar{q}Sb}$
C_y	side-force coefficient, $\frac{\text{side force}}{\bar{q}S}$
$\bar{c}$	wing mean aerodynamic chord, m (ft)
$\bar{c}_e$	elevator mean aerodynamic chord, m (ft)
D	aerodynamic drag, N (lb)
F_C, F_W, F_P	pilot control force on column, wheel and pedals, respectively, N (lb)
g	acceleration due to gravity, 9.8 m/sec^2 (32.2 ft/sec^2)
h	airplane altitude, m (ft)
I_{xx}, I_{yy}, I_{zz}	body axes rolling, pitching, and yawing moments of inertia, respectively, kg-m^2 (slug-ft^2)
L	aerodynamic lift force, N (lb)
M	Mach number
m	airplane mass, kg (slugs)
n_z	normal load factor, $\frac{\text{lift force}}{\text{gross weight}}$

p	roll angular velocity (right roll, positive), deg/sec
q	pitch angular velocity (ANU, positive), deg/sec
$\bar{q}$	dynamic pressure, $\rho \frac{V^2}{2}$, N/m^2 (lb/ft^2)
r	yaw angular velocity (nose right, positive), deg/sec
S	wing reference area, m^2 (ft^2)
S_e	elevator reference area, m^2 (ft^2)
T	total thrust, N (lb)
T_A	asymmetric thrust, N (lb)
V	airspeed, knots
V_{EF}	speed at which engine failure occurs, knots
V_{MC}	minimum control speed, knots
V_s	stall speed, knots
V_2	takeoff safety speed, knots
W	gross weight, kg (lb)
y_{LE}, y_{RE}	distance from fuselage plane of symmetry to left and right engines, respectively, m (ft)
α	angle of attack, deg
β	angle of sideslip (relative wind from right, positive), deg
γ	flight path angle (climb, positive), deg or percent
δ_a	total aileron deflection (right aileron up, positive), deg
δ_c	control column deflection (aft, positive), cm (in.)
δ_e	elevator deflection (AND, positive) deg
δ_F	flap deflection, deg or percent
δ_p	rudder pedal deflection (airplane nose right, positive), cm (in.)
δ_r	rudder deflection (trailing edge left, positive), deg
δ_s	horizontal stabilizer deflection, deg

δ_w	control wheel deflection (right wing down, positive), deg
θ	pitch angle of airplane body axis relative to horizon (ANU, positive), deg
ϕ	bank angle (right wing down, positive), deg
ψ_i	heading, deg
$(\dot{})$	derivative with respect to time, $\frac{d}{dt}$

Abbreviations:

ANU,AND	airplane nose up, airplane nose down
CG	center of gravity
CAR	Civil Air Regulations
FAR	Federal Aviation Regulations
FSAA	Flight Simulator for Advanced Aircraft
GU,GD	landing gear up, landing gear down
IFR	instrument flight rules
MCT	maximum continuous thrust
OEI	one engine inoperative
PIO	pilot induced oscillation
RAD	rapid access device
TE	trailing edge of control surface
TO	maximum takeoff thrust
TR	thrust required for flight condition
VFR	visual flight rules

CERTIFICATION STUDY OF A DERIVATIVE MODEL OF A SMALL JET TRANSPORT AIRPLANE USING A PILOTED RESEARCH SIMULATOR

Raymond D. Forrest

Federal Aviation Administration

SUMMARY

The Flight Simulator for Advanced Aircraft (FSAA) at Ames Research Center was used to evaluate the flying qualities of a small jet transport and those of a derivative model of that airplane. The objective was to define technical criteria that piloted simulations must meet to enable their increased use for demonstrating compliance with transport category aircraft airworthiness requirements. Flying-qualities data were obtained for numerous test configurations and conditions using conventional certification flight test procedures. These data correlated well with the basic airplane data from the manufacturer's certification test report. Analysis of the simulator data showed valid results in critical test cases, such as the demonstration of static longitudinal stability and minimum control speed, with confidence that all influencing and limiting factors were identified. An important aspect was the accurate simulation of the control force-feel qualities of the reversible flight control system. The simulator was judged to have duplicated actual flight results with a high degree of confidence. It is concluded that it is technically feasible to pursue the increased use of simulation in conducting derivative airplane certification evaluations of the scope reported in this report.

INTRODUCTION

For many years, flight simulators have been used in varying degrees by the aircraft industry in the development of new aircraft. In such phases of aircraft development as conceptual design, preliminary design, flight test, and training, the contributions of flight simulators have proved invaluable (ref. 1). However, simulators have limitations that must be understood if they are to be used effectively.

In the past, the certification of an aircraft design primarily involved demonstrations that were performed entirely on the first flight model. In recent years, however, several additional methods have been used to show regulatory compliance, including varying degrees of simulation. The extent to which simulators are used in this phase of certification is determined by the complexity of the aircraft design and the cost of building and validating an adequate simulator.

Even with the recent advances in simulation technology, the cost of validating a simulator for demonstrating acceptable aircraft characteristics in critical flight regimes can exceed the cost of demonstration by flight test alone. Because of the uncertain cost of validation, simulation has not been extensively used for routine demonstrations of compliance.

However, simulators have been used to demonstrate compliance in cases where flight tests are considered to be hazardous or impossible. From these experiences it was hypothesized that demonstrations of compliance through simulation might be useful in support of flight demonstrations in other areas.

Intending to explore this supporting function, the Federal Aviation Administration (FAA) issued an advisory circular (ref. 2) stating the opinion that greater use could be made of simulation in the certification process. If simulation could be more extensively used in the certification process, significant savings might be realized, particularly when new technology is involved. Attention was directed at defining the technical criteria that simulators must meet to demonstrate aircraft compliance with certification regulations.

To test the hypothesis, the FAA undertook (1) to explore with industry potential uses of simulation in the certification process and to minimize limitations presently preventing such uses; and (2) to study on the Flight Simulator for Advanced Aircraft (FSAA) the certification of the Rockwell International Sabreliner airplane to determine how a high fidelity simulation could be used in lieu of, or in support of, flight tests to show compliance with the Federal Aviation Regulations (ref. 3). The initial effort in accomplishing the first task is reported in reference 4; this report discusses progress toward accomplishing the second task.

The objectives of this second task were agreed on by the FAA and Rockwell International. First, it was necessary to compare data from a real-time simulation of a Rockwell International Sabreliner Model 75A airplane with data from flight tests. Acceptable correlation of the flight test and simulator data formed the basis for establishing a valid baseline Model 75A. Then, a derivative of the Model 75A, the Model 75B, was defined by Rockwell International and the demonstration of compliance with some of the flying-qualities certification requirements was accomplished on the simulator. Finally, based on the analyses of the Model 75B simulation data, Rockwell International could modify flight control system characteristics, where necessary, to overcome any flying-qualities deficiencies exposed during the simulation. The experiment was designed so that results of the Model 75B simulation tests could be compared with flight tests of the prototype airplane had the decision been made to build it.

SIMULATION

Description of the Simulator

The Flight Simulator for Advanced Aircraft (FSAA) is the designation given to the simulator and supporting equipment used in this certification

study program. This facility, in operation since 1969 at Ames Research Center, National Aeronautics and Space Administration (NASA), is capable of high-fidelity simulation of a wide range of flight vehicles. Reference 5 describes the facility in detail and provides useful information regarding checkout and operating procedures. The facility is composed of the following major systems or elements: motion-base system, visual display system, crew cab, flight instruments and controls, control loader (force-feel) system, digital computer, analog computers, data conversion and interface linkage, and data input-output devices. Figure 1, a simplified block diagram, shows the interconnection of these major elements. Details pertinent to the present study are discussed in the following paragraphs.

Motion capability.- The motion-base system consists of a complex movable structure (fig. 2) that can drive the cab in a combination of six directions at once (six degree-of-freedom capability). The motion drive logic is designed to convert the computed pilot station accelerations of the simulated airplane into six velocity drive signals which move the simulator cab, within its physical limits, such that the combined effects of acceleration and gravity subject the pilot to forces that approximate those that he would experience in flying the real airplane. These forces provide the pilot with motion cues that can influence his control of the airplane. The motion capability of the FSAA is given in table 1. The most dramatic feature of this system is its unique 80 ft of lateral travel.

Visual and aural cues.- The pilot in the cab was provided with visual and aural cues as well as motion cues. The visual cues are derived from a visual flight scene displayed on a collimated color TV monitor mounted above the instrument panel. There were no side window displays available to aid the pilot in his testing by providing peripheral visual flight cues. The visual flight scene was generated by a computer driven six degree-of-freedom TV camera that followed the motion of the simulated airplane with respect to the Earth. During approach and landing, a view of the runway and nearby terrain was generated by driving the camera over a three-dimensional color model (scaled at 600:1). During cruise a view simulating flight over a low level cloud base was generated by positioning the camera over a color painting of the scene and limiting the camera to pitch, roll, and yaw motion.

The aural cues consisted of engine noise modulated by computed engine revolutions; they were introduced through stereo speakers located in the cab. Other aural cues, such as aerodynamic noise and landing gear noise, which can also be introduced on these speakers, were not provided.

Flight instruments and controls.- The cab was equipped with seats for a crew of three: pilot, copilot, and observer. However, instruments and flight controls were provided only at the pilot's station (fig. 3). The test program was planned so that the pilot could accomplish the VFR or IFR task without crew assistance. Controls were provided for engine thrust, landing gear and wing flap position, as well as the conventional column, wheel, and pedals for controlling elevator, aileron, and rudder surface deflection. Horizontal stabilizer and aileron trim was actuated by a switch on the wheel. Rudder trim was actuated by a switch on the center console.

The column, wheel, and pedals were equipped with hydraulically actuated control loaders. The control loaders were programmed to produce realistic dynamic force-feel characteristics during all phases of flight. This action of the control loaders on the pilot's controls thereby provided kinesthetic cues that were essential to the evaluation of the reversible flight control system and of airplane longitudinal stability and control. A detailed description and discussion of the operating characteristics of the control loader system is given in appendix A.

Computer laboratory details.- Data for setting the initial conditions of a specific test and for changing the configuration variables of the mathematical models were read into the computer from files in a rapid access device (RAD) memory. The RAD file was read by entering instructions from a keyboard-CRT control station in the computer laboratory. Changes in the file could also be made from this station if necessary. Test operations were directed from the laboratory via an intercom to the cab. Test data were automatically output to an electrostatic printer, strip chart recorders, and a magnetic tape recorder. Pilot comments from the intercom were recorded on a tape recorder.

Modeling

Two airplane aerodynamic models were programmed for use in this simulation study. They were a baseline Model 75A and a derivative Model 75B. Two flight control system models were also programmed; that is, a baseline system and a modified system.

Airplane models.- The baseline Model 75A is a representation of the Rockwell International Sabreliner 75A airplane (NA-265-80), a twin-engine airplane equipped with General Electric CF700-2D2 aft-mounted turbofan engines. Certificated maximum takeoff gross weight is 23 000 lb. Figure 4 is a three-view drawing of the airplane.

The derivative Model 75B design is the same airframe as the Model 75A with the fuselage lengthened by the addition of a 2.5-ft section aft of the entrance door. The design is configured with larger Lycoming ALF-502 high bypass ratio engines in place of the General Electric engines. The design maximum takeoff gross weight is 28 000 lb.

The maximum takeoff thrust characteristics under standard temperature conditions for the General Electric and Lycoming engines as modeled for the simulation are compared in figure 5. Thrust was computed by the engine model program as a function of Mach number, altitude, and throttle position.

The longitudinal stability derivatives of the Model 75B differed slightly from those of the Model 75A but the lateral-directional stability derivatives were essentially the same. Reference 6 provides the basic data which determined the values of the stability derivatives of the two airplane models, as well as data used to define the flight control system models. The equations from reference 6, which determine how the data are combined to form the aerodynamic coefficients, are listed in appendix B.

Flight control system models.- The flight control surfaces (elevator, ailerons, and rudder) of the Sabreliner Model 75A are mechanically operated from a conventional set of dual controls by means of linkages, pushrods, bellcranks, and cables. A schematic of the Sabreliner 75A flight control system is shown in figure 6. A spring-type bias bungee is incorporated to establish a no-load center position for the elevator controls by interconnecting the elevator and horizontal stabilizer. This no-load position varies automatically with horizontal stabilizer position to improve longitudinal stability. A bobweight is installed in the longitudinal control system to obtain a positive column force of approximately 10 lb/g of normal acceleration, and a bobweight balance bungee is used to statically balance the system at +1g conditions.

Trim is accomplished by electromechanical actuators that position the trim tabs on the left aileron and rudder and position the horizontal stabilizer. When the landing gear is retracted, trimming of the horizontal stabilizer is accomplished at a low-speed rate; when the gear is extended trimming is accomplished at a high-speed rate.

The characteristics of the models of the flight control system that were tested during this simulation are given in table 2. The baseline system was tested with the Model 75A and Model 75B airplanes and the modified system was tested only with the Model 75B airplane. The modified system was a simplification of the baseline system which resulted from the elimination of (1) the bobweight balance bungee, (2) the elevator bias bungee, and (3) the nonlinear gearing mechanism.

The longitudinal and lateral flight control system models were developed to accurately simulate the real systems including the reversible force characteristics that result from elevator and aileron hinge moments being fed back to the pilot's controls. The directional flight control system model, however, was treated as a simple irreversible system with a constant pedal force gradient of 40 lb/in. The reversible forces in the longitudinal and lateral system were generated during the simulation by the variable digitally-computed gradient which augmented the basic control loader gradient. Equations that determine how the system parameters are combined to form the variable force gradients are listed in appendix C. A complete discussion of the development of the flight control system models and of how they were mechanized for this simulation is contained in reference 7.

CERTIFICATION TEST PROGRAM

The test program conducted on the simulator included the following flying-qualities tests: longitudinal, directional, and lateral trim; longitudinal control during configuration changes; static longitudinal stability; static directional and lateral stability; directional and lateral control; dynamic longitudinal, directional, and lateral stability; longitudinal maneuvering characteristics; roll rate characteristics; minimum control speed; longitudinal out-of-trim control; and crosswind landing. These tests were first

conducted on the baseline Model 75A and then most of them were repeated on the derivative Model 75B. In addition, the following tests were conducted on the Model 75B with the modified flight control system: static longitudinal stability, longitudinal maneuvering characteristics, and longitudinal out-of-trim control.

Evaluation Pilots

Four pilots participated in the simulator tests. A Rockwell International pilot was the principal simulator pilot during the validation phase; he had 1400 hr in the Sabreliner 75A, most of which was gained during acceptance flying. Two FAA test pilots, one with USAF T-39 airplane experience and one with Sabreliner 40 airplane certification experience, flew the simulator while most of the test data were obtained, and an FAA engineer-pilot with no flight experience in this type of aircraft assisted while the remaining data were obtained.

Test Procedure

The test procedures were the same as those used in conducting the actual certification flight test program on the Sabreliner 75A airplane. With a few exceptions, no tests were attempted in the simulator that could not be safely conducted in flight. The pilot was given guidance regarding any unusual technique necessary to satisfy the special requirements of a particular test and was allowed to make as many runs as he considered necessary to accomplish the task. A more detailed discussion of specific tests and the required test procedures is contained in references 6, 8, and 9.

Each test on the baseline Model 75A was performed until the quantitative results and subjective qualities duplicated the particular flight test of the Sabreliner 75A airplane. This was necessary (although not sufficient in itself) to prove the simulation valid as a method of demonstrating compliance with the certification requirements. Following a judgment of the simulation team that the baseline simulation was acceptable, tests were repeated for the derivative Model 75B configurations at similar flight conditions. Finally, test data were gathered to assist Rockwell International in the design evaluation of the modified flight control system.

Data Acquisition

The data collected during the simulation program were in several forms. During the validation phase, the pilot's comments provided the most important information. Quantitative data were recorded on analog strip charts and on digital magnetic tapes (at four samples per second) during the test program runs. Table 3 lists the variables that were recorded on magnetic tape. Copies of the tapes were provided to Rockwell International for analysis. Initial flight conditions and run duration were listed on an electrostatic printer; the printer also has a plot capability which was used during processing and analysis of the data.

Test Conditions

Table 4 lists the airplane configuration and loading for all the test program items; baseline Model 75A, derivative Model 75B, and Model 75B with the modified flight control system. Also listed in this table are record run numbers and total record length. The airplane gross weight, center of gravity, and inertia did not vary during any given run.

Variable density, pressure, and temperature conditions were precisely determined by a basic digital computer subroutine based on international standard atmosphere equations.

DISCUSSION AND RESULTS

Nonpiloted Verification of Models

A mathematical model of the Sabreliner 75A airplane was first used for piloted simulation studies on the FSAA 6 months prior to the present study. The objective at that time was to study pilot response to simulated failures of the integrated automatic flight control system. Although this simulation was completed, some discrepancies in the model were not resolved during the time available. All of the pilots who flew the simulator during that period commented that the pitch stability characteristics of the simulator were not representative of the real airplane. The discrepancies were (1) low damping of the short-period pitch response to elevator control inputs, and (2) pilot induced oscillation (PIO) which occurred when attempting precise pitch attitude control. The PIO tendency was more pronounced at airspeeds above 250 knots and thus did not interfere with the study, which was limited to terminal area speeds. However, the poor fidelity in pitch control dynamics that existed in the simulation increased the pilot's workload and reduced the overall confidence in the quality of the simulation.

During a 2-month period prior to the present study, a nonpiloted investigation was undertaken by the FSAA Projects Staff at Ames Research Center to isolate the source of these discrepancies. The results of this investigation are described in an unpublished working paper. The investigation resulted in the identification of the following problem areas: (1) aerodynamic pitch rate damping was too low and (2) the software model of the elevator control system did not accurately predict the dynamic behavior of the elevator.

During the investigation, the effect of pitch rate damping was first examined using a linear stability analysis program available on the FSAA digital computer. This program was used to compute the frequency and damping of the characteristic modes of motion of the aerodynamic model which had been specified by Rockwell International. The analysis showed that the computed short-period damping ratio of 0.32 was low compared to that expected to produce satisfactory pilot ratings in this class of airplane. In fact, the computed damping ratio was less than the minimum of 0.35 specified by reference 10 as adequate for the takeoff, approach, and landing flight phases. Approximate equations from reference 11 were used next to calculate values for the

stability derivatives, C_{L_q}, C_{m_q}, $C_{L_{\dot{\alpha}}}$, and $C_{m_{\dot{\alpha}}}$, which affect primarily the short-period mode damping. A comparison with data in the model showed the model C_{m_q} to be several times smaller than the calculated C_{m_q}. The difference was then isolated to an error in the original estimated value of the wing-body contribution to C_{m_q}.

There had been a reluctance to significantly change C_{m_q}, during the first simulator operating period on the FSAA, even though the value was suspect, without a thorough analysis. It was apparent after the above described investigation that C_{m_q} must be increased by at least a factor of 5 in order to increase the damping ratio to a satisfactory level. The short-period pitch response to elevator input of the model is compared with flight test records in figure 7. Figure 7(a) compares the first model with $C_{m_q} = -3.8$. Figure 7(b) shows a similar comparison after C_{m_q} was increased by a factor of 5 ($C_{m_q} = -19.0$); the increase provided a good match with the flight test measured response. The comparison was made more exact by shaping the simulation elevator input using a signal generating function to duplicate the elevator control surface dynamics contained in the flight test input. The maximum excursions of pitch attitude, normal acceleration, and angle of attack to an elevator input pulse were slightly reduced when simulated elevator dynamics were included.

In preparing the simulation data package (ref. 6) for the present study, Rockwell International reviewed the results of the investigation by the FSAA staff and decided to form a new baseline Model 75A. Originally, the tail contribution was combined with the wing-body contribution to form the composite aerodynamic model in pitch, which introduced complications such as equations for computing downwash angle at the horizontal tail. The model was simplified by providing complete airplane aerodynamic data input. This effort to reformulate the data was aided by application of a computer program for predicting the major static and dynamic stability derivatives of a complete airplane. The method utilizes potential flow theory to compute the surface flow fields and pressures on any configuration that can be synthesized from arbitrary lifting bodies and nonplanar, thick lifting panels. Reference 12 includes the theoretical development of the method, a user's guide, and example output data. A sample of Models 75A and 75B data output obtained at Rockwell International on a computer graphics terminal (CRT) is shown in figure 8; for the sample shown in figure 8(a) the Model 75A was disturbed in pitch at a rate of 1 rad/sec. The parameter values of interest in the figure are enclosed in boxes with the letters "CZ" and the word "PITCH." These are values for C_{L_q} and C_{m_q} at the flight condition selected. The Model 75B was disturbed in yaw at a 1 rad/sec rate to determine C_{ℓ_r} and C_{n_r} (fig. 8(b), "ROLL" and "YAW" boxes). This "vortex lattice" program, as it is referred to by users, was useful to the designer and to the simulation team as an independent check on the values of stability derivatives that were determined by other methods (i.e., textbook equations, Datcom, etc.).

When the Model 75A and Model 75B as defined by reference 6 had been programmed, checks were made to verify that the FSAA Xerox Sigma 8 (Σ8) digital

computer program results agreed with results of similar programs at Rockwell International (RI). This verification process was accomplished during the early phases of experiment design and setup for the present study. A set of five equilibrium check cases was selected for verification of trimmed airplane attitudes and control surface deflections (static checks). Each case was defined by flight condition, airplane loading, and airplane configuration. The dynamic response to fixed control input disturbances (dynamic checks) was verified by comparing both time histories of flight parameters and the factors (frequency, period, damping, and time constants) that describe the characteristics modes. The linear stability analysis program on the FSAA digital computer was used to extract the factors of the characteristic modes. Figure 9 illustrates part of the computer printout for the Model 75A at Case 1 conditions. The results of this analysis for both models for all five cases are summarized in tables 5 and 6. The FSAA programs were accepted as the principal source of data for documenting the models.

At this point, the software of the simulation aerodynamic models was judged to be ready for the "pilot-in-the-loop" validation phase. The objective of this phase was to demonstrate that the simulator (including all mechanical and electrical hardware elements as well as the aerodynamics) was sufficiently like the real airplane for the purpose intended. In this case, it was intended that the baseline Model 75A be developed into a high fidelity model of the Sabreliner airplane so that decisions concerning the use of simulation in the certification of a derivative airplane could be formulated. It was intended that the data collected in the course of the simulation experiment with the Model 75B be considered valid for the real airplane if a prototype had been built. The validation of certain simulator qualities critical to achieving good results was extended into the data acquisition period and is discussed in sections that follow. The validation of the model of the reversible flight control system was particularly difficult.

Flight Control Systems

An important aspect of this study was the intention to accurately simulate the true force-feel qualities of the airplane flight control system. Figure 6 is a schematic drawing of the longitudinal, lateral, and directional axis flight controls of the Model 75A. The longitudinal axis (fig. 6(a)) is clearly the most complex and the development of an accurate simulation of this axis was very difficult.

A significant part of the task was the development of software describing the reversible characteristics of the longitudinal control axis. Most present day flight simulations use a simplified irreversible control system model. The elevator hinge moment, bobweight force, and deflection of the springs in the system were perceived by the pilot as forces (generated by the control loader device) that tended to move the control column. A complicating factor was that the elevator hinge moment and bobweight force are both dependent on the state of the airplane (i.e., change in airspeed or normal acceleration causes a change in elevator hinge moment or bobweight force). Therefore, the system equations were developed to continuously solve for the equilibrium

column position with and without applied pilot force (i.e., control-fixed and control-free).

The following quote about the importance of modeling control force-feel characteristics is from reference 13:

> Unfortunately, these characteristics are rarely modeled with a high confidence level. Even if all the data are available, which is seldom the case, an extremely complex mathematic model may be needed. Uncertainties arise when attempts are made to simplify the model in order to match available computational capacity since there is no easy guide as to the degree of fidelity that is really necessary. Faithful modeling of control forces for an unpowered manual control system is extremely difficult and this aspect is often the source of complaint from the pilot if he is familiar with the aircraft being simulated.

Although this reference provides a good treatment of the essentials of simulation development and validation, it provides no guidance for overcoming the noted difficulty in modeling the reversible flight control system.

The Rockwell International pilot, during his first experience with the Model 75A simulation, commented that it did not reproduce the airplane pitch response when thrust was applied for a go-around. The simulation pitched more rapidly to a higher attitude than did the airplane. If allowed to continue control-free, the simulation would go through a large amplitude pitch oscillation and either stall or dive until the pilot took control again. The airplane, on the other hand, required very little control or retrimming to settle on the correct pitch attitude for climb with maximum available thrust. Two other pilots with less time in the airplane did not comment adversely on this simulation deficiency. When they accomplished a go-around in the simulator they remained in-the-loop and trimmed to the necessary pitch attitude, since they anticipated a requirement to do so.

Attempts were made to determine the cause of the pitch-up identified by the validation pilot. Control-fixed static stability and pitch rate damping of the aerodynamic model were confirmed to be at the previously verified values. Repeated tests while applying thrust with different values of thrust line offset showed no significant effect on the dynamic response. Then an investigation of the control system dynamics showed that the addition to the model equations of a small friction force of 1.5 lb had a pronounced effect on the control-free response.

The control system was modeled assuming that the elevator was aerodynamically balanced so the elevator hinge moment did not vary with angle of attack at the horizontal tail. Thus, it was determined that the difference in control-fixed and control-free stability was not due to aerodynamic effect but rather to a force imbalance in the control system. The imbalance was caused by variation of the bobweight force (due to change in effective moment arm of the weight with change in angle of attack) which caused a destabilizing elevator deflection. The addition of the friction force resisted the movement in the control system and reduced the elevator deflection.

Ultimately the friction force and the dynamic force of the bobweight caused by normal acceleration were added to the summation of forces in the column trim position computation. The control-free response to a throttle burst before and after the addition of these forces is compared in figure 10. The divergent pitch oscillation shown in figure 10(a) was forced by an elevator deflection of ±2° and reached a pitch attitude of 32° at the first peak. The friction force resists motion in the control system until the force at the column exceeds 1.5 lb. As shown in figure 10(b) this resulted in less elevator deflection and a lower amplitude pitch oscillation (first peak of 25°), although it was still divergent. From a pilot's view, the addition of friction was perceived as a lower pitch rate response to the throttle burst. The bobweight acceleration force had the beneficial effect of additionally damping the pitch oscillation, as shown in figure 10(c). However, the effect of the bobweight acceleration force alone was not as pronounced as the effect of the friction force alone.

The effect of friction force and bobweight acceleration force on the long-period, control-free response to an elevator pulse was also investigated. All of the pilots had commented about an unrealistic divergent phugoid oscillation while performing static longitudinal stability tests in the simulator. The above forces were not included initially in the column trim position computation, although they were included in the computation of the force felt by the pilot.

The time histories of the Model 75A control-free response to an elevator pulse are shown in figures 11(a) and (b). In figure 11(a) there is no friction force or bobweight acceleration force; once the equilibrium trim condition was upset by the pulse, the elevator deflection varied with angle of attack (again due to variation in bobweight moment arm) and forced a divergent oscillation with a period of approximately 42 sec. With the addition of friction force and bobweight acceleration force the response to the same elevator pulse is damped. Since the friction force never exceeded 1.5 lb the elevator deflection after the pulse remained fixed at the initial trim value.

Another flight control system simulation problem occurred and had to be solved before the comparatively routine data gathering phase of the test plan could begin. The problem appeared when the pilot would pump the control column at frequencies of 0.3 to 0.4 Hz. Such action resulted in low column forces measured for relatively high airplane normal acceleration (i.e., low column force per g during the transient inputs). This problem was more pronounced at flight conditions of high dynamic pressure, but until resolved it was perceptible at all conditions and the pilots were forced to modify their control input technique accordingly.

This problem was solved by adding a digital low-pass filter (first order lag) in the computation of column force gradient. The filter time constant of 1 sec was empirically determined. It is believed that the primary cause of the problem was the low apparent inertia of the control loader device. Recall that this device is basically a force generating servomechanism with an input command which is the digitally computed column force gradient (pounds force per inch of column displacement). The addition of the low-pass filter in the

input (forward flow) path had the effect of filtering out the high-frequency components of the gradient. This prevented the column loader position and force from getting out of phase and causing pilot-induced oscillations in the simulation that did not occur in the Sabreliner airplane. Such oscillations have been experienced in some high performance real airplanes that have inherently low force gradients and a bobweight in the control system.

A comparison of the transient control characteristics with and without the low-pass filter is provided by figures 12(a) and (b). These data were taken from the simulation with the pilot-in-the-loop. Although the phase angle between measured column force and position is difficult to determine, the transient column force per g unit of acceleration is 7.5 lb/g without the filter and 23 lb/g with the filter.

Other problems were experienced which initially degraded the pilot's feel and precision of simulator control. Pilots felt occasional control-loader force imbalance due to electronic circuit drift and due to change in the attitude of the FSAA cab. This problem was corrected by periodically rebalancing the electronic circuits of the control loader device for optimum performance. Work is under way at Ames Research Center to develop a means of automatically compensating for force imbalance.

The addition of springs and a bobweight in the longitudinal control system of high-performance light airplanes with low levels of stability can improve pilot-in-the-loop force-feel characteristics. However, if system friction is low, these same devices (bobweight and springs) can cause the long-period, control-free response to be less stable. The control system dynamics may also couple with the short-period response of the airplane. These problems were certainly evident during the development of the flight control system model for this simulation. An acceptable compromise between model complexity and force-feel fidelity was found. The capability of modeling the reversible flight control system and of realistically and accurately including the effects discussed above is considered a major contribution to the state of the art in hybrid real-time simulation. The confidence level in the validity of the Model 75A was greatly increased as a result. Details of the formulation of the flight control system model equations and of mechanization of the control loader device are presented in reference 7.

This simulation capability was of benefit to Rockwell International in studying a design modification to the control system proposed for the Model 75B. The modification consisted of eliminating (1) the bobweight balance bungee, (2) the elevator bias bungee, and (3) the nonlinear gearing mechanism. Evaluations of this modification when piloted and an analysis of longitudinal control data with respect to speed change and during accelerated flight are discussed in the following section on longitudinal stability and control.

Longitudinal Stability and Control

Once the Model 75A and Model 75B were validated, the longitudinal stability and control tests were readily accomplished in the simulator. Data were

recorded for the numerous test plan configurations and flight conditions. The data selected for analysis in the following paragraphs were those obtained for critical configurations and conditions with respect to compliance with civil airworthiness requirements and those obtained to predict the characteristics of the derivative Model 75B

Static longitudinal stability of the Model 75A in climb configuration.- Static longitudinal stability was demonstrated during the certification flight tests of the Sabreliner 75A airplane in the climb, cruise, approach and landing configurations. The climb configuration test was found to be critical when demonstrating compliance with the requirements. The column force versus airspeed data taken during flight established an average gradient of 1 lb/6.5 knots. The gradient of column force versus airspeed is important since it is an index of the pilot's feel for speed change. A steep gradient, especially close to the trim speed, will tend to keep the airplane flying at trim speed with a minimum of pilot effort, and it will enable him to easily retrim after an airspeed change. It should be noted that the airplane, when first certified in 1962 under CAR 4b regulations, was required to demonstrate only positive stability which was perceptible to the pilot. During the certification of the 75A airplane in 1973 the quantitative requirement of FAR 25.173(c) (1 lb/6 knots) was used as guidance, and a special qualitative evaluation was flown to verify safe flight characteristics. In figure 13, the simulator test data are compared with flight test data and with computer data obtained by Rockwell International during the certification. The computer analysis was used to account for CG variation. The measured friction band of the simulator (the breakout force and mechanical hysteresis of the control loader device are included) was 2 lb; it was 1.5 lb in flight. The average column force gradients (pounds per knot) from simulator, flight, and computer were all less than the FAR 25.173(c) standard. The simulator gradient which was the lowest differed from the flight gradient by as much as 25 percent depending on how the flight test data were faired. A better comparison was between the simulator gradient and the computer gradient which were both obtained at 0.37 $\bar{c}$ CG. The difference between simulator and computer gradients was only about 1 lb of column force at 50 knots below trim airspeed.

The average gradient of elevator deflection with airspeed showed good agreement. The flight elevator deflection data differed in value from the other data by about 1° (more trailing edge up). Apparently this difference was caused by a small variation in basic aerodynamic pitching moment which was not included in the model.

The quantitative agreement shown between simulation and flight was judged acceptable considering that very low force-feel gradients were satisfactorily generated and that the results of the simulator evaluations should be conservative with regard to showing compliance with civil requirements. It was the opinion of the simulation team that the match with flight could be improved with continued refinement of the model but such refinement was not necessary for the purposes of this study. It was shown that the precision of the simulation was adequate to produce almost imperceptible (to the pilot) changes in column force versus airspeed gradients. Qualitatively, the most significant comment was made by the pilot during the final data run for the configuration:

"That is the best (control system) configuration - it may be better than the airplane's with less slop (in the controls)."

Static longitudinal stability of the Model 75B in climb configuration.- Climb configuration static longitudinal stability tests of the Model 75B were conducted to evaluate a modification to the flight control system. This modification consisted of eliminating (1) the bobweight balance bungee, (2) the elevator bias bungee, and (3) the nonlinear gearing (see fig. 6(a)). The objective of these tests was to determine whether the column force versus airspeed gradient would be significantly reduced by the modification and thus necessitate a more restrictive aft center of gravity limit.

Figure 14 shows the effect of center of gravity position in this test configuration. Data were taken for three CG's, 0.325, 0.345, and 0.365 $\bar{c}$, at constant 28 000 lb gross weight (GW). The average gradients obtained were 0.167, 0.125, and 0.1 lb/knot, decreasing as the center of gravity was moved aft. If the gradient of 0.167 lb/knot (i.e., 1 lb/6 knots) specified in FAR 25.173(c) must be met in certificating the derivative airplane, then based on these limited simulation tests the center of gravity must be restricted to 0.325 $\bar{c}$ during climb. From a designer's viewpoint it is not obvious that a lesser gradient of 0.1 lb/knot would provide insufficient force-feel characteristics to maintain the trim airspeed during climb, or whether this would increase the potential for airplane upsets. On the other hand, the advantages of the modified flight control system are clear. It is possible to plan a more comprehensive simulation experiment to accomplish an equivalent safety analysis of these factors. Acceptance of the modified system without a CG restriction could result in a cost savings in the design, development, certification, and operation of a derivative airplane while maintaining an adequate level of safety. In concept, the final validation check of acceptable characteristics would occur in flight test prior to certification.

Longitudinal maneuvering characteristics of the Model 75A and Model 75B.- Flight data for maneuvering were not taken during certification tests of the Sabreliner airplane because there was no specific civil requirement. It is assumed that a qualitative flight evaluation was sufficient to show compliance with the general requirement of CAR 4b.130(a): "The airplane shall be safely controllable and maneuverable during takeoff, climb, level flight, descent, and landing."

Flight data for maneuvering were taken during piloted operation of the simulator, however. A sample plot of data for the Model 75A and Model 75B at cruise conditions is shown in figure 15. The data were obtained using a "windup turn" flight test procedure in the simulator. The procedure consisted of maintaining constant trim speed and thrust while pulling increasingly higher normal acceleration with increasing angle of bank. Rate of descent was varied to maintain constant speed and data were recorded at normal acceleration intervals during quasi-steady-state conditions.

The flight data for maneuvering are important because the stable variations of column force and elevator deflection with normal acceleration indicate that the airplane short-period mode is stable. This means that there is

a restoring moment developed which tends, at least in the short term, to return the airplane to 1-g flight following a disturbance.

A study of figure 15 shows that column force versus normal acceleration gradients, F_c/n_z, of the Model 75A and Model 75B, are linear over the maneuvering range tested in the simulator. The magnitude of the gradients is within the acceptable range given in reference 10 for normal maneuvering flight. The F_c/n_z gradient of 26 lb/g for the Model 75B is less than the 31 lb/g for the Model 75A as a result of eliminating the elevator bias bungee from the flight control system of the Model 75B and making a slight reduction in the effectiveness of the bobweight. Also obtained from figure 15 is the variation of normal acceleration with elevator deflection, n_z/δ_e, and with angle of attack, n_z/α. These are gradients which are also significant to the airplane short-period response.

Additional maneuvering-flight data plots similar to those of figure 15 were prepared from which the gradients defined above were determined at other test conditions. The results are summarized in table 7.

Longitudinal control tests with the horizontal stabilizer jammed.- Special longitudinal control tests were conducted to demonstrate that the airplane could be adequately maneuvered and landed with the horizontal stabilizer jammed in the most adverse position without excessive control forces. This requirement was satisfied during the certification flight tests of the Sabreliner 75A airplane by (1) executing a landing with the stabilizer at the trim position for cruise flight at 0.8 Mach number and 40 000 ft and by (2) executing an approach and go-around with full airplane nose up stabilizer (-8°).

When the modification to the flight control system was made to the Model 75B, the mechanical stop for airplane nose up stabilizer was changed from -8° to -14° in order to trim at all test conditions. It was decided to run the Model 75B special control tests with the stabilizer in four positions: -14°, -8°, -6.9° (cruise trim position), and 0° (full airplane nose down position). The airplane loading was 25 000 lb with a 0.18 $\bar{c}$ center of gravity. Maneuverability was acceptable for approach and landing or go-around with the stabilizer in all four positions, although control was very marginal during landing with the stabilizer at 0°. Column force exceeded 60 lb during this maneuver (see fig. 16). It appears that the stabilizer mechanical stops may be better adjusted for the required CG range of the Model 75B - a trade-off test for which the simulation is ideally suited.

Minimum Control Speed

The object of this certification test was to determine the minimum airspeed at which, following a sudden loss of thrust after takeoff, the pilot could safely recover and continue the takeoff climb maintaining straight flight. Satisfactory demonstration of the minimum control airspeed required that the transient motions following sudden engine failure be such that dangerous conditions could be avoided and a steady flight path with constant heading could be reestablished. Thus, there were steady-state and transient characteristics which had to be certified as acceptable. The safety aspects of this

flight test dictated a technique where (1) the engine was made inoperative at an airspeed above the probable minimum and the airspeed then slowly reduced until a minimum was reached, and (2) the minimum was then checked by failing the engine at that airspeed to verify that control could be maintained. The minimum control speed, V_{MC}, is an absolute type-certificate limitation and the takeoff safety speed, V_2, for operating transport airplanes must be at least equal to 1.1 V_{MC}.

Minimum control speed requirement and guidance for flight test.- The requirement to determine minimum control speed as a precedent to type-certification of transport airplanes is contained in Federal Aviation Regulations Part 25 (ref. 3). The pertinent paragraphs are quoted here.

§25.149 Minimum Control Speed:

(a) V_{MC} is the calibrated airspeed at which, when the critical engine is suddenly made inoperative, it is possible to recover control of the airplane with that engine still inoperative, and maintain straight steady flight either with zero yaw or, at the option of the applicant, with an angle of bank of not more than 5 degrees.

(b) (Paragraph (b) is not pertinent to turbine engine powered airplanes.)

(c) For turbine engine powered airplanes, V_{MC} may not exceed 1.2 V_S with:

(1) Maximum available takeoff power or thrust on the engines;

(2) The most unfavorable center of gravity;

(3) The airplane trimmed for takeoff;

(4) The maximum sea level takeoff weight (or any lesser weight necessary to show V_{MC});

(5) The airplane in the most critical takeoff configuration existing along the flight path after the airplane becomes airborne, except with the landing gear retracted; and

(6) The airplane airborne and the ground effect negligible.

(d) The rudder forces required to maintain control at V_{MC} may not exceed 180 pounds nor may it be necessary to reduce power or thrust of the operative engines. During recovery, the airplane may not assume any dangerous attitude or require exceptional piloting skill, alertness, or strength to prevent a heading change of more than 20 degrees.

Methods and procedures that have been employed to establish V_{MC} are contained in reference 8; it provides guidance in particular problem areas for flight test personnel. Depending on the nature of a particular problem,

however, it may be necessary to deviate from the methods and procedures outlined in reference 8. Any major deviation should be coordinated with the FAA, Washington, D. C.

Because of the inherent danger of dynamic engine failure testing at low speed, low altitude, and high thrust-to-weight ratio (T/W), and because of the many factors that influence V_{MC}, the FAA permits extensive use of steady-state methods (static methods) to establish the variation of V_{MC}. Dynamic checks must still be made, however, in order to ensure that the minimum speeds obtained are valid. The dynamic condition could cause an unacceptable control situation if response of the airplane is violent, or if the response is difficult to discern (such that pilot corrective action is delayed) and hard to overcome once begun. Obviously, the pilot must be able to diagnose the situation and take corrective action before any of the limiting factors specified in FAR 25.149(d) occur.

Method used in tests on the Model 75A airplane.- Flight test data were obtained to determine minimum control speed using procedures described in reference 9. The data were obtained over a range of 19 840 to 17 160 lb gross weight and 0.312 to 0.318 $\bar{c}$ center of gravity. First static points were run with one engine shut down and the other engine at various thrust settings. The airplane was banked approximately 5° into the operating engine while holding a constant heading. The speed was systematically reduced starting at approximately 1.45 V_S, then reduced to 1.3 V_S, and 1.1 V_S. Points were obtained with flaps in both the takeoff and landing positions. Three dynamic cut demonstrations were made. With both engines operating at maximum available thrust, one engine was cut to represent a failure.

Asymmetric thrust, T_A, was calculated for all data points. The rudder deflection, δ_r, used in each case was plotted versus asymmetric thrust divided by free-stream dynamic pressure, $T_A/\bar{q}$. The data were plotted in figure 17 just as was done in reference 9. A line was faired through the flight data points and extrapolated to maximum rudder deflection. Only two dynamic cut points approached maximum rudder, with the remainder between zero and half rudder. This put heavy reliance on the two high-deflection points, but it was felt that the resulting faired curve was conservative because the airplane did not maintain a 5° bank angle.

The minimum control speed was determined using the $T_A/\bar{q}$ value corresponding to maximum measured rudder deflection. The maximum controllable $T_A/\bar{q}$ value was used with a plot of airspeed versus $T_A/\bar{q}$ and extrapolated to maximum takeoff thrust under sea level standard conditions to obtain a flight test value of V_{MC} = 93 knots (see fig. 17). Because the airplane is limited by aerodynamic stall and engine stall warning speeds that are above 93 knots for most gross weights, V_{MC} will be either 93 knots, aerodynamic stall speed, or engine stall warning speed, whichever is greater.

Piloted simulator data were obtained for comparison with flight test data in figure 17. This comparison and the determination of cause where the results differed was a necessary step in the validation of the simulator mathematical model for subsequent use in minimum control speed tests on the derivative model. The simulator data were obtained at 15 000 lb gross weight

and 0.37 $\bar{c}$ center of gravity. The light gross weight was selected so tests could be completed without being limited by stall speed. The steady-state static test points were run with one engine shut down and the other engine at maximum available thrust. The airspeed was decreased until a limiting control condition was reached. Airspeed was not reduced below aerodynamic stall speed or engine stall warning speed. The pilots were instructed to maintain a 5° bank angle into the operating engine, but it was difficult to control bank angle accurately and the results were grouped more near zero sideslip angle. If a fairing of the simulator data were accepted without correction for test technique or conditions a V_{MC} value would be obtained that is about 10 knots greater than the flight test value. Only steady-state simulator data are shown in figure 17. The dynamic cut demonstrations made in the simulator are discussed in a paragraph which follows.

The scatter in the simulation data was due primarily to the pilots' difficulty in precisely maintaining a straight course, constant heading and 5° bank. An FAA pilot with extensive certification flight test experience and a good familiarity with research flight simulators stated that the addition of sensitive attitude information to the simulator visual display would aid in the control task and enable a better match with the actual flight test data. During flight tests of this nature, it is common practice to mark horizontal reference angles on the pilot's windshield. Thus, the pilot has a very sensitive bank angle indicator which enables more accurate control. In the simulator, the attitude gyro was the primary bank angle reference. The fact that the aileron control system model had less inertia than the real control system induced some over-control for small deflections around zero and also contributed to scatter in the data.

The need for a more sensitive attitude information display can also be argued from an opposing viewpoint. While the addition would allow more precise pilot control, it may not be necessary to obtain large amounts of steady-state data using piloted simulator operations. Once the simulation mathematical model is sufficiently validated and the analyst is confident that all influencing factors are identified, the necessary steady-state V_{MC} data can be obtained during non-piloted operation, that is, during fast-time computer solution of the mathematical model at many specific conditions. This illustrates the advantage which could come from more extensive use of simulation in the certification process. A very large data base generated from computer solutions of the more precise and accurate mathematical model which can be formulated, can be satisfactorily verified and then validated by a few selected piloted simulation maneuvers, which in turn can be confirmed with even fewer flight tests (pyramid effect). The success of this approach, while making cost-effective use of simulation, is dependent on ensuring that all influencing and limiting factors are properly accounted for in the analysis.

Factors which influence the determination of V_{MC}.- The minimum control speed is clearly influenced by the thrust delivered by the operating engine. It is also influenced by many other variable factors including airplane attitude, gross weight, center of gravity, flap position, landing gear position, altitude, temperature, effectiveness of the control surfaces, effectiveness of the trim surfaces, which engine fails, and last but not least, the skill and strength of the pilot.

The maximum rudder pedal force during simulator tests and flight tests was 140 lb, significantly less than the maximum of 180 lb set by FAR 25.149(d). Thus, the need for a subjective determination that the average pilot's strength was not exceeded was eliminated. Experience has shown (ref. 14) that the evaluations of five or six pilots may be needed to determine minimum speed when it is limited by pilot force, whereas three pilots can establish the minimum speed when it is limited by control displacement.

Insight into the significance of some of the factors identified and the sensitivity of V_{MC} to variation in these factors during the present experiment was gained by a theoretical simultaneous solution of the approximate sideforce and yaw moment equations of motion using a hand-held calculator. The form of solutions derived from these equations is as follows:

The yaw moment, N, equation is solved for $T_A/\bar{q}$, assuming the left engine to be inoperative.

$$N = 0 = \bar{q}SbC_{n_\beta}\beta + \bar{q}SbC_{n_{\delta_r}}\delta_r - T_A y_{RE}$$

or

$$\frac{T_A}{\bar{q}} = K_1\delta_r + K_2\beta \tag{1}$$

where

$$K_1 = \frac{Sb}{y_{RE}} C_{n_{\delta_r}} \quad \text{and} \quad K_2 = \frac{Sb}{y_{RE}} C_{n_\beta}$$

The steady angle of sideslip β which is needed in equation (1), is obtained from a solution of the sideforce, F_y, equation as follows:

$$F_y = 0 = \bar{q}SC_{y_\beta}\beta + \bar{q}SC_{y_{\delta_r}}\delta_r + W \sin \phi + T_A\beta$$

or

$$\beta = \frac{W \sin \phi + K_3\bar{q}\delta_r}{T - K_4\bar{q}} \tag{2}$$

where

$$K_3 = SC_{y_{\delta_r}} \quad \text{and} \quad K_4 = SC_{y_\beta}$$

The net yaw moment contribution due to thrust asymmetry, rudder deflection and sideslip angle must sum to zero for steady-state conditions. The net sideforce must be zero in order to maintain straight flight at constant heading. The term $W \sin \phi$ is the sideforce due to the horizontal component of the lift vector. The $K_3\bar{q}\delta_r$ term is the sideforce caused by the deflected rudder. $T_A\beta$ is the sideforce due to the y component of the thrust vector inclined to the direction of the flight path and $K_4\bar{q}\beta$ is the sideforce due to the inclination of the fuselage and vertical tail. Although these equations are approximations they do include the principal sources of sideforce and yaw moment.

The constants K_1, K_2, K_3, and K_4 are design factors that are functions of the airplane geometry and aerodynamic stability derivatives. The values for the stability derivatives are provided in reference 6; they were originally estimated using analytical, wind tunnel and flight test methods.

It is important to note that equations (1) and (2) are solved simultaneously and assuming that rates and accelerations are zero. Also note that there is no explicit relationship of $T_A/\bar{q}$ versus δ_r except for the case when sideslip angle is zero. The significance of this second statement is that independent effects of T_A and $\bar{q}$ on the required δ_r can cause variability in the determination of V_{MC} when extrapolating flight test $T_A/\bar{q}$ values to the maximum rudder deflection and maximum asymmetric thrust conditions. Nonlinear effects in rudder effectiveness at maximum deflection can also cause variability in the results.

Validation of Model 75A minimum control speed determination.- The solution of the approximate sideforce and yaw moment equations for theoretical rudder deflection was of benefit in comparing the exact simulator solution with flight test (fig. 18). It would otherwise have been difficult to compare the simulator results with Sabreliner 75A flight tests because of the scatter in the data and different test technique. The comparison of theoretical and simulator rudder deflections showed very good correlation. This was not too surprising since equations (1) and (2) are close approximations of the exact equations that were solved in real-time by the simulator computer. The good correlation between theoretical and flight test rudder deflections provided confidence that all the influencing factors were included. The bias (1° to 1.5°) seen in the comparison with flight test was apparently due to an instrumentation system error in rudder deflection. Only steady-state data were included in this comparison. The three dynamic cut points shown in figure 17 were not included. The simulator tests covered the full range of rudder deflection whereas the flight tests were limited to approximately half rudder.

The above comparison was one step in demonstrating that the simulator was sufficiently like the airplane for the purpose of V_{MC} determination. Next, the approximate equations were solved for the various conditions necessary to encompass all simulator and flight test data. The results of these calculations are given in figure 19, which shows the variation of δ_r versus $T_A/\bar{q}$ as was done in figure 17. Although data points are omitted from figure 19, the scales of the two figures are identical so that they can be directly compared. Six lines were drawn on figure 19 in addition to the faired lines obtained from the simulator and flight test data. These lines encompass all the data and graphically show the effect of the different conditions and test techniques. The two test techniques described are,

1. constant throttle (thrust asymmetry of 4000 lb) with airspeed and bank angle varied

2. constant 5° bank angle (airspeed 106 and 149 knots) with throttle (thrust asymmetry) varied.

Dynamic pressure, $\bar{q}$, varies as the square of the airspeed. The theoretical variation of $T_A/\bar{q}$ versus δ_r is linear to 20° δ_r. The nonlinear variation in the range of 20° to 25° δ_r is due to nonlinear variation in rudder effectiveness, $C_{n_{\delta_r}}$, and sideforce due to rudder, $C_{y_{\delta_r}}$.

Either test technique will result in the same V_{MC} for the same conditions; however, correction for independent T_A and $\bar{q}$ effect may be needed when extrapolating to maximum rudder deflection from low rudder deflections. The conditions shown are for 0°, 3.5°, and 5° bank angles. The 3.5° bank angle condition is shown because it corresponds to zero sideslip. Gross weight does not affect the theoretical $T_A/\bar{q}$ versus δ_r relationship at zero bank. Gross weight lines of 15 000 and 20 000 lb are shown for the 5° bank angle condition. The simulator data compared favorably with the theoretical variations and when corrected to the flight test conditions agreed, within 1 knot, with the flight test determined V_{MC} of 93 knots. This was considered excellent agreement and validated the simulation for V_{MC} determination using these steady-state techniques.

Determination of steady-state minimum control speed for the derivative Model 75B.- A major change to the airplane which described the derivative Model 75B was the engine modification. Such a modification was judged to have a large effect on V_{MC} and flight tests to demonstrate V_{MC} would be required prior to certification of a prototype 75B airplane. Therefore, preflight tests on the simulator could be of benefit.

Data points from the piloted steady-state V_{MC} tests with the Model 75B are shown in figure 20; the data were obtained at 20 000 lb gross weight a 0.325 $\bar{c}$ center of gravity. Figure 20 also shows the theoretical calculations of $T_A/\bar{q}$ versus δ_r for bank angles of 0°, 2.6°, and 5°. The 2.6° bank angle condition corresponds to 0° sideslip. The calculations assume a constant throttle (thrust asymmetry, T_A, of 5000 lb) and variable airspeed which resulted in variable $T_A/\bar{q}$.

The theoretical lines encompass the piloted data points at rudder deflections of 22° and less. The points at maximum δ_r were scattered at $T_A/\bar{q}$ values greater than calculated. Data points for the piloted tests in the simulator at the maximum conditions were difficult to obtain while maintaining perfectly balanced sideforce and zero yaw rate. Yaw rates as low as 0.6°/sec to 0.8°/sec were seen to provide an assisting sideslip angle allowing temporory airspeed reduction (see fig. 21). Loss of directional control was gradual and occurred very near stall onset. Directional control could be regained and steady flight reestablished by trading climb performance for acceleration in order to increase airspeed.

The difficulty in both lateral-directional and longitudinal control of the Model 75B increased over that experienced with the Model 75A; the difficulty was aggravated by test conditions nearer to the stall angle of attack. Temporary airspeed reduction near stall resulted in nonsteady-state values of $T_A/\bar{q}$ higher than those that could be sustained. Care was exercised when selecting time points for reading data to ensure that the airplane was indeed steady about all axes. The number of acceptable data points appears sufficient and the V_{MC} thus determined was predicted to be 119 knots.

Simulator demonstrations of dynamic V_{MC} for the Model 75A and Model 75B.- The dynamic V_{MC} demonstration tests in the simulator were made by three pilots. The airplane was initially trimmed at the airspeed to be demonstrated with both engines operating at maximum available thrust. This resulted in a very nose high pitch attitude. A 3-sec countdown to failure was given the pilot. The left engine was then failed to simulate instantaneous loss of thrust on that engine. The motion cues generated during these demonstrations were judged to be realistic. The pilots commented that the simulator provided particularly good training in flight-test procedures for this hazardous maneuver.

The maneuver in the Model 75A was successfully accomplished at an airspeed of 95 knots by a pilot without actual flight experience in the airplane (fig. 22). The loading and configuration were: 15 000 lb gross weight, 0.37 $\bar{c}$ center of gravity, 15° flaps, and gear up. The thrust of the engine was 2260 lb at the instant of failure. The rudder was smoothly deflected to the limit of 25° to counter the yaw caused by engine failure. Control of the airplane was excellent: it rolled to a maximum of 14° during the recovery as a result of the yaw and the heading change was held within 10°. Longitudinal control was accomplished with a 14° decrease in pitch attitude to complete the recovery in a level flight attitude. Repeated attempts would probably result in a lower minimum control speed if not limited by airplane stall.

Instantaneous failures of the left engine on the Model 75B were tried by two other pilots; both pilots had Sabreliner and T-39 flight experience. The configuration and loading were: gear up, 15° flaps, 20 000 lb gross weight, and a 0.325 $\bar{c}$ center of gravity. Attempts to recover when the airspeed at time of engine failure, V_{EF}, was below 119 knots were unsuccessful due to control deficiencies and to very rapid rotation to dangerous attitudes caused by the upsetting moments on the airplane. Figure 23 is a time history with V_{EF} of 103 knots. The engine thrust at time of failure was 4940 lb. The rudder, aileron, and elevator control surfaces were all deflected to their limit in the recovery maneuver. The elevator input was immediate following the engine failure and the airplane rotated 40° nose down and accelerated from a stalled flight condition. This recovery maneuver required exceptional pilot skill. For that reason, and because 300 ft of altitude were lost and heading changed 35° during recovery, it was an unsuccessful demonstration of compliance with FAR 25.149.

A test at the above conditions is not realistic because it could not be safely attempted in flight. However, it does provide a check on the range of angle of attack and sideslip for which the Models 75A and 75B were judged valid. The maximum values during this maneuver were 15.2° angle of attack and 20.4° sideslip angle. These values slightly exceed those demonstrated during flight tests. The maximum sideslip angle rate was 10.7°/sec. Conclusive matching of the model response during such rapid, large angular perturbations was not possible because comparable flight histories were not available. The simulation mathematical model assumes the vertical tail yaw moment to be linear with sideslip angle (ref. 6). Care must be taken in analyzing the data to be sure that sideslip angle excursions do not exceed in magnitude or rate those values which matched the flight test; if they do, the results obtained will not be valid.

Reference 14 is an excellent and useful manual of procedures for planning safe progressive flight tests to determine V_{MC}. An interesting comment on aerodynamic characteristics is quoted:

> The violence with which a *given* aircraft reacts to an engine failure depends mainly upon the airspeed and the power being used. High power, low airspeed will result in a more violent reaction than low power and high airspeed. Various types of reaction will also depend upon the design characteristics of the aircraft and generally speaking an aircraft inclined to "Dutch Roll" characteristics reacts more violently than an aircraft inclined to spiral instability. *The more "nose-high" the attitude* the more rapid is the deceleration and hence faster recovery action is required. . . The quickness and ease with which control is regained depends entirely upon the interval between the engine failing and pilot commencing recovery action. However, before any of the tests for (takeoff) safety speed or for landing and overshooting, a careful investigation for any evidence of rudder lock or fin stalling is made since the occurrence of these conditions in an emergency can be very serious. . . It should be noted that an airplane that normally will not exhibit either of these characteristics due to the inability to develop the large yaw angles required, may do so when an engine fails causing a yawing velocity such that a large yaw angle is reached.

Figure 24 is a time history showing a successful demonstration of V_{MC} of 120 knots. The configuration and loading were the same as in figure 23. Thrust was 4805 lb at the time the left engine was failed. Recovery control required considerable pilot skill predominately in the pitch axis. About 50 percent of elevator control was used to pitch the airplane nose down (pitch attitude change was 34°). The altitude goes through an oscillation of approximately ±300 ft amplitude but does not decrease below that at the time of engine failure. The heading change exceeds the 20° criteria slightly but the pilot believed it could be reduced with repeated attempts. This demonstration confirmed the earlier steady-state determination of V_{MC} of 119 knots.

Since one-engine-inoperative climb performance requirements would be satisfied at these conditions with the larger engine of the Model 75B, the FAR 25 constraint on takeoff safety speed, V_2, is 1.2 V_S or 1.1 V_{MC}, whichever is greater. Stall speed, V_S, was about 105 knots at these conditions and V_2 would therefore be limited by V_{MC}; however, at design maximum takeoff weight of 28 000 lb the estimated stall speed was 115 knots in which case V_2 would again be limited by V_S. Thus, there is a range of gross weights where minimum control speed is predicted to be critical with respect to safe takeoff operations of the derivative airplane.

General Discussion

Although data were recorded for all of the test program items and are available for detailed analysis, only a limited amount of the simulation data obtained has been presented in this report. No significant unanswered questions regarding the validity of the data remained at the completion of the

test program. The simulator appears to be an effective means of routinely evaluating these airplane characteristics and large amounts of data can be obtained in a relatively short period of time.

The critical items analyzed herein were: the reversible flight control system, longitudinal stability and control, and minimum control speed. The simulator experience gained in these areas has contributed toward defining the technical criteria which the simulator must meet to provide an acceptable means of demonstrating compliance with the applicable FAR paragraph.

A preliminary step in defining the technical criteria has been completed by comparing the simulator results with flight results from the baseline airplane. However, additional steps essential to a complete solution of the problem remain to be taken. Since a prototype of the derivative Model 75B will not be produced as was originally planned, the logical step of comparison of the simulator preflight data with flight data from the prototype can no longer be accomplished. This was planned to answer the question: How much flight testing is necessary to validate a simulation for accomplishing specific test requirements? An efficient flight test approach may have been the antithesis - that is, show in the minimum amount of flight time that the simulator results are not valid. In any case, it is still important to the proof of concept that a direct concurrent comparison be made of the quantitative and subjective results in each critical test area. Only in this way will we be able to study in detail those characteristics about which the flight test specialists have suspicions regarding the simulation.

Questions of a less technical nature also exist. For example: What is the best form in which the criteria should be drafted? It may be possible to include tentative criteria in appropriate sections of such FAA test procedure manuals as reference 8. It is clear that the intent of Advisory Circular 21-14 (ref. 3) must be preserved so that industry may have the option to extend the use of simulation in the certification process where it is economically attractive to do so. What is the best time in the design development cycle of the aircraft for conducting a "certificability" assessment? Will substitution of simulation for flight during the certification process create a legal technicality with regard to demonstrating reliability of a product? This last question is truly difficult to answer because the mathematical models used in the simulation are abstractions of the physical systems and exact conformity with the aircraft hardware cannot be shown. The importance of such questions is obvious, and the absence of a reasonable answer can inhibit implementation of the concept even though it is technically feasible.

Some of the FAR flight-test paragraphs which were not considered technically feasible for simulation study at this time are: (1) paragraphs 25.103 and 25.201 through 25.207 concerning stall speed and stall characteristics; and (2) paragraphs 25.105 through 21.115 concerning takeoff performance. The nonsteady aerodynamic flow characteristics in the stall flight regime cannot be modeled with sufficient precision at present to use the simulator for actual compliance demonstrations. Efforts to mathematically describe this phenomenon and develop real-time simulation models (both deterministic and stochastic) should be continued. Although the certification of actual takeoff performance by simulation is not feasible at present, simulation experiments,

such as those described in reference 15, have shown that the related effects of airplane handling qualities on performance can be evaluated. If a real data base of sufficient accuracy existed or could be developed concurrently, the digital hybrid simulator would have the potential, which early analog simulators did not have, for precise generation of takeoff performance information.

CONCLUDING REMARKS

An advanced research simulator was used to investigate the feasibility of increasing the use of piloted simulations as a means of demonstrating compliance with transport airplane airworthiness requirements. Evaluations of the flying qualities required to certificate a small jet transport and a derivative model of that airplane were performed in the simulator. The evaluations were satisfactorily accomplished in less time and with less cost than required to do the same flight tests.

Results of the simulator evaluations using the basic airplane model were compared with flight tests performed during the certification of that airplane. The data from these evaluations correlated well with that shown in the manufacturer's certification test report. The longitudinal static stability gradient for the climb configuration, which was a critical test case, agreed closely with flight results. The difference was only 1 lb column force at 50 knots below trim airspeed. Very good agreement was also demonstrated in the critical determination of minimum control speed. Agreement was within 1 knot after corrections were made for different test conditions. The evaluation pilots' comparison of the simulator flying qualities with those of the airplane were favorable.

Several flight tests were identified where simulation would assist in the certification of the derivative airplane. Special longitudinal control tests and equivalent safety analysis of static longitudinal stability levels are examples. The greater potential for increasing the use of the simulator is in the determination of minimum control speed for the large engine modification. An extensive analysis of the many factors which influence minimum control speed is included in the report. All of the above flight tests are candidates for additional simulator testing to further explore this concept. It is possible that such simulator testing can result in savings in the design, development, certification, and operation of a derivative airplane.

In general, it can be said that the accuracy and extent of the simulation models needed for certification testing applications is greater than that needed for equivalent basic research studies. This was evident during the development of the reversible flight control system model, which provided a faithful representation of the control force-feel characteristics of the airplane. The overall confidence level in the validity of the simulation was greatly increased as a result. This experience will be useful in developing models of new airplanes of similar designs; for example, business jet airplanes and general aviation airplanes with reversible flight controls.

The simulation problems encountered during this study were solved using available technology at this facility. The principal constraint on use of the hybrid simulator as it was used in this study is the development of efficient software and the formulation of complex mathematical models. Procedures that will result in a minimum but sufficient number of independent verification checks of these models should be developed.

It is concluded that it is technically feasible to pursue the increased use of simulation in conducting certification evaluations of the scope of those reported here. Test requirements should be thoroughly analyzed during concurrent simulation and flight investigations in order to develop appropriate guidelines in each specific test area. Regulatory changes to remove restrictions on the future application of this concept are in the legal province of the Flight Standards Service, FAA.

APPENDIX A

CONTROL LOADER SYSTEM CHARACTERISTICS

General Description

A control loader system which is mounted in the FSAA cockpit to provide control force-feel simulation is described in reference 5. The system consists of a three-axes set of cockpit controls (column, wheel, and pedals) with integral rotary hydraulic actuators, valves, and transducers. It also includes an associated console of servo control and function generating electronics. By interfacing these loaders with the central digital computer through an analog computer, it is possible to simulate a wide range of control force characteristics. These characteristics may be functions of control position, rate, and aircraft parameters such as airspeed, normal acceleration, and angle of attack. The system can simulate variable spring gradient, viscous friction (damping), breakout (preload), deadband (backlash), coulomb friction (hysteresis), and control travel limits. Column and wheel trim is available through a trim button on the wheel; trim rate is variable.

A rate limiting feature is provided that limits the rate of force buildup. It is designed to prevent runaway operation or a response to inadvertent computer commands. The system resets when the limit is reached.

An hydraulic rotary actuator, connected directly to the column, provides a more compact package than the typical linear actuator. The actuator is supported on hydrostatic bearings to minimize friction. In addition, the actuator is sealed by a vacumn return system, thus eliminating the need for seals with their attendant friction. A standard servo valve is mounted on the actuator and a differential pressure transducer is utilized as the force sensing element. A position transducer and tachometer provide the feedback position and velocity signals, respectively. A similar setup is used with the wheel and rudder pedal controls. The important performance characteristics are listed in table 8.

Control Loader Operation

An overview block diagram of the loader is shown in figure 25. Each axis of the loader system is basically configured as a force servo. Valve position is controlled by the difference between a commanded force and the actuator force. The actuator force is the force applied to the system by the hydraulic actuator and is measured by a differential pressure transducer. The feedback compensation for this loop has been carefully designed to achieve a high loop bandwidth (>10 Hz).

Because of this high bandwidth, the force felt by the pilot will closely approximate the force command. The force command is an electronically generated function of control displacement and rate. This command generation can be done either in the special loader electronics unit or by an analog computer.

However, the loader electronics can only simulate a fixed gradient and damping. For more complex force-feel system characteristics, or to provide variations with flight condition, it is necessary to use the analog computer.

The force command is generated on an EAI 231R analog computer with inputs from the digital computer. The following parameters can be varied by the digital computer: gradient, damping (viscous friction), hysteresis (coulomb friction), breakout (preload), bias force, trim position, and stops (position limits). If any of the parameters listed in table 8 do not vary, the constant values can be set external to the digital computer. On the other hand, desired variations with flight condition can be simulated by providing the appropriate computations in the digital computer.

One parameter which cannot be independently controlled is the effective loader mass. If the loader is set to simulate only the gradient K and damping B terms, the dynamic response transfer function (control deflection/pilot force) is closely approximated by:

$$\frac{\delta}{F_P} = \frac{1}{m_e s^2 + Bs + K}$$

The effective mass, m_e, is not the physical mass of the system but is a complex function of the force loop, valve, and actuator characteristics.

APPENDIX B

AIRPLANE AERODYNAMIC MODEL EQUATIONS

This appendix summarizes the modeling data and necessary equations for combining the data to obtain aerodynamic coefficients of lift, drag, pitching moment, rolling moment, yawing moment, and sideforce. These six components of aerodynamic forces and moments are the basis of the computer subroutines that determine the static and dynamic characteristics of the airplane being simulated. These subroutines communicate with other subroutines which describe the FSAA standard kinematic model (ref. 16). The equations below apply to both the Model 75A and Model 75B except where noted.

Lift coefficient:

$$C_L = C_{L_o} + \Delta C_{L_{o_{flaps}}} + \left(C_{L_\alpha} + \Delta C_{L_{\alpha_{flaps}}}\right)\alpha + C_{L_{\delta_s}} \cdot \delta_s + C_{L_{\delta_e}} \cdot \delta_e \cdot K_e$$

$$+\left[C_{L_{\dot{\alpha}}} + \Delta C_{L_{\dot{\alpha}(CG)}}\right]\left(\frac{\dot{\alpha}\bar{c}}{2V}\right) + \left[C_{L_q} + \Delta C_{L_{q(CG)}}\right]\left(\frac{q\bar{c}}{2V}\right)$$

$$+\Delta C_{L_{gear}} + \Delta C_{L_{power}}$$

Drag coefficient:

$$C_D = C_{D_o} + \Delta C_{D_{o_{antennas}}} + \Delta C_{D_{o_{slats}}} + \Delta C_{D_{o_{flaps}}} + \Delta C_{D_{o_{gear}}}$$

$$+\Delta C_{D_{o_{windmill}}} + \Delta C_{D_{o_{rudder}}} + \Delta C_{D_{o_{(\beta)}}} + \Delta C_{D_{o_{ailerons}}}$$

$$+K_{P_d}\left(C_L - C_{L_K}\right)^2$$

Pitching-moment coefficient:

$$C_m = C_{m_o} + \Delta C_{m_{flaps}} + C_{m_\alpha} \cdot \alpha + C_{L_s}(CG - 0.25) + C_{m_{\delta_s}} \cdot \delta_s \cdot \frac{1}{K_{CG}}$$

$$+C_{m_{\delta_e}} \cdot \delta_e \cdot \frac{Ke}{K_{CG}} + \left[C_{m_{\dot{\alpha}}} + \Delta C_{m_{\dot{\alpha}(CG)}}\right]\left(\frac{\dot{\alpha}\bar{c}}{2V}\right) + \left[C_{m_q} + \Delta C_{m_{q(CG)}}\right]\left(\frac{q\bar{c}}{2V}\right)$$

$$+\Delta C_{m_{gear}} + C_{m_{power}}$$

Rolling-moment coefficient:

$$C_\ell = C_{\ell_\beta} \cdot \beta + C_{\ell_{\delta\alpha}} \cdot \delta\alpha + C_{\ell_{\delta_R}} \cdot \delta_R + C_{\ell_p}\left(\frac{pb}{2V}\right) + \left(C_{\ell_r}{}_{C_L=o} + \frac{\partial C_{\ell_r}}{\partial C_L} \cdot C_L\right)\left(\frac{rb}{2V}\right)$$

Yawing-moment coefficient:

$$C_n = \left[C_{n_\beta} + \Delta C_{n_{\beta_{(CG)}}}\right] \cdot \beta + C_{n_{\delta_R}} \cdot \delta_R + \left(C_{n_p}{}_{C_L=o} + \frac{\partial C_{n_p}}{\partial C_L} \cdot C_L\right) \cdot \left(\frac{pb}{2V}\right) + C_{n_r}\left(\frac{rb}{2V}\right) + \Delta C_{n_{eng.\ out}}$$

Sideforce coefficient:

$$C_y = C_{y_\beta} \cdot \beta + C_{y_{\delta_R}} \cdot \delta_R + \left(C_{y_p}{}_{C_L=o} + \frac{\partial C_{y_p}}{\partial C_L} \cdot C_L\right)\left(\frac{pb}{2V}\right) + C_{y_r}\left(\frac{rb}{2V}\right)$$

where

$$\Delta C_{L_o}{}_{flaps} = 0.0158\delta_F$$

$$\Delta C_{L_\alpha}{}_{flaps} = -0.000128\delta_F$$

$$K_e = 1.0 \qquad \text{for } \delta_e \text{ from } +11° \text{ to } -12°$$

$$= 1.0 - 0.001(\delta_e + 12)^2 \qquad \text{for } \delta_e \text{ from } -12° \text{ to } -22°$$

$$\Delta C_{L_{\dot\alpha(CG)}} = -1.1(CG - 0.25)\ (1/RAD)$$

$$\Delta C_{L_{q(CG)}} = K_{L_q}(CG - 0.25)\ (1/RAD) \qquad K_{L_q} = -10 \text{ Model 75A}, \ -9 \text{ Model 75B}$$

$$\Delta C_{L_{gear}} = 0.011 - 0.0004\delta_F$$

$$\Delta C_{L_{power}} = C_T\left[\sin(\alpha + 2°) - K_{L_s}C_{L_{\delta_s}}\right] \qquad K_{L_s} = 4.615 \text{ Model 75A}, \ 3.231 \text{ Model 75B}$$

$$C_{L_s} = \left[C_{L_o} + \Delta C_{L_o}{}_{flaps} + \left(C_{L_\alpha} + \Delta C_{L_\alpha}{}_{flaps}\right)\alpha + \Delta C_{L_{gear}}\right]$$

$$K_{P_d} = 0.0726 \text{ Model 75A}$$
$$= 0.0750 \text{ Model 75B}$$

$$\text{Low speed } C_{D_o} = 0.0198 \text{ Model 75A}$$
$$= 0.0218 \text{ Model 75B}$$

$$\Delta C_{D_o}{}_{\text{antennas}} = 0.0005 \text{ Model 75A}$$
$$= 0.0010 \text{ Model 75B}$$

$$\Delta C_{D_o}{}_{\text{slats}} = 0 \qquad \text{for } C_L \leq 0.43$$
$$= 0.0130\left(\frac{C_L - 0.43}{0.37}\right) \qquad \text{for } 0.43 \leq C_L \leq 0.80$$
$$= 0.0130 \qquad \text{for } C_L > 0.80$$

$$\Delta C_{D_o}{}_{\text{flaps}} = 0.0070 \quad \text{for } \delta_F = 15°$$
$$= 0.0180 \quad \text{for } \delta_F = 25°$$

$$\Delta C_{D_o}{}_{\text{gear}} = 0.0230$$

$$\Delta C_{D_o}{}_{\text{windmill}} = K_{D_W}\left(\frac{1 + 0.70M^2}{1 + 2.96M^2}\right) \qquad K_{D_W} = 0.0025 \text{ Model 75A}$$
$$= 0.0061 \text{ Model 75B}$$

$$\Delta C_{D_o}{}_{\text{rudder}} = 0.0064\left(\frac{\delta_R{}^o}{25}\right)^2$$

$$\Delta C_{D_o}{}_{(\beta)} = 0.0002(\beta^o)^2$$

$$\Delta C_{D_o}{}_{\text{ailerons}} = 0.000018(\delta_a{}^o)^2$$

$$C_{L_K} = \Delta C_{L_K}{}_{\text{slats}} + C_{L_K}{}_{\text{flaps}} + C_{L_K}{}_{\text{gear}}$$

$$\Delta C_{L_K}{}_{\text{slats}} = 0 \qquad \text{for } C_L \leq 0.43$$
$$= 0.050\left(\frac{C_L - 0.43}{0.37}\right) \qquad \text{for } 0.43 \leq C_L \leq 0.80$$
$$= 0.050 \qquad \text{for } C_L > 0.80$$

$$C_{L_K}{}_{\text{flaps}} = 0.030 \quad \text{for } \delta_F = 15°$$
$$= 0.050 \quad \text{for } \delta_F = 25°$$

$$C_{L_{K_{gear}}} = 0.040$$

$$\Delta C_{m_{flaps}} = -0.00328\delta_F$$

$$K_{CG} = 0.895 + 0.42\,\frac{X}{c} \qquad K_{CG} = 1.0 \quad \text{for} \quad \frac{X}{c} = 0.25$$

$$\Delta C_{m_{\dot{\alpha}_{(CG)}}} = 5.0(CG - 0.25)\ (1/RAD)$$

$$\Delta C_{m_{q_{(CG)}}} = K_{m_q}(CG - 0.25)\ (1/RAD) \qquad K_{m_q} = 17.0 \text{ Model 75A}, \ 15.5 \text{ Model 75B}$$

$$\Delta C_{m_{gear}} = -0.0050$$

$$\Delta C_{m_{power}} = -C_T\left(K_{m_T} + K_{L_s}C_{m_{\delta_s}}\right) \qquad K_{m_T} = 0.187 \text{ Model 75A}, \ 0.157 \text{ Model 75B}$$

$$C_T = \frac{T}{\bar{q}S} \qquad \text{where} \quad T = \text{total net thrust}$$

$$\alpha_{max} = \alpha_{max} + \Delta\alpha_{max_{flaps}}$$

$$\Delta\alpha_{max_{flaps}} = -0.04\delta_F$$

Effect of asymmetric thrust on yawing moment:

$$\Delta C_{n_{eng.\ out}} = \frac{\Delta N}{\bar{q}Sb} = K_{NE}\left(\frac{F_n + D_{w_m}}{\bar{q}S}\right) \qquad K_{NE} = 0.1032 \text{ Model 75A}, \ 0.1201 \text{ Model 75B}$$

where

F_n = net thrust on left engine

$$D_{w_m} = \frac{K_{we}q(1 + 0.70M^2)}{(1 + 2.96M^2)} \qquad K_{we} = 0.8416 \text{ Model 75A}, \ 2.093 \text{ Model 75B}$$

$$\Delta C_{n_{\beta_{(CG)}}} = -0.00271(CG - 0.25)$$

APPENDIX C

FLIGHT CONTROL SYSTEM MODEL EQUATIONS

Longitudinal Control System Equations

The sign convention used in the column force equations is shown in the sketch below. The pilot force F_{CP}, which is opposed by the column force F_C when in equilibrium conditions, is given by equation (C1).

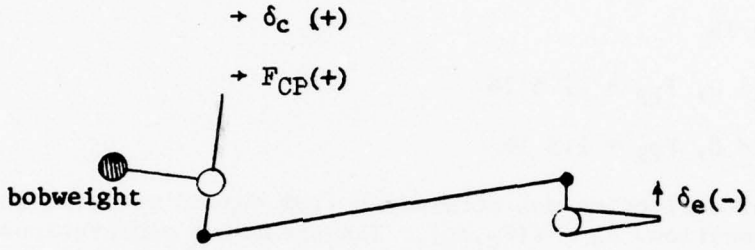

$$F_{CP} = -F_C = F_{BW} + F_{BWB} + F_{BB} + F_{HM} + F_{FR} \tag{C1}$$

where

$$F_{BW} = \Delta F_{p_{bw}} n_z + X_{BW} \Delta F_{p_{bw}}\Big|_{\alpha=o} \frac{\dot{q}}{g} \tag{C2}$$

where

$\Delta F_{p_{bw}} = f(\delta_c,\alpha)$, lb, is the pilot force due to the bobweight mass

$X_{BW} = 18.3$ ft, is the distance from the bobweight to the CG

where

$$F_{BWB} = \Delta F_{p_{bwb}} = f(\delta_c), \text{ lb} \tag{C3}$$

is the pilot force due to the bobweight balance bungee

where

$$F_{BB} = \Delta F_{p_{bb}} = f(\delta_e,\delta_s), \text{ lb} \tag{C4}$$

is the pilot force due to the bias bungee

where

$$F_{HM} = C_{h_e} \bar{q} S_e \bar{C}_e \delta_e G_R \tag{C5}$$

where

C_{h_e} = f(M), per deg, is the elevator hinge moment coefficient

G_R = $f(\delta_e, \delta_s)$, lb/ft lb, is the gearing ratio and F_{FR}, lb, is the control system friction force which is obtained as follows:

(1) If $\dot{\delta}_e = 0$,

$$F_{FR} = -(F_C + F_{BW} + F_{BWB} + F_{BB} + F_{HM}) \tag{C6}$$

but $|F_{FR}| \leq 1.5$ lb

(2) If $\dot{\delta}_e > 0$, $F_{FR} = -1.5$ lb

(3) If $\dot{\delta}_e < 0$, $F_{FR} = 1.5$ lb

The elevator deflection was determined from column position and horizontal stabilizer position, $\delta_e = f(\delta_c, \delta_s)$. The preceding computations were performed in the digital computer. In addition, computations were performed to determine the column trim position, $\delta_{c_{trim}}$, with zero pilot force. Finally, the digital gradient G defined as

$$G \equiv \frac{F_{CP}}{\delta_c - \delta_{c_{trim}}} = \left| \frac{F_{CP}}{\delta_c - \delta_{c_{trim}}} \right| \tag{C7}$$

was computed and transmitted to the control loader.

The column breakout force was added by computation in the analog computer. Viscous damping force and force servo loop compensation was introduced by the loader system electronics.

The above equations and computations apply to the modified flight control system as well as to the baseline system. The following parametric functions were changed as indicated for the modified system.

(1) $\Delta F_{p_{bw}} = 10$ lb/g constant bobweight effect

(2) $\Delta F_{p_{bw}} = 0$ and $\Delta F_{p_{bb}} = 0$, since the bobweight balance bungee and the bias bungee were elimianted

(3) Constant values of $G_R = 0.055$ lb/ft lb and $\delta_e/\delta_c = 2.66$ °/in., since the nonlinear gearing mechanism was eliminated.

Lateral Control System Equations

The wheel force equations were developed using the sign convention in the sketch below. The absence of springs and bobweights makes the system less complex than the baseline longitudinal system. The force equations were solved in the digital computer and breakout force and viscous damping force were introduced as in the longitudinal system.

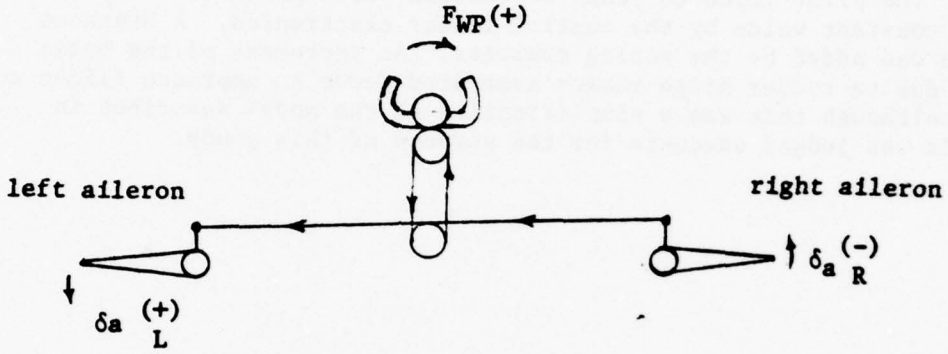

$$F_{WP} = -F_W = F_{HMA} + F_{FRA} \tag{C8}$$

where

$$F_{HMA} = C_{h_a} \cdot \bar{q} S_a \bar{c}_a \cdot \delta_a G_R \tag{C9}$$

$C_{h_a} = f(\delta_a, \delta_F)$, per deg, is the aileron hinge moment coefficient

$G_R = f(\delta_{a_L}, \delta_{a_R})$, lb/ft lb, is the gearing ratio and F_{FRA} is the friction force in the aileron control system which is obtained as follows:

(1) If $\dot{\delta}_a = 0$,

$$F_{FRA} = -(F_{HMA} + F_W) \tag{C10}$$

but $|F_{FRA}| \leq 1.0$ lb

(2) If $\dot{\delta}_a > 0$, $F_{FRA} = -1.0$ lb

(3) If $\dot{\delta}_a < 0$, $F_{FRA} = 1.0$ lb

The left and right aileron surface deflection was determined from the wheel position, $\delta_{a_{L,R}} = f(\delta_W)$. The total aileron deflection was

$$\delta_a = \delta_{a_L} - \delta_{a_R} \tag{C11}$$

The digital gradient was then computed as defined by

$$G_W \equiv \frac{F_{WP}}{\delta_W - \delta_{W_{trim}}} = \left| \frac{F_{WP}}{\delta_W - \delta_{W_{trim}}} \right|$$

Directional Control System

The directional control force-feel system was simulated without digital computation. The pilot force to pedal deflection basic gradient of 40 lb/in. was set as a constant value by the control loader electronics. A breakout force of 4 lb was added by the analog computer. An increment of the basic gradient was due to rudder hinge moment generated force at approach flight conditions, and although this was a simplification of the model described in reference 6 it was judged adequate for the purpose of this study.

REFERENCES

1. Lee, A. H.: Flight Simulator Mathematical Models in Aircraft Design. AGARD Conference Proceedings No. 79 on Simulation, January 1971.

2. The Role of Simulation in the Aircraft Certification Process. Federal Aviation Administration, Advisory Circular No. 21-14, June 12, 1975.

3. Federal Aviation Regulations, Part 25 - Airworthiness Standards: Transport Category Airplanes. Federal Aviation Agency, February 4, 1965.

4. Archibald, D. M.: The Role of Simulation Methods in the Aircraft Certification Process. Federal Aviation Administration, FAA-RD-77-17, March 1977.

5. Sinacori, J. B.; Stapleford, R. L.; Jewell, W. F.; and Lehman, J. M.: Researcher's Guide to the NASA Ames Flight Simulator for Advanced Aircraft (FSAA). System Technology, Inc., Report No. 1074-1, February 1977.

6. Husher, C.: Data Package for Sabreliner Models 75A and 75B Simulation. Rockwell International, Report No. TFD-76-801, July 9, 1976.

7. Haug, C.: Real-Time Simulation of a Reversible Flight Control System in a Light Jet Transport Aircraft. Computer Sciences Corp., Report CSCR No. 7, February 1977.

8. Engineering Flight Test Guide for Transport Category Airplanes. Federal Aviation Administration Order 8110.8, September 26, 1974.

9. FAA Type Inspection Report Model NA-265-80 Sabreliner. Rockwell International, Report No. SR-74-016, 1973.

10. Chalk, C. R.; Neal, T. P.; Harris, T. M.; Pritchard, F. E.; and Woodcock, R. J.: Background Information and User Guide for MIL-F-8785B(ASG), Military Specification - Flying Qualities of Piloted Airplanes. USAF AFFDL-TR-69-72, August 1969.

11. Etkin, B.: Dynamics of Flight. John Wiley & Sons, Inc., New York, 1959.

12. Tulinius, J.; Clever, W.; Niemann, A.; Dunn, K.; and Gaither, B.: Theoretical Prediction of Airplane Stability Derivatives at Subcritical Speeds. NASA CR-132681, 1973.

13. Approach and Landing Simulation. AGARD Report No. 632, October 1975.

14. Pilot Techniques for Stability and Control Testing. U. S. Naval Test Pilot School, Patuxent River, Maryland, 1958.

15. Synder, C. T.; Drinkwater, F. J., III; Fry, E. B.; and Forrest, R. D.: Takeoff Certification Considerations for Large Subsonic and Supersonic Transport Airplanes Using the Ames Flight Simulator for Advanced Aircraft. NASA TN D-7106, March 1973.

16. McFarland, R. E.: A Standard Kinematic Model for Flight Simulation at NASA-Ames. NASA CR-2497, January 1975.

TABLE 1.- MOTION LIMITS, FLIGHT SIMULATOR FOR ADVANCED AIRCRAFT

Motions generated	Displacement	Velocity	Acceleration
Roll	38°	1.75 rad/s	2.09 rad/s^2
Pitch	20°	1.01 rad/s	2.62 rad/s^2
Yaw	25°	0.90 rad/s	1.68 rad/s^2
Vertical	±1.3 m (±4.2 ft)	2.6 m/s (8.6 ft/s)	3.66 m/s^2 (12 ft/s^2)
Longitudinal	±1.0 m (±3.5 ft)	2.1 m/s (7.0 ft/s)	2.44 m/s^2 (8 ft/s^2)
Lateral	±12.2 m (±40 ft)	8.7 m/s (28.6 ft/s)	2.44 m/s^2 (8 ft/s^2)

TABLE 2.- FLIGHT CONTROL SYSTEMS CHARACTERISTICS

	Baseline system	Modified system
Control column:		
Basic force gradient, N/cm (lb/in.)	10.5 (6)	10.5 (6)
Digital force gradient, N/cm (lb/in.)	variable	variable
Bobweight force, N/g (lb/g)	variable	44.5 (10)
Breakout force, N (lb)	±6.7 (±1.5)	±6.7 (±1.5)
Travel, aft/fwd., cm (in.)	17.8/12.7 (7/5)	17.8/12.7 (7/5)
Control wheel:		
Basic force gradient, N/deg (lb/deg)	0.85 (0.19)	0.85 (0.19)
Digital force gradient, N/deg (lb/deg)	variable	variable
Breakout force, N (lb)	±4.4 (±1)	±4.4 (±1)
Travel, deg	±105	±105
Rudder pedals:		
Basic force gradient, N/cm (lb/in.)	70.1 (40)	70.1 (40)
Breakout force, N (lb)	±17.8 (±4)	±17.8 (±4)
Travel, cm (in.)	±8.26 (±3.25)	±8.26 (±3.25)
Maximum control surface deflection:		
Elevator, T.E. up/down, deg	22/11	22/11
Aileron, deg	±31	±31
Rudder, deg	±25	±25
Horizontal stabilizer, ANU/AND, deg	-8/0	-14/0
Aileron trim, deg	±12	±12
Rudder trim, deg	±15	±15
Control system gearing:		
Elevator, deg/cm (deg/in.)	nonlinear	1.05 (2.66)
Aileron, deg/deg	0.44	0.44
Rudder, deg/cm (deg/in.)	3.03 (7.69)	3.03 (7.69)
Horizontal stabilizer rate limit:		
Gear up, deg/sec	0.4	0.4
Gear down, deg/sec	1.0	1.0

TABLE 3.- VARIABLES RECORDED ON DIGITAL MAGNETIC TAPE

Variable	Notation	Units or Position	Fortran name
Time	t	sec	DT
Center of gravity/$\bar{c}$	CG	-	CG
Calibrated airspeed	V_c	knots	VCAL
Mach number	M	-	XMACH
Gross weight	GW	lb	WAITIC
Moment of inertia, x axis	I_{xx}	slug-ft^2	XIXXIC
Moment of inertia, y axis	I_{yy}	slug-ft^2	XIYYIC
Moment of inertia, z axis	I_{zz}	slug-ft^2	XIZZIC
Product of inertia, xz	I_{xz}	slug-ft^2	XIXZIC
Heading	ψ_i	deg	PSI
Pitch angle	θ	deg	THET
Roll angle	ϕ	deg	PHI
Altitude	h	ft	HWEEL
Rate of climb	$\dot{h}_{cg}$	ft/min	HDOT
Net thrust	F_n	lb	FNET
Flap deflection	δ_F	deg	DF
Gear position	GU/GD	up/down	RIWELC
Stabilizer deflection	δ_s	deg	DS
Wind velocity	V_{TW}	ft/sec	VTW
Wind direction	ψ_w	deg	PSIW
Localizer error	E_{LOC}	deg	EPSLOC
Glide slope error	E_{GS}	deg	EPSGS
Computed column force	F_c	lb	FPCOLR
Column position	δ_c	in.	CALPOS
Computed wheel force	F_W	lb	FPWELP
Wheel position	δ_w	deg	WHEEL
Computed pedal force	F_p	lb	FPPEDR
Pedal position	δ_p	in.	PEDALS
Rudder deflection	δ_r	deg	DR
Elevator deflection	δ_e	deg	DE
Aileron deflection	δ_a	deg	DA
Angle of attack	α	deg	ALFA
Angle of sideslip	β	deg	BETA
Normal load factor (body axis)	n_z	g	ANZ
Pitch rate (body axis)	q_B	deg/sec	QB
Roll rate (body axis)	P_B	deg/sec	PB
Yaw rate (body axis)	r_B	deg/sec	RB
Net thrust, No. 1 engine	Fn_1	lb	THO
Net thrust, No. 2 engine	Fn_2	lb	THO+1
Throttle position, No. 1 engine	δt_1	deg	THPAZD
Throttle position, No. 2 engine	δt_2	deg	THPAZD+1
Longitudinal acceleration (pilots station)	Ax_p	ft/sec^2	AXP
Lateral acceleration (pilots station)	Ay_p	ft/sec^2	AYP
Vertical acceleration (pilots station)	Az_p	ft/sec^2	AZP

TABLE 3.- VARIABLES RECORDED ON DIGITAL MAGNETIC TAPE - Concluded

Variable	Notation	Units or position	Fortran name
Turbulence intensity, rms value	σ	ft/sec	DISP
Roll velocity gust	P_g	deg/sec	PTURBD
Initial vertical flight path angle	γ_{vic}	deg	GAMVIC
Initial horizontal flight path angle	γ_{hic}	deg	GAMHIC
Measured column force	F_{CM}	lb	CFORCE
Measured wheel force	F_{WM}	lb	WFORCE
Measured pedal force	F_{PM}	lb	PFORCE

TABLE 4.- CERTIFICATION TEST PROGRAM

Baseline Model 75A Test Conditions

Requirement paragraph	Description of test	Config.	Gear	Flaps, deg	Thrust	Run numbers	Duration min:sec
4b.142	Longitudinal trim	Cruise	Up	0	TR	187,188	3:58
4b.142	Longitudinal trim	Landing	Down	25	Idle	189	2:34
4b.143	Long., direct. and lateral trim	Cruise	Up	0	MCT(OEI)	126	2:23
4b.151,4b.154	Static longitudinal stability	Climb	Up	0	MCT(OEI)	33,34	4:30
4b.151,4b.155	Static longitudinal stability	Cruise	Up	0	TR	31	10:38
4b.151,4b.153	Static longitudinal stability	Approach	Up	15	TR	28-30	9:21
4b.151,4b.152	Static longitudinal stability	Landing	Down	25	Idle	36-38	5:08
4b.131	Long. control, flap extension	-	Down	-	Idle	127	0:56
	Long. control, flap retraction	-	Down	-	TO	128	0:50
	Long. control, gear extension	-	-	0	TR	129	1:23
	Long. control, thrust application	-	Down	25	-	130	0:45
	Long. control, flap retraction and thrust application	-	Down	-	-	131,132	2:16
4b.132	Directional control	-	Up	15	TR(OEI)	39,41	3:18
4b.132	Lateral control	-	Up	0	MCT(OEI)	42	1:54
4b.130	Long. maneuvering	Climb	Up	0	MCT	43	3:03
4b.130	Long. maneuvering	Cruise	Up	0	TR	44,45	3:50
4b.156	Dynamic long. stability	Climb	Up	0	MCT	133	3:19
4b.156	Dynamic long. stability	Cruise	Up	0	TR	134-136	7:02
4b.156	Dynamic long. stability	Approach	Up	15	TR	137	2:56
4b.157	Static direct. and lateral stability	Cruise	Up	0	TR	46-51	13:45

TABLE 4.- CERTIFICATION TEST PROGRAM - Continued

Baseline Model 75A Test Conditions

Requirement paragraph	Description of test	Config.	Gear	Flaps, deg	Thrust	Run numbers	Duration min:sec
4b.157	Static direct. and lateral stability	Approach	Up	15	TR	52	2:18
4b.157	Static direct. and lateral stability	Landing	Down	25	TR	53	2:11
4b.158	Dynamic direct. and lateral stability	Cruise	Up	0	TR	139,141,142,145	12:10
↓	Dynamic direct. and lateral stability	Loiter	Up	0	TR	146	3:39
↓	Dynamic direct. and lateral stability	Approach	Up	15	TR	143	1:35
↓	Dynamic direct. and lateral stability	Landing	Down	25	TR	144	1:15
4b.132(e)	Roll rate response	Climb	Up	0	MCT	147	4:30
↓	Roll rate response	Cruise	Up	0	TR	148	1:29
↓	Roll rate response	Approach	Up	15	TR	149	1:32
↓	Roll rate response	Landing	Down	25	TR	150	1:46
4b.133	Minimum control speed	Takeoff	Up	15	TO	54,55,158-161	12:10
4b.320	Long. out-of-trim control	Landing	Down	25	TR	151-153,155-157	19:42
4b.173	Crosswind landing	Landing	Down	25	TR	190-193	7:56
Derivative Model 75B Test Conditions							
25.161	Longitudinal trim	Cruise	Up	0	TR	179	3:36
↓	Longitudinal trim	Landing	Down	25	TR	180	3:20
↓	Long., direct. and lateral trim	Cruise	Up	0	MCT(OEI)	163	6:14
25.173,25.175	Static long. stability	Climb	Up	0	MCT	71-76	12:24
↓	Static long. stability	Cruise	Up	0	TR	77,78	5:04
↓	Static long. stability	Approach	Up	15	TR	79,80	4:01
↓	Static long. stability	Landing	Down	25	TR	81-83	5:13
25.145	Long. control, flap extension	-	Down	-	TR	164	1:20
25.145	Long. control, thrust application	-	Down	25	TR	165,166	2:42

TABLE 4.- CERTIFICATION TEST PROGRAM - Continued

Derivative Model 75B Test Conditions

Requirement paragraph	Description of test	Config.	Gear	Flaps, deg	Thrust	Run numbers	Duration min:sec
25.145	Long. control, flap retraction and thrust application	-	Down	-	TR	167-169	1:45
25.143	Longitudinal maneuvering	Climb	Up	0	MCT	67,68	2:40
25.143	Longitudinal maneuvering	Cruise	Up	0	TR	69,70	4:11
25.181	Dynamic long. stability	Climb	Up	0	MCT	114	4:29
25.181	Dynamic long. stability	Cruise	Up	0	TR	115,116	11:54
25.181	Dynamic long. stability	Approach	Up	15	TR	117	3:43
25.177	Static direct. and lateral stability	Cruise	Up	0	TR	59-63	20:00
25.177	Static direct. and lateral stability	Approach	Up	15	TR	64,65	3:53
25.177	Static direct. and lateral stability	Landing	Down	25	TR	66	1:46
25.181	Dynamic direct. and lateral stability	Cruise	Up	0	TR	170-173,177	8:18
	Dynamic direct. and lateral stability	Loiter	Up	0	TR	178	1:39
	Dynamic direct. and lateral stability	Approach	Up	15	TR	175	1:30
	Dynamic direct. and lateral stability	Landing	Down	25	TR	176	1:46
25.147(e)	Roll rate response	Climb	Up	0	MCT	118-120	5:11
	Roll rate response	Cruise	Up	0	TR	121,122,185,186	10:16
	Roll rate response	Approach	Up	15	TR	123	1:40
	Roll rate response	Landing	Down	25	TR	124	1:09
25.149	Minimum control speed	Takeoff	Up	15	TO	103-113	18:25
25.237	Crosswind landing	Landing	Down	25	TR	181-184	7:46

TABLE 4.- CERTIFICATION TEST PROGRAM - Concluded

Test Conditions for Model 75B with Modified Flight Control System

Requirement paragraph	Description of test	Config.	Gear	Flaps, deg	Thrust	Run numbers	Duration min:sec
25.173,25.175	Static long. stability	Climb	Up	0	MCT	89-94	13:07
25.173,25.175	Static long. stability	Cruise	Up	0	TR	86,88	23:10
25.173,25.175	Static long. stability	Landing	Down	25	TR	84,85,99	15:42
25.143	Longitudinal maneuvering	Climb	Up	0	MCT	95	1:45
25.143	Longitudinal maneuvering	Cruise	Up	0	TR	97,98	3:47
Special cond.	Long. out-of-trim control	Landing	Down	25	TR	100-102	7:29

TABLE 5.- VERIFIED MODEL 75A AERODYNAMIC CHARACTERISTICS

Loading: gross weight 22 000 lb, center of gravity 0.25 $\bar{c}$
Inertias, slugs-ft^2: I_x 26 300, I_y 52 600, I_z 75 000, I_{xz} 1750
Geometry: span 44.4 ft, chord 8.4 ft, wing area 342 ft^2

Characteristic	Case 1[a]		Case 2		Case 3		Case 4		Case 5	
	Σ8[b]	RI[b]	Σ8	RI	Σ8	RI	Σ8	RI	Σ8	RI
Trim Conditions										
Altitude, ft	95	0	10 000	10 000	20 000	20 000	20 000	20 000	30 000	30 000
Calibrated airspeed, knots	133	133	222	222	275	275	324	324	304	304
Mach number	0.20	0.20	0.40	0.40	0.60	0.60	0.70	0.70	0.80	0.80
Angle of attack, deg	9.60	10.71	5.40	5.43	3.59	3.58	2.70	2.58	2.90	2.79
Thrust, lb	2796	3150	1759	1837	2117	2171	2617	2659	2622	2516
Stabilizer defl., deg	-6.48	-6.01	-3.63	-3.39	-2.82	-2.58	-2.30	-2.02	-2.50	-2.26
Elevator defl., deg	-2.90	-1.98	0.18	0.19	0.44	0.41	0.46	0.44	0.46	0.43
Longitudinal Mode Analysis										
Phugoid, period, sec	36		63		83		90		175	
Phugoid, freq., rad/sec	0.176		0.100		0.076		0.070		0.036	
Phugoid, damping ratio	0.085		0.071		0.079		0.090		0.384	
Short period, period, sec	3.1	3.1	1.8	2.1	1.5	1.5	1.2	1.2	1.3	1.3
Short period, freq., rad/sec	2.06	2.04	3.42	3.04	4.29	4.30	5.10	5.10	4.90	4.80
Short period, damping ratio	0.504	0.502	0.440	0.490	0.381	0.380	0.390	0.390	0.333	0.330
Lateral Mode Analysis										
Spiral, sec to 1/2 ampl. or sec to 2x ampl.	25	92	181	258	286	549	180	2512	189	878
Roll, sec to 1/2 ampl.	0.43	0.44	0.31	0.31	0.29	0.29	0.24	0.24	0.31	0.31
Dutch roll, period, sec	4.8	4.9	3.2	3.2	2.6	2.5	2.0	2.2	2.3	2.3
Dutch roll, freq., rad/sec	1.32	1.28	1.99	1.99	2.43	2.47	3.16	2.91	2.72	2.74
Dutch roll, damping ratio	0.144	0.160	0.145	0.143	0.125	0.116	0.115	0.126	0.108	0.108

[a]Case 1 configuration is gear down, flaps 25°; all other cases are gear up, flaps up.
[b]Column headed Σ8 lists Sigma 8 computer results; column headed RI lists Rockwell International results.

TABLE 6.- VERIFIED MODEL 75B AERODYNAMIC CHARACTERISTICS

Loading: gross weight 20 225 lb, center of gravity 0.25 $\bar{c}$
Inertias, slugs-ft^2: I_x 14 989, I_y 74 295, I_z 84 109, I_{xz} 0
Geometry: span 44.4 ft, chord 8.4 ft, wing area 342 ft^2

Characteristic	Case 1[a]		Case 2		Case 3		Case 4		Case 5	
	Σ8[b]	RI[b]	Σ8	RI	Σ8	RI	Σ8	RI	Σ8	RI
Trim Conditions										
Altitude, ft	95	0	10 000	10 000	20 000	20 000	20 000	20 000	30 000	30 000
Calibrated airpseed, knots	133	133	222	222	275	275	324	324	304	304
Mach number	0.20	0.20	0.40	0.40	0.60	0.60	0.70	0.70	0.80	0.80
Angle of attack, deg	9.08	9.49	5.53	5.53	3.84	3.83	2.96	2.95	3.07	2.87
Thrust, lb	2620		1800		2253		2851		2781	
Stabilizer defl., deg	-6.17		-3.18		-2.54		-2.14		-2.44	
Elevator defl., deg	-2.51		0.38		0.52		0.50		0.48	
Longitudinal Mode Analysis										
Phugoid, period, sec	36		62		86		101		143	
Phugoid, freq., rad/sec	0.175		0.102		0.073		0.062		0.044	
Phugoid, damping ratio	0.081		0.077		0.098		0.112		0.408	
Short period, period, sec	4.1		2.5		2.0		1.6		1.7	
Short period, freq., rad/sec	1.54		2.55		3.20		3.86		3.79	
Short period, damping ratio	0.526		0.460		0.400		0.406		0.347	
Lateral Mode Analysis										
Spiral, sec to 1/2 ampl. or sec to 2x ampl.	29	40	256	71	365	145	196	260	220	496
Roll, sec to 1/2 ampl.	0.26	0.30	0.18	0.18	0.17	0.17	0.14	0.14	0.18	0.18
Dutch roll, period, sec	4.9	5.0	3.3	3.3	2.7	2.7	2.1	2.3	2.4	2.4
Dutch roll, freq., rad/sec	1.29	1.26	1.91	1.90	2.33	2.34	3.01	2.76	2.60	2.61
Dutch roll, damping ratio	0.217	0.216	0.191	0.195	0.160	0.162	0.139	0.153	0.137	0.133

[a]Case 1 configuration is gear down, flaps 25°; all other cases are gear up, flaps up.
[b]Column headed Σ8 lists Sigma 8 computer results; column headed RI lists Rockwell International results.

TABLE 7.- MANEUVERING FLIGHT CHARACTERISITCS

MODEL 75A AND MODEL 75B

Model	Config.	Flight condition			Loading		F_c/n_z, lb/g	n_z/δ_e, g/deg	n_z/α g/rad
		Airspeed, knots	Mach no.	Altitude, ft	GW, lb	CG			
75A	Climb	252	0.47	10 000	22 800	0.37 $\bar{c}$	31	0.44	19.0
75A	Cruise	327	0.70	20 000	22 000	0.37 $\bar{c}$	31	0.67	28.6
75A	Cruise	227	0.73	40 000	22 000	0.37 $\bar{c}$	31	0.35	13.7
75B	Climb	256	0.48	10 000	28 000	0.345 $\bar{c}$	27	0.39	14.3
75B	Cruise	328	0.70	20 000	27 000	0.345 $\bar{c}$	27	0.56	22.9
75B	Cruise	200	0.66	40 000	27 000	0.345 $\bar{c}$	27	0.21	7.7

TABLE 8.- CONTROL LOADER SYSTEM CHARACTERISTICS

Characteristic	Axis		
	Column	Wheel, 17.8 cm (7 in.) radius	Pedals
Maximum total travel, mechanical stops	35.6 cm (14 in.)	±105°	±8.3 cm (±3.25 in.)
Maximum control force or control torque	±667 N (±150 lb)	±7909 cm-N (±700 in.-lb)	±890 N (±200 lb)
Threshold force or torque	0.89 N (0.2 lb)	15.8 cm-N (1.4 in.-lb)	0.89 N (0.2 lb)
Maximum control velocity	±127 cm/sec (±50 in./sec)	±350°/sec	±127 cm/sec (±50 in./sec)

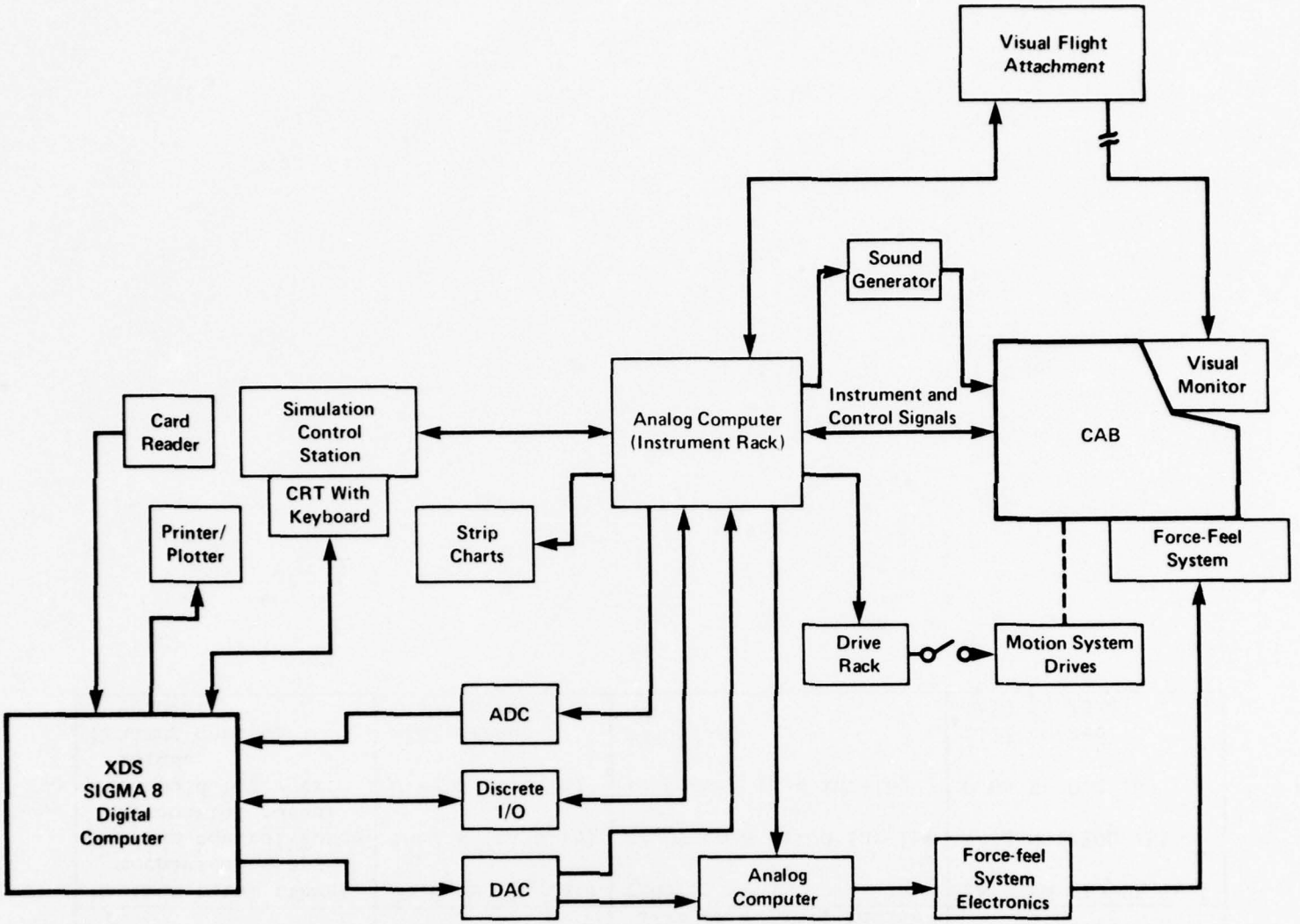

Figure 1.- Interconnection diagram of simulation systems, Flight Simulator for Advanced Aircraft.

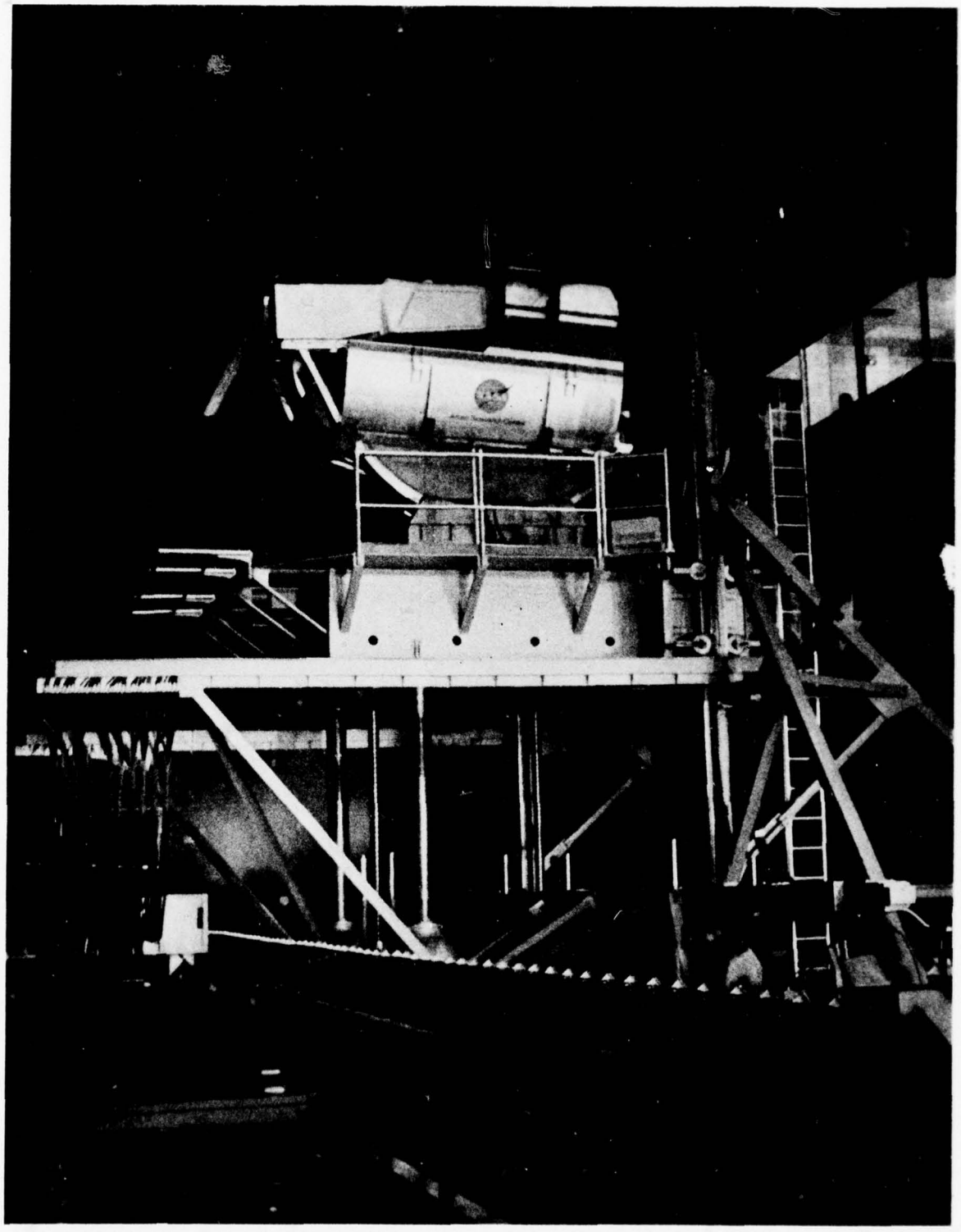

A71-1912

Figure 2.- Flight simulator cab and motion system.

Figure 3.- Cockpit layout, flight instruments, and controls. 613

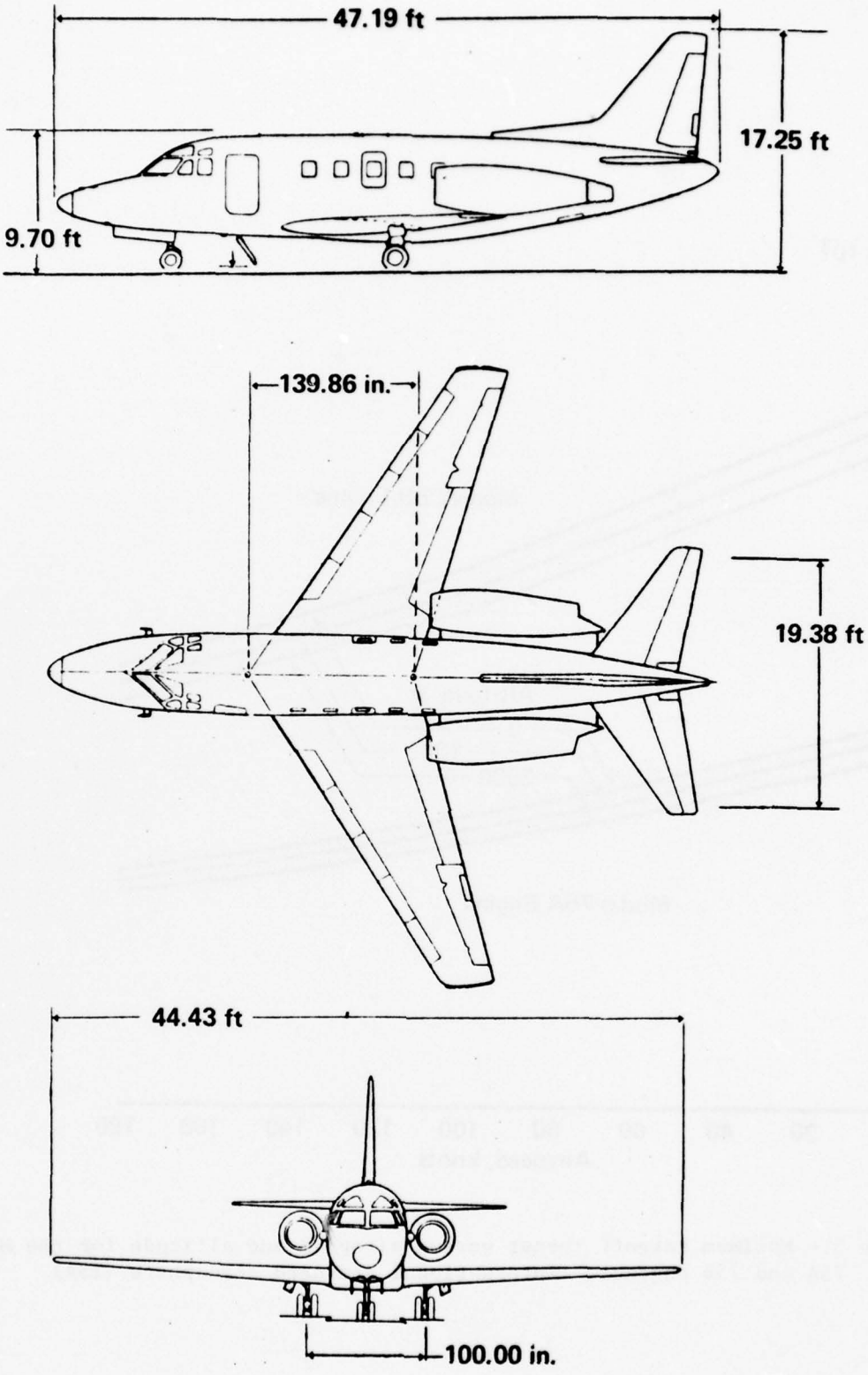

Figure 4.- Three-view drawing of the Sabreliner 75A airplane.

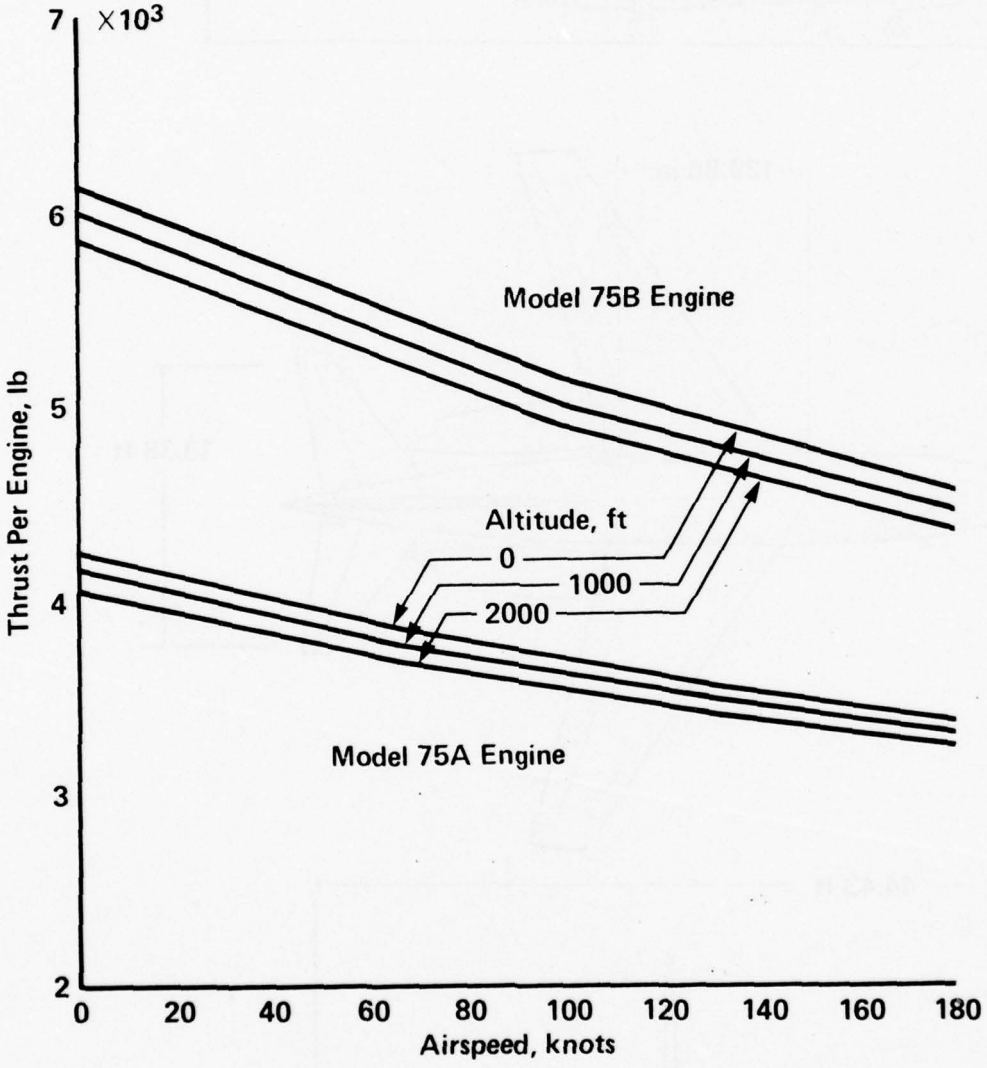

Figure 5.- Maximum takeoff thrust versus airspeed and altitude for the Model 75A and 75B engines. International Standard Atmosphere (ISA).

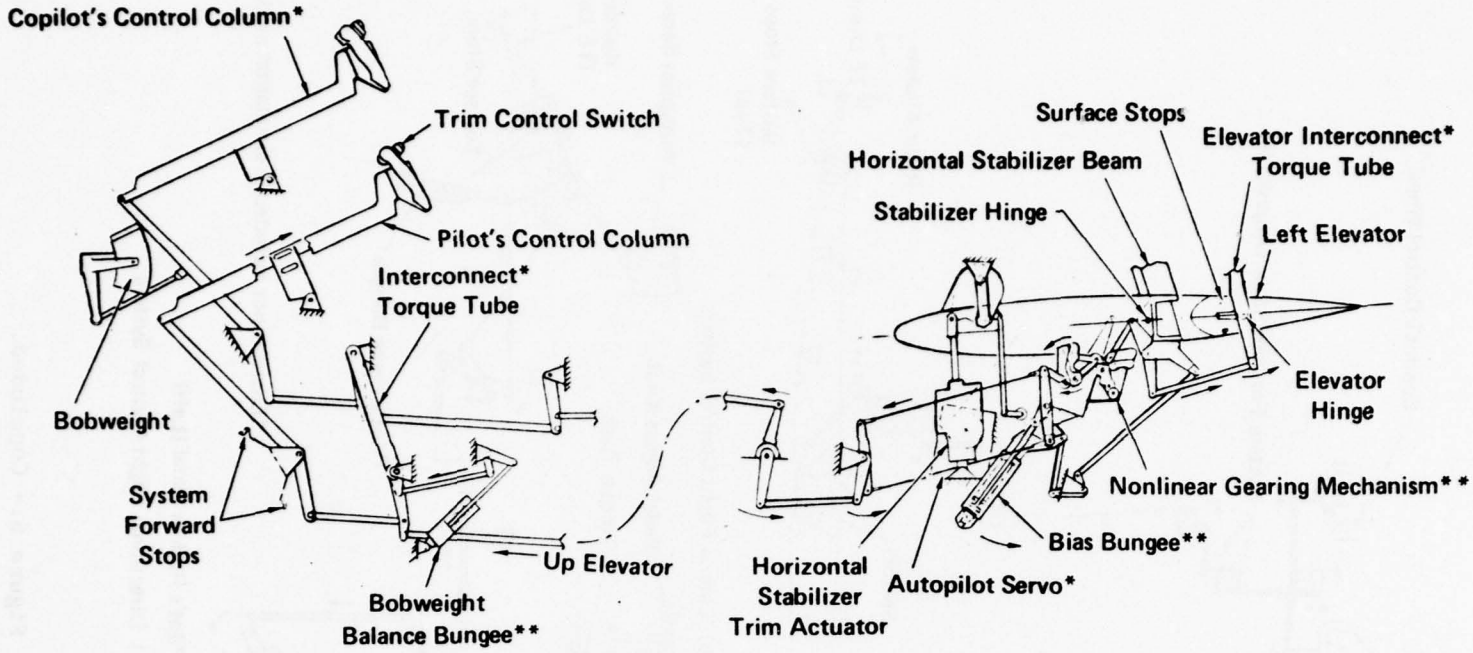

*This element not included in simulation models.
**This element not included in Model 75B with modified flight control system.

(a) Longitudinal Flight Control System.

Figure 6.- Schematic of the Sabreliner 75A flight control system.

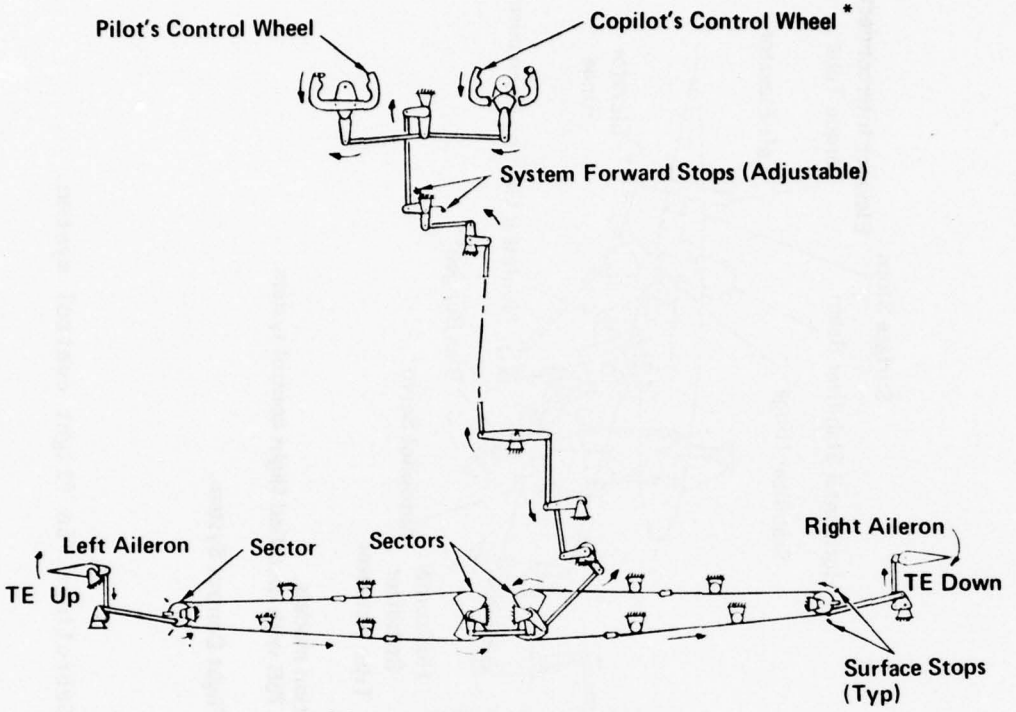

(b) Lateral Flight Control System.

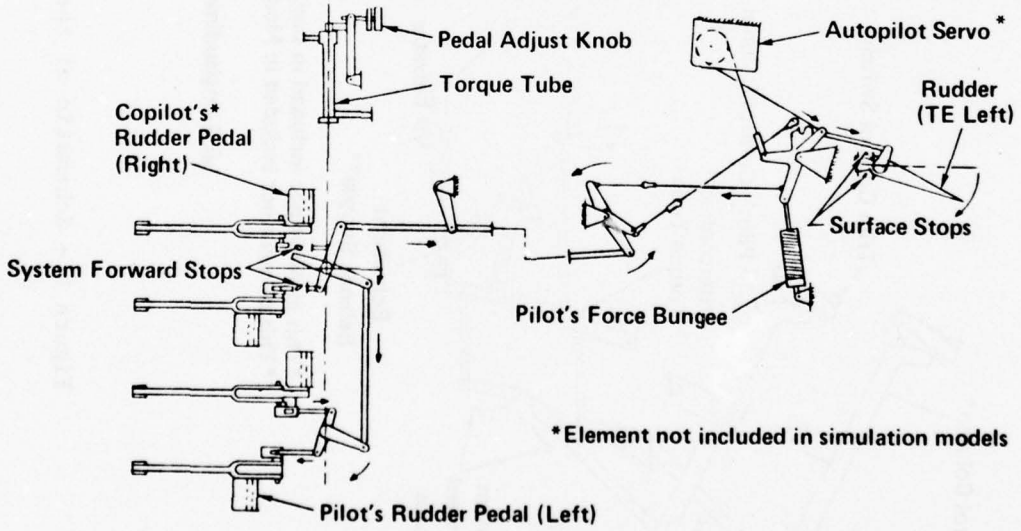

(c) Directional Flight Control System.

Figure 6.- Concluded.

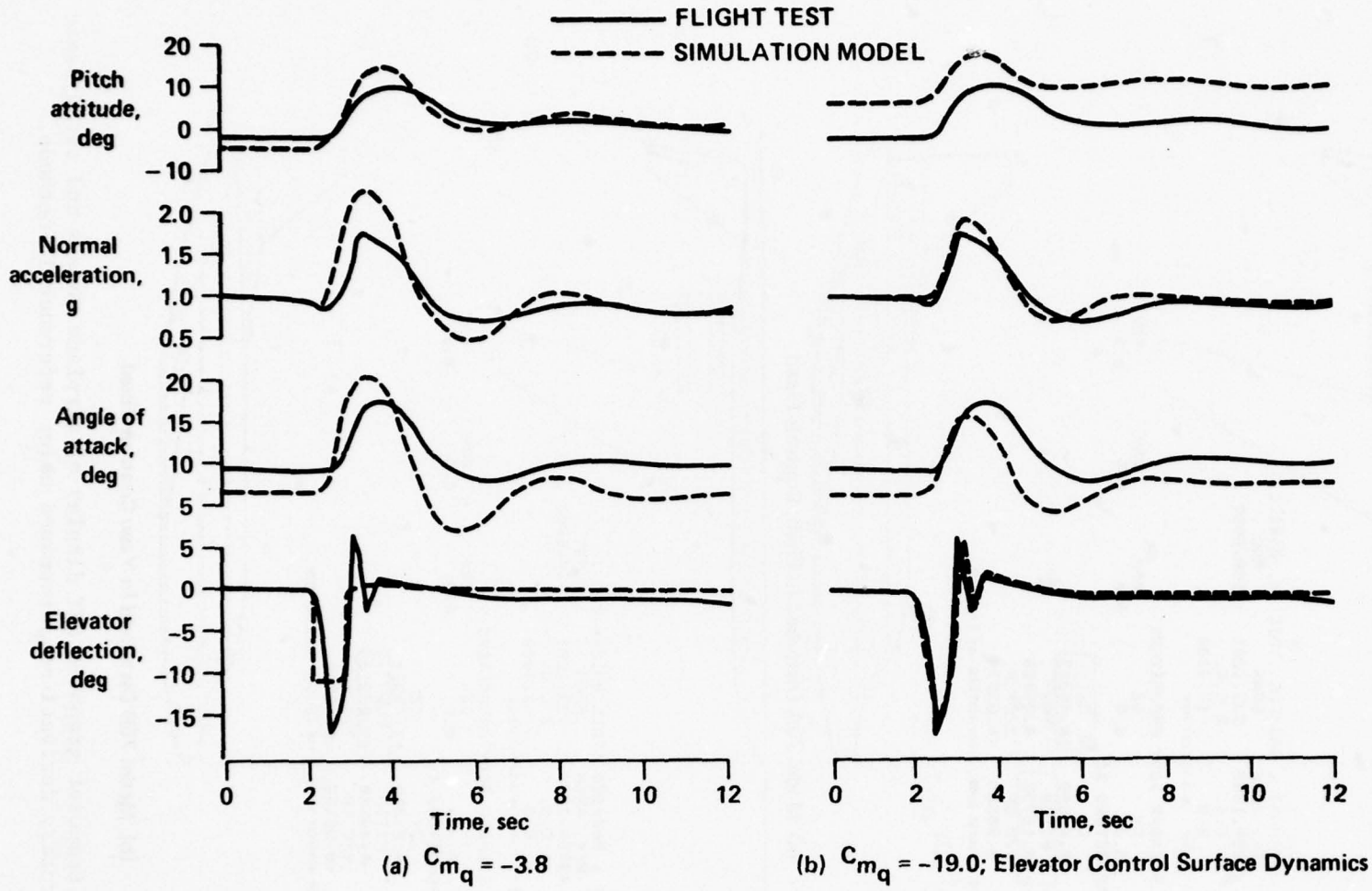

Figure 7.- Comparison of short-period pitch response to an elevator pulse for flight test and simulation model.

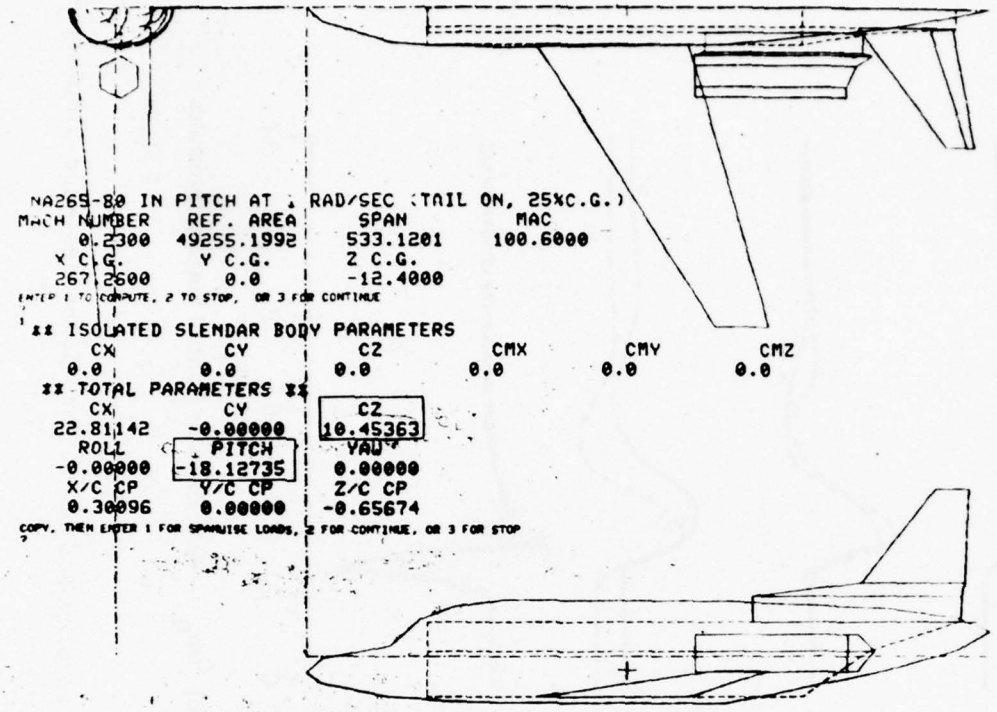

(a) Model 75A Disturbed In Pitch, Controls Fixed

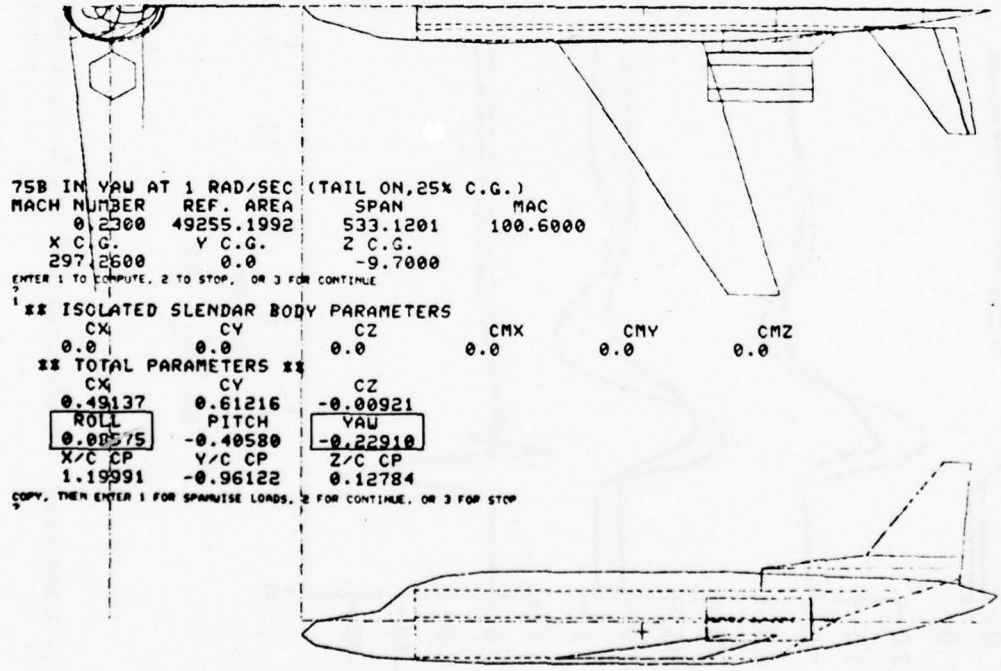

(b) Model 75B Disturbed In Yaw; Controls Fixed.

Figure 8.- Computer graphics CRT display of airplane models and aerodynamic rotary derivatives determined using reference 12 methods.

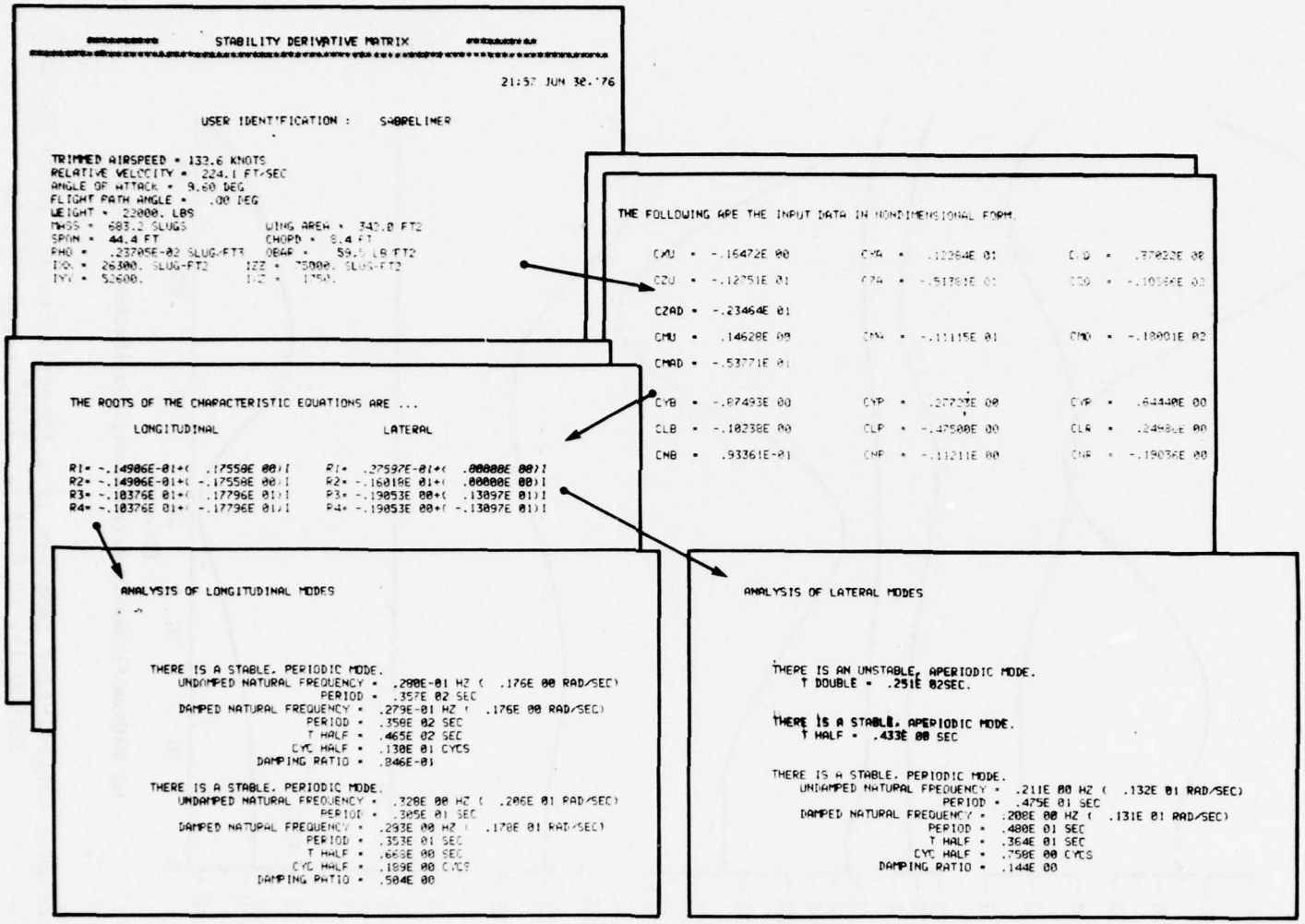

Figure 9.- Sample of stability analysis Sigma 8 computer printout; Model 75A controls fixed, Case 1 conditions, GW 22 000 lb, cg 0.25 $\bar{c}$, gear down, flaps 25°, -6.48° δ_s, -2.90° $\delta_{e_{trim}}$.

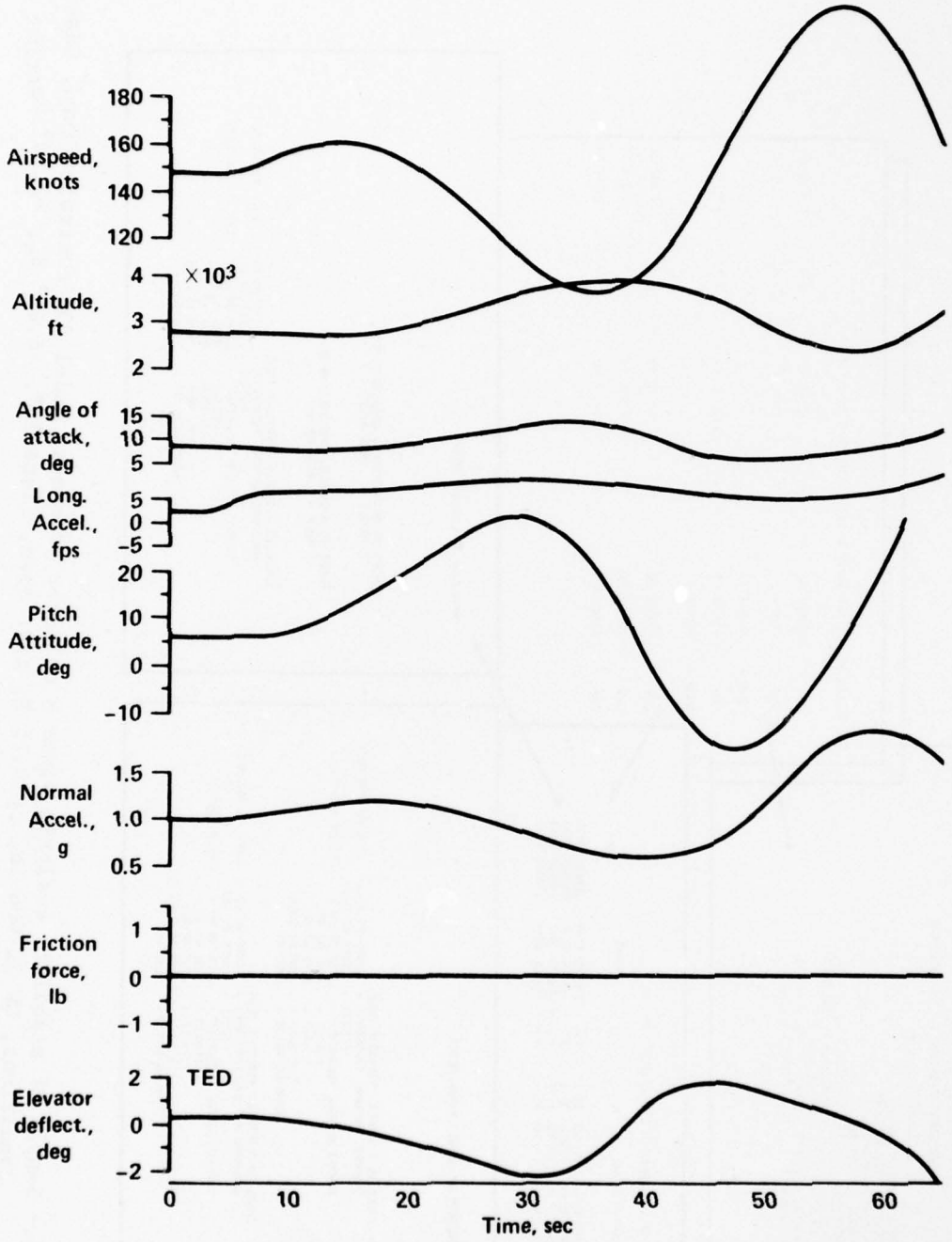

(a) Without Friction Force or Bobweight Acceleration Force.

Figure 10.- Control-free response to a throttle burst. Model 75A GW 22,000 lb, cg 0.37 $\bar{c}$, -3.74° δ_{stab}, 15° δ_f.

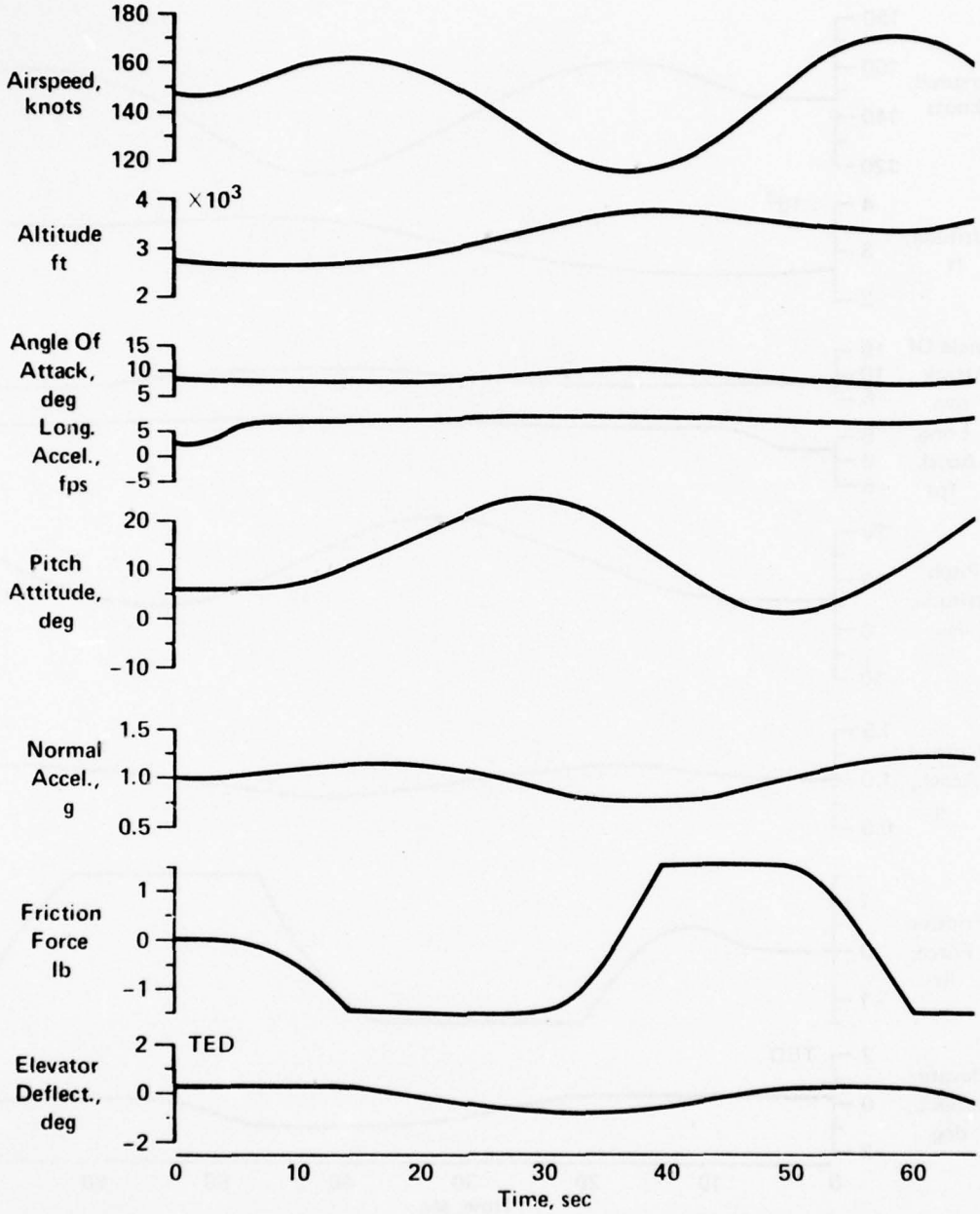

(b) With Friction Force, Without Bobweight Acceleration Force.

Figure 10.- Continued.

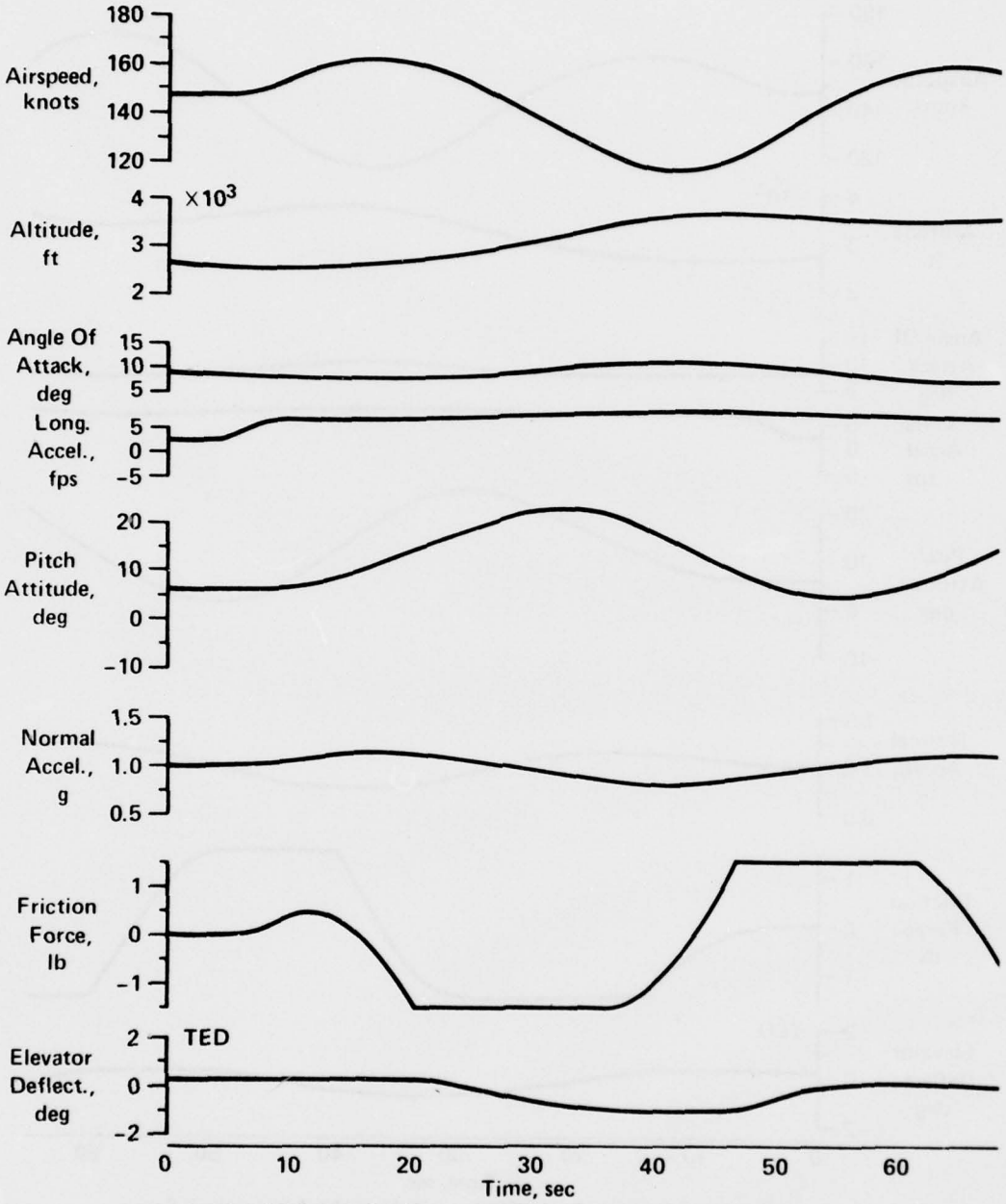

(c) With Friction Force and Bobweight Acceleration Force.

Figure 10.- Concluded.

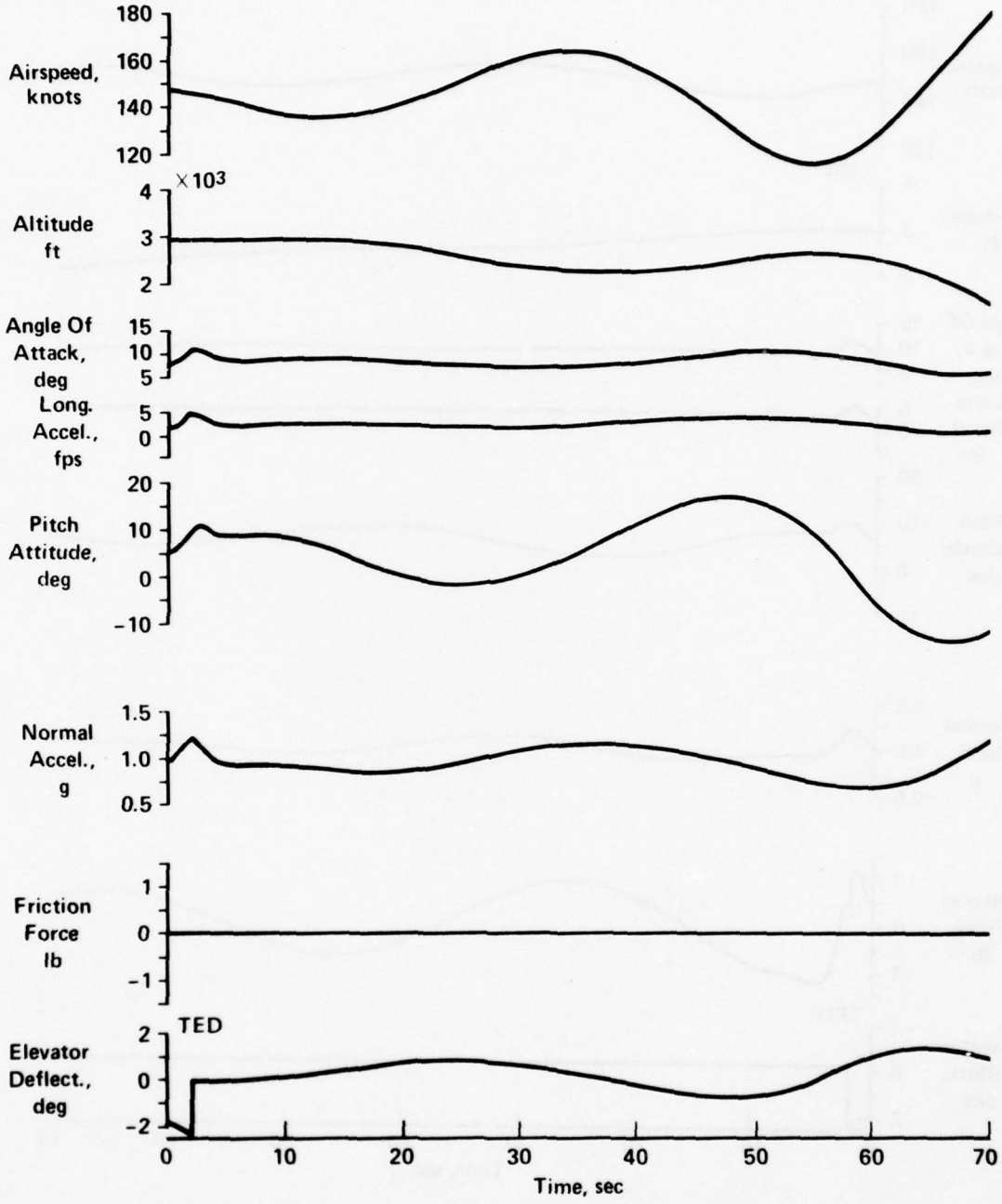

(a) Without Friction Force or Bobweight Acceleration Force.

Figure 11.- Control-free response to an elevator pulse. Model 75A GW 22 000 lb, cg 0.37 $\bar{c}$, -3.74° δ_{stab}, 15° δ_f.

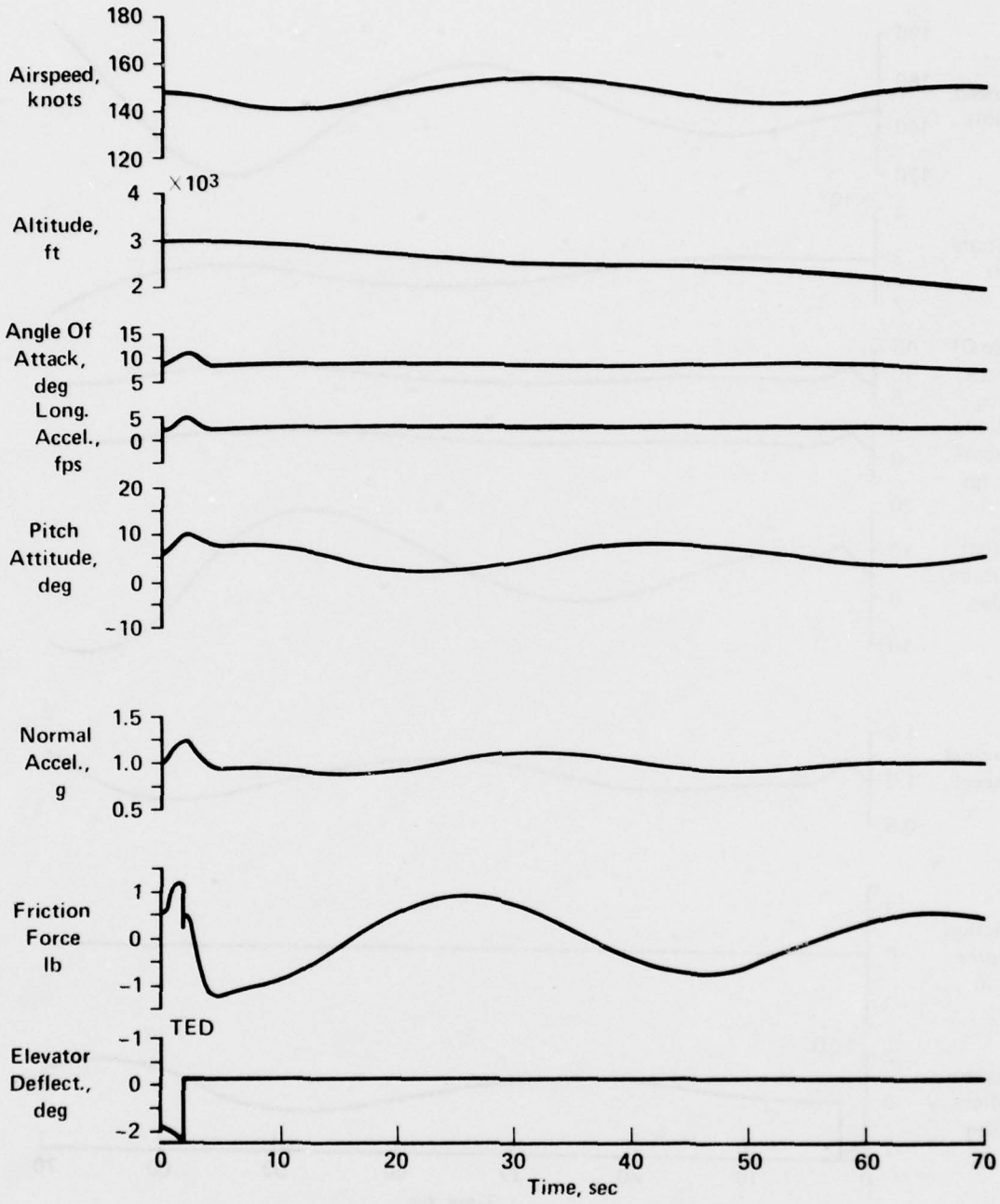

(b) With Friction Force and Bobweight Acceleration Force.

Figure 11.- Concluded.

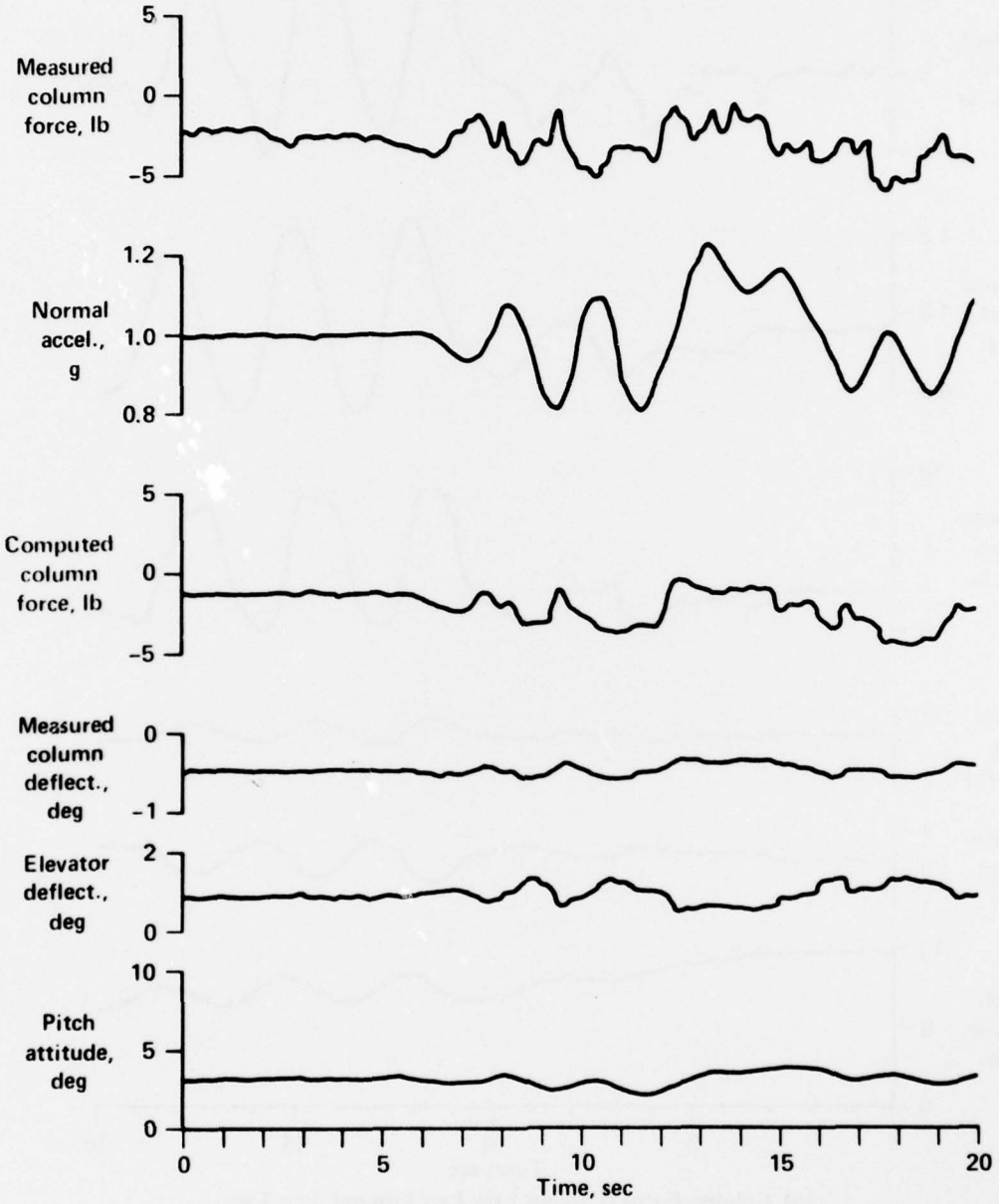

(a) Column Force Gradient Not Filtered.

Figure 12.- Pilot in-the-loop transient control characteristics.

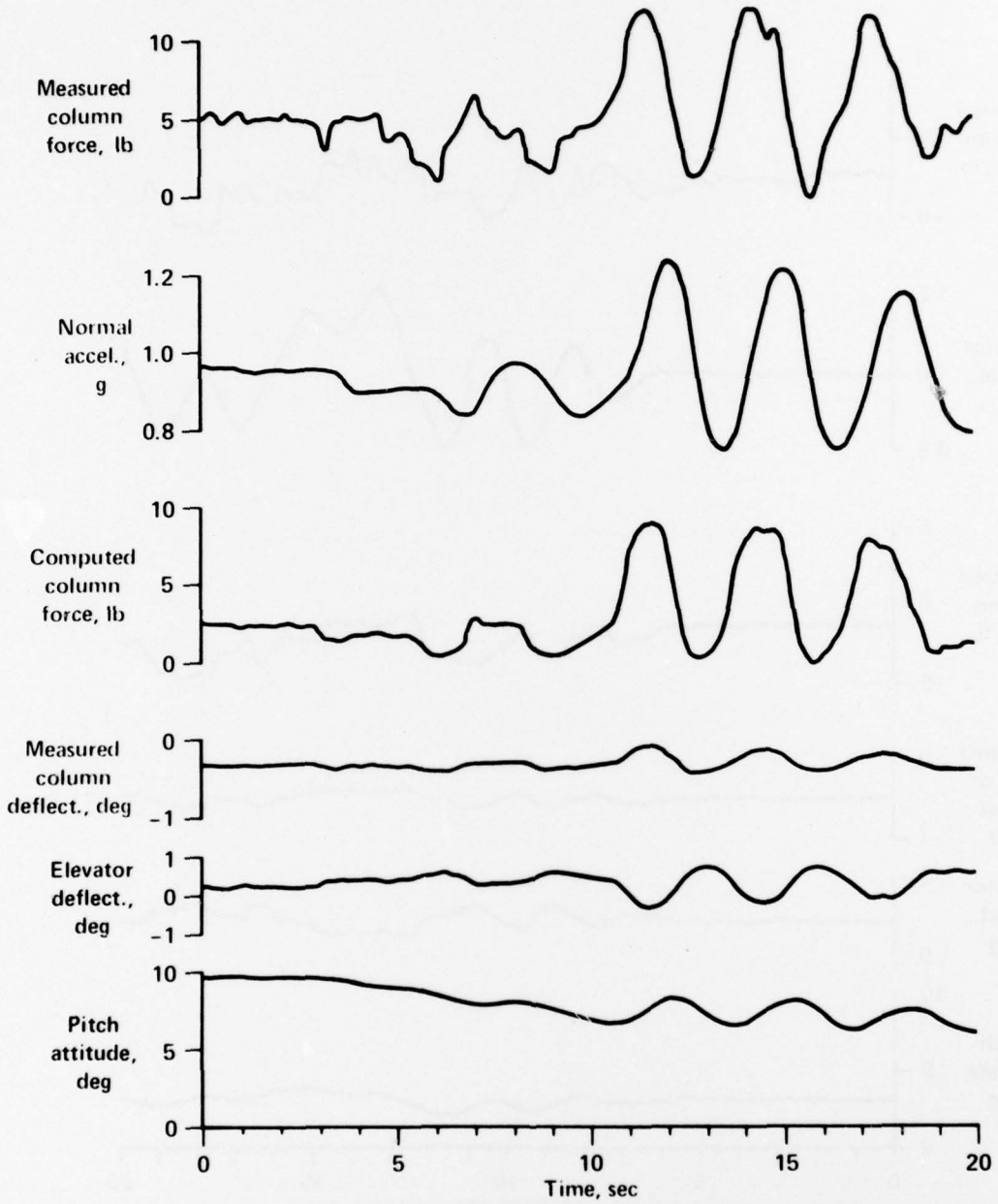

(b) Column Force Gradient Low Pass Filtered (τ = 1 sec)

Figure 12.- Concluded.

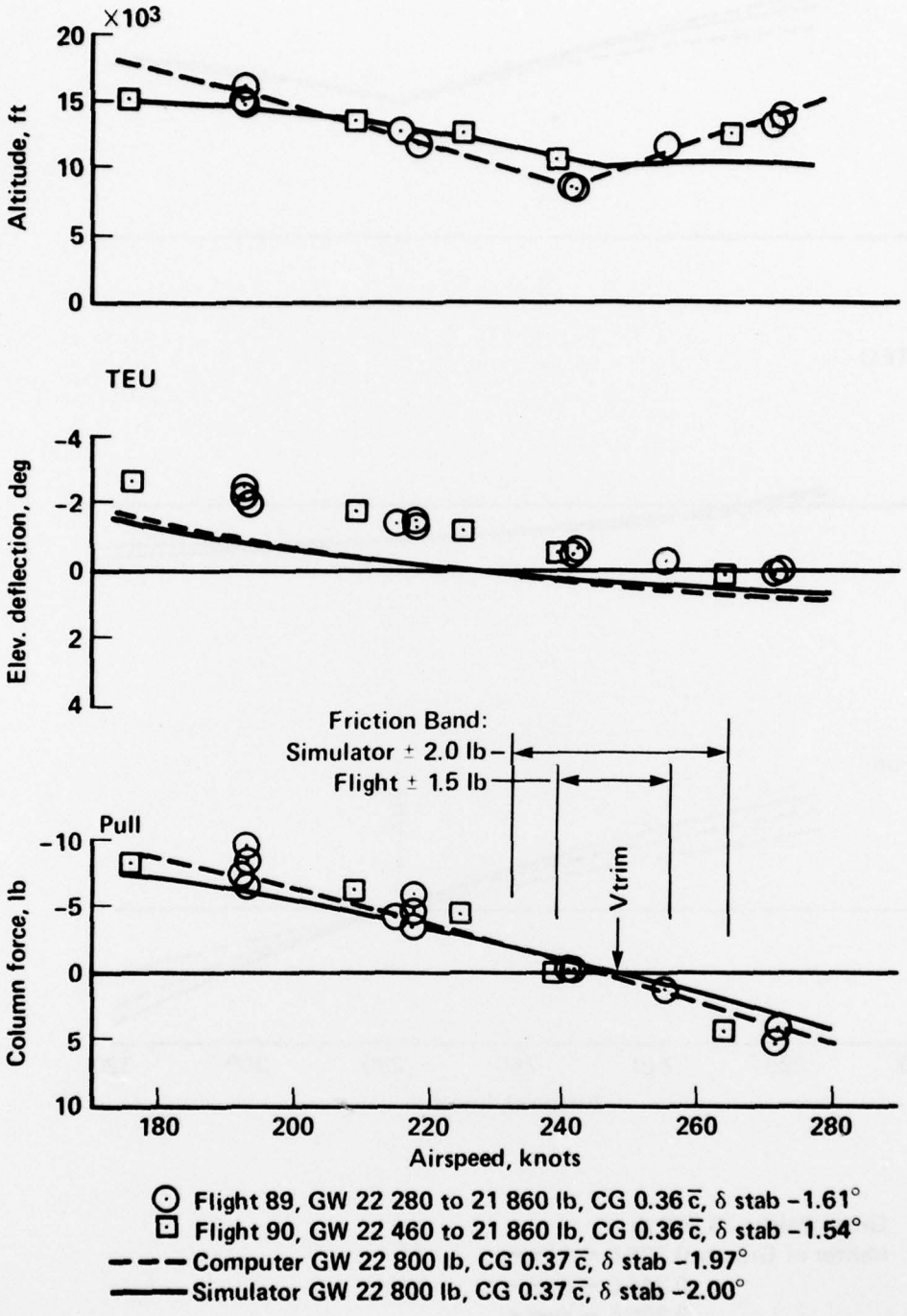

Figure 13.- Static longitudinal stability of Model 75A compared with reference 9, flight and computer results, and climb configuration.

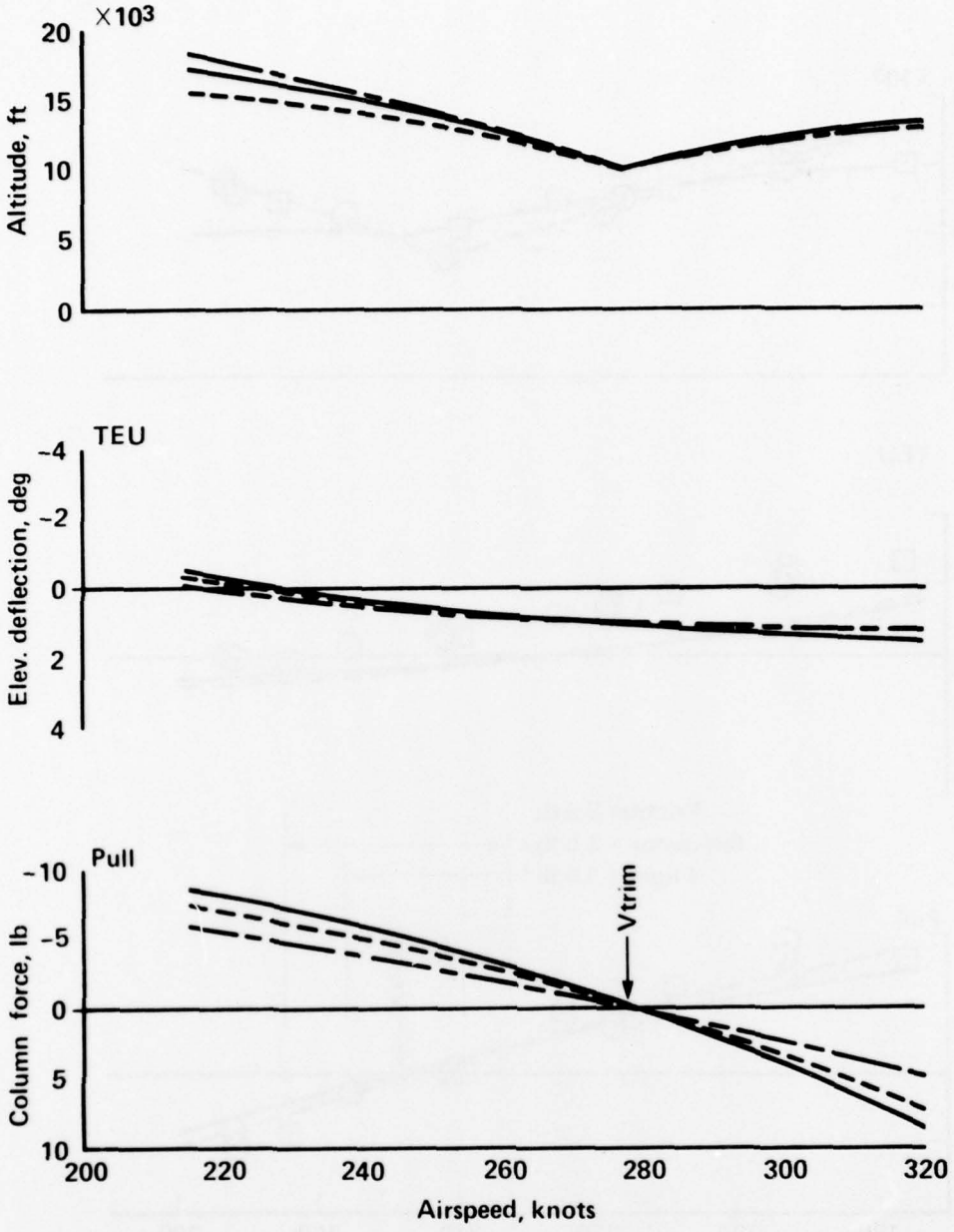

Figure 14.- Static longitudinal stability of Model 75B with modified flight control system, climb configuration.

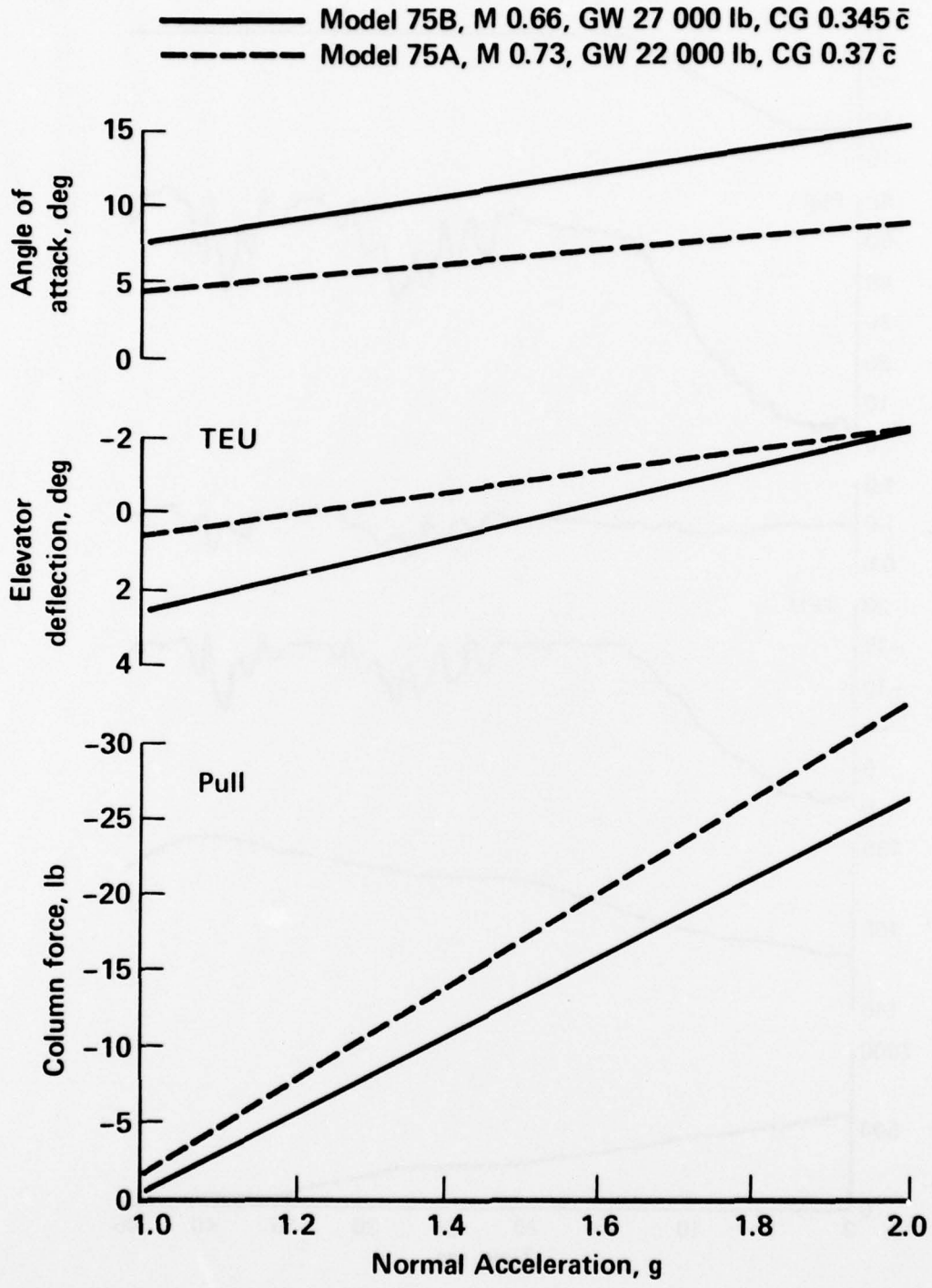

Figure 15.- Comparison of maneuvering characteristics in cruise configuration at 40,000 ft altitude.

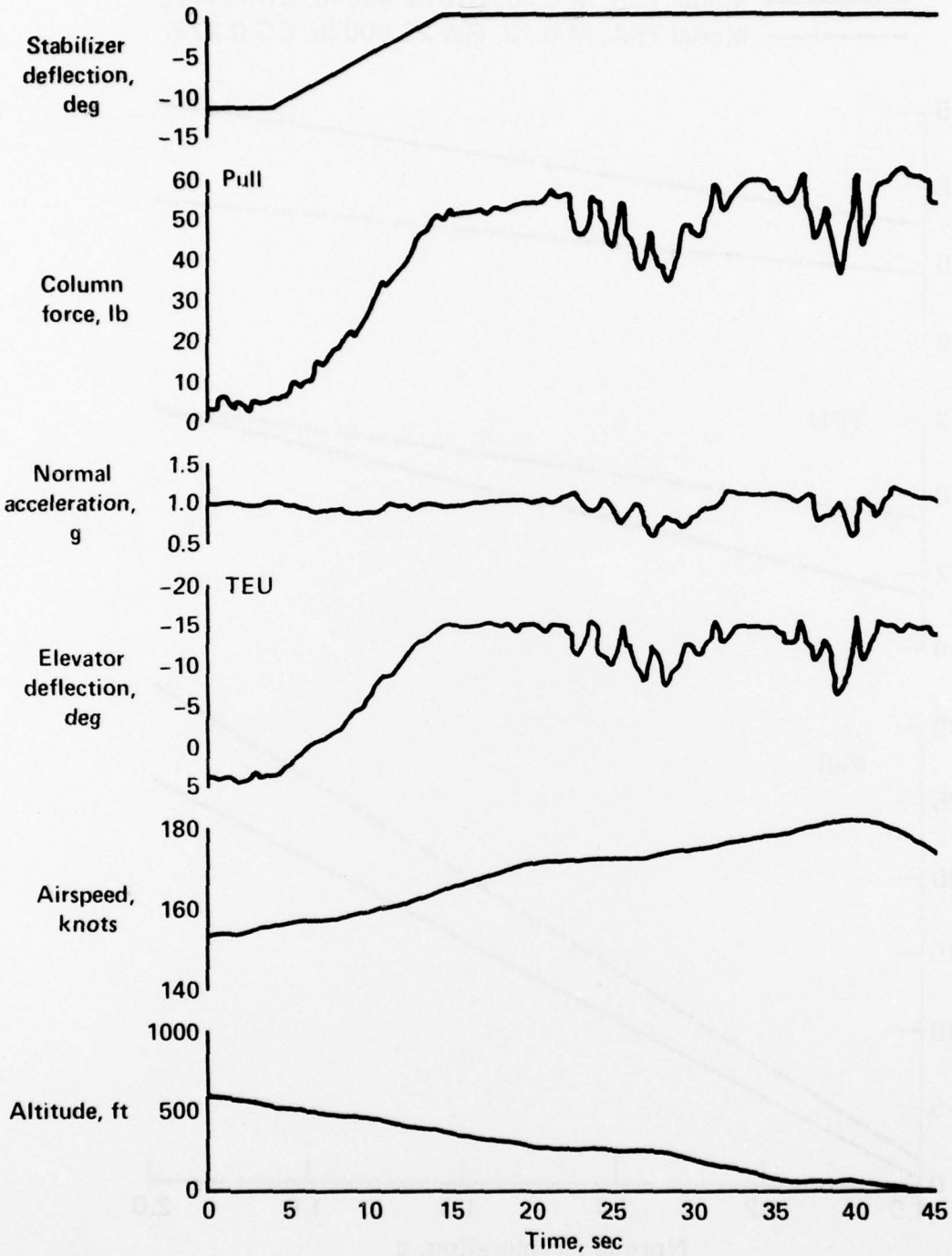

Figure 16.- Longitudinal control test with full nose-down horizontal stabilizer; Model 75B with modified flight control system. GW 25,000 lb, 0.18 $\bar{c}$, cg, gear down, flaps 25°.

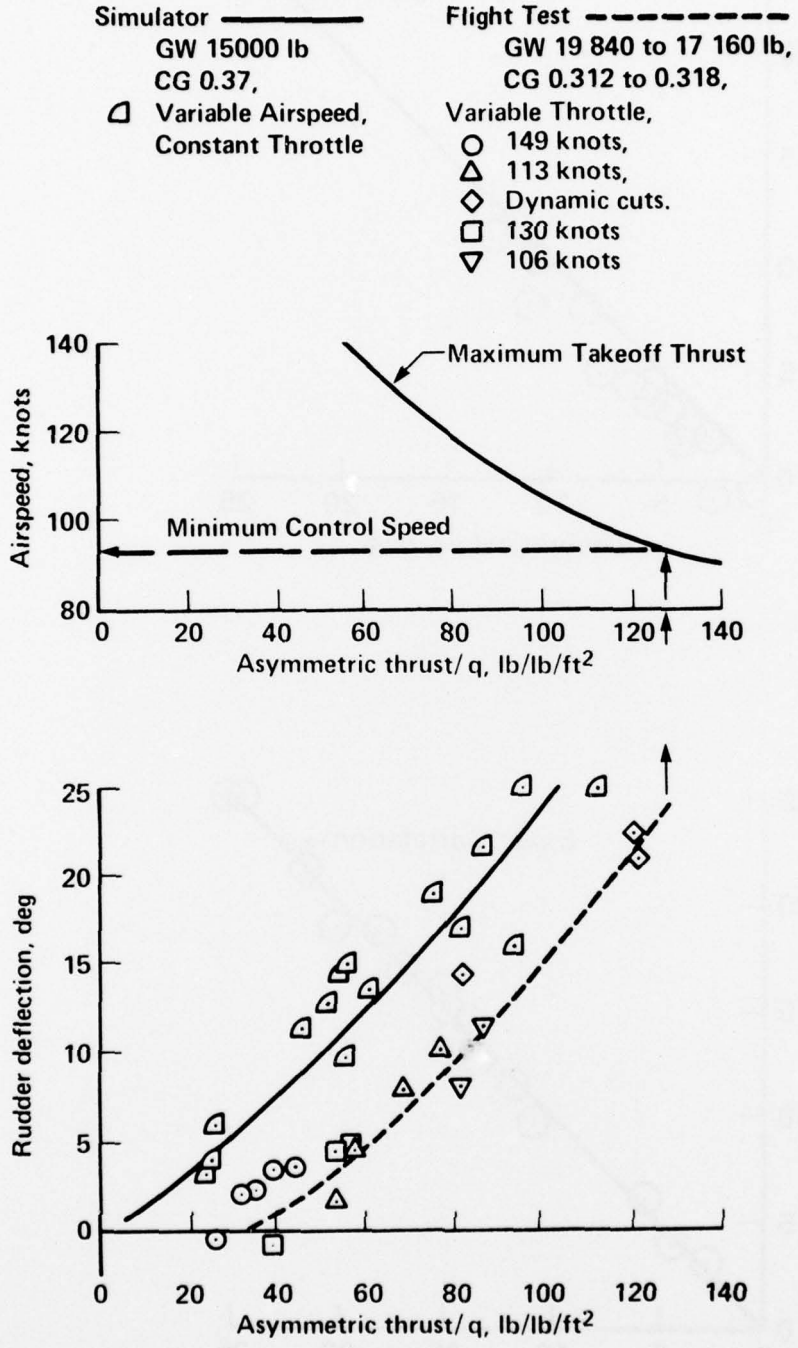

Figure 17.- Minimum control speed data from flight test (ref. 9) and the Model 75A simulation.

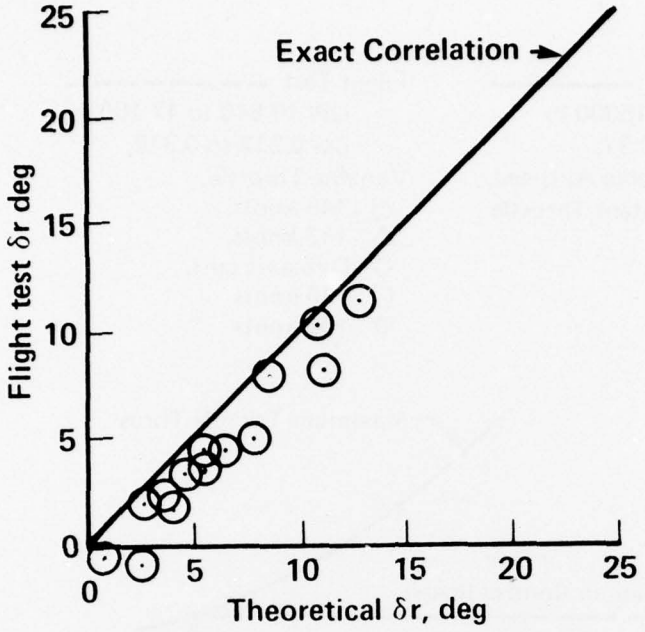

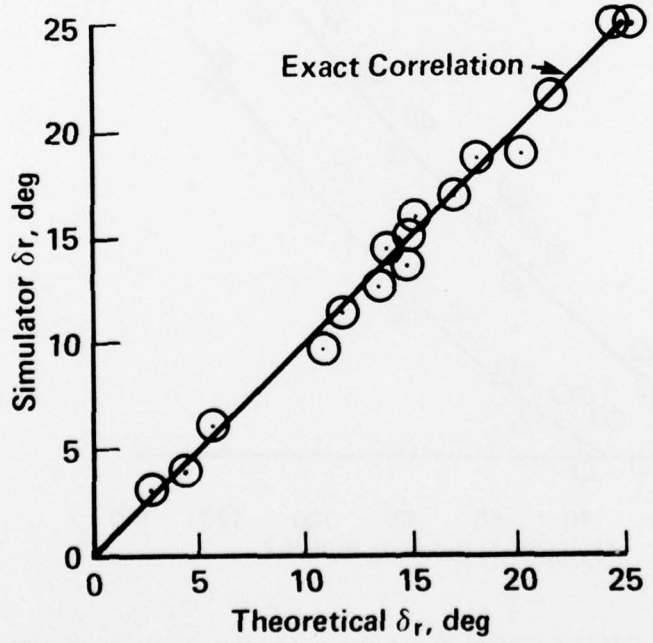

Figure 18.- Comparison of theoretical rudder deflections, δ_r, with simulator and flight test during steady-state air minimum control speed tests.

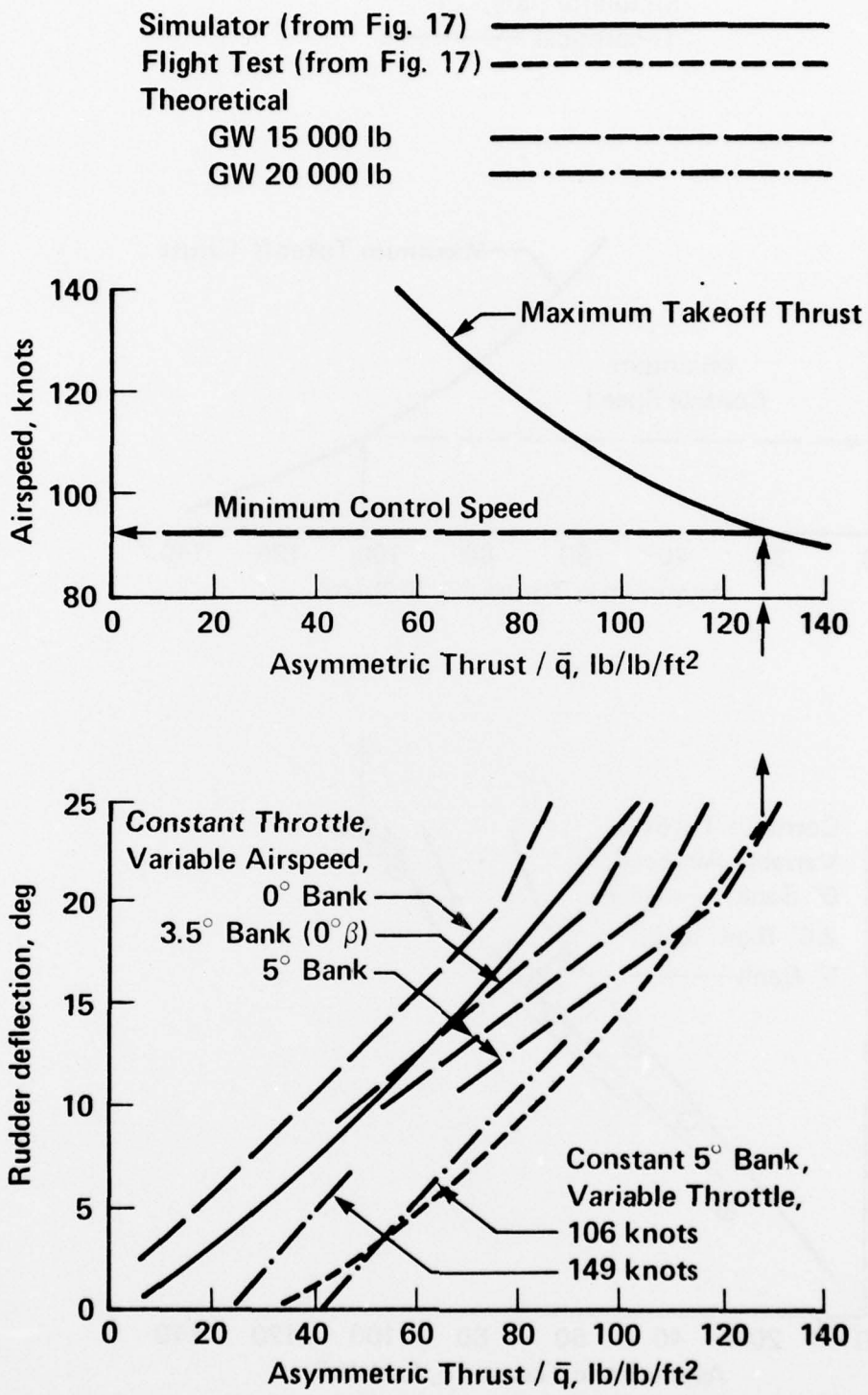

Figure 19.- Determination of minimum control speed by reference 9, steady-state flight test method compared with values for a solution of theoretical mathematical model: Model 75A.

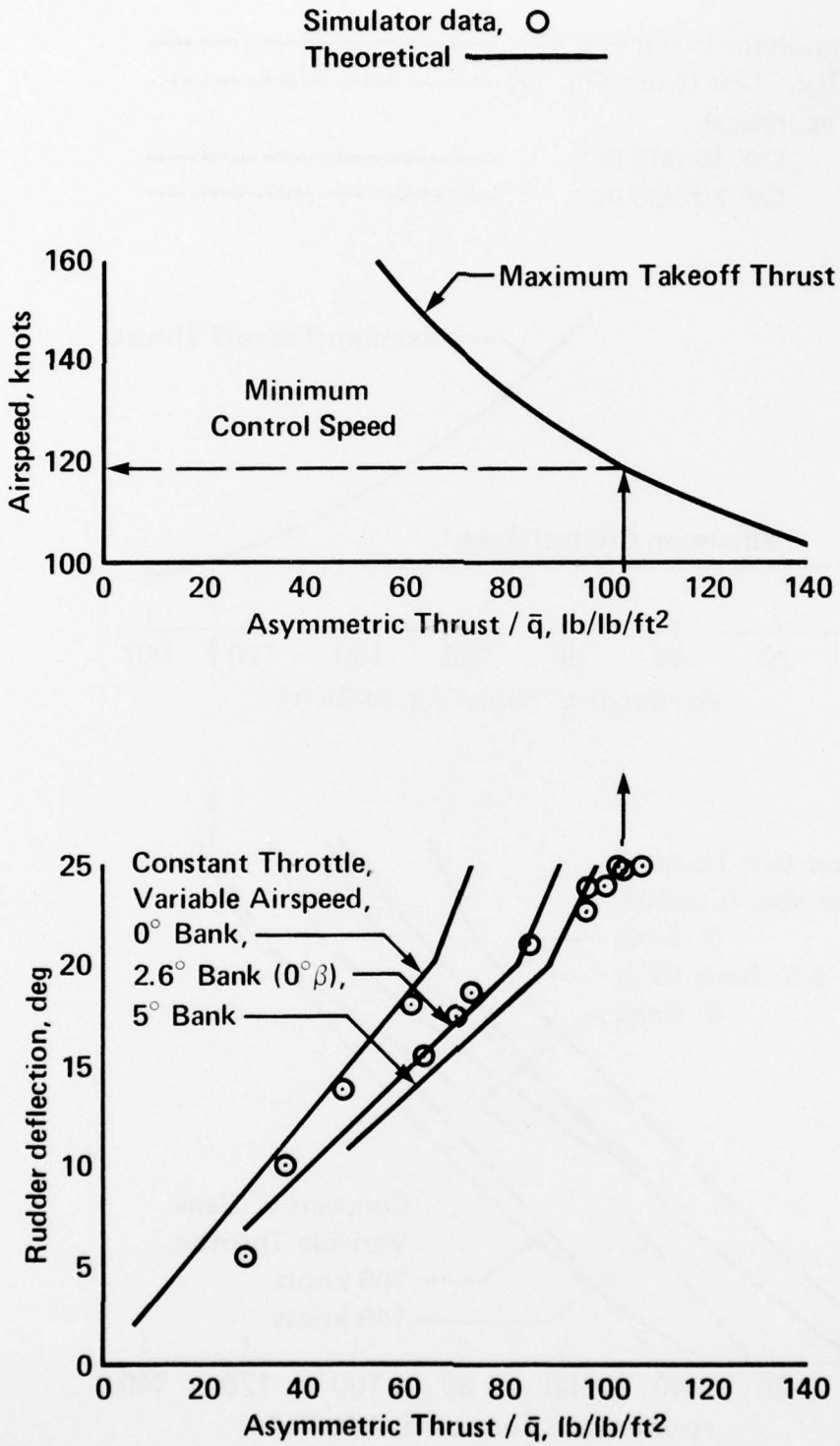

Figure 20.- Determination of minimum control speed by reference 9, steady-state flight test method compared with values from a solution of theoretical mathematical model: Model 75B.

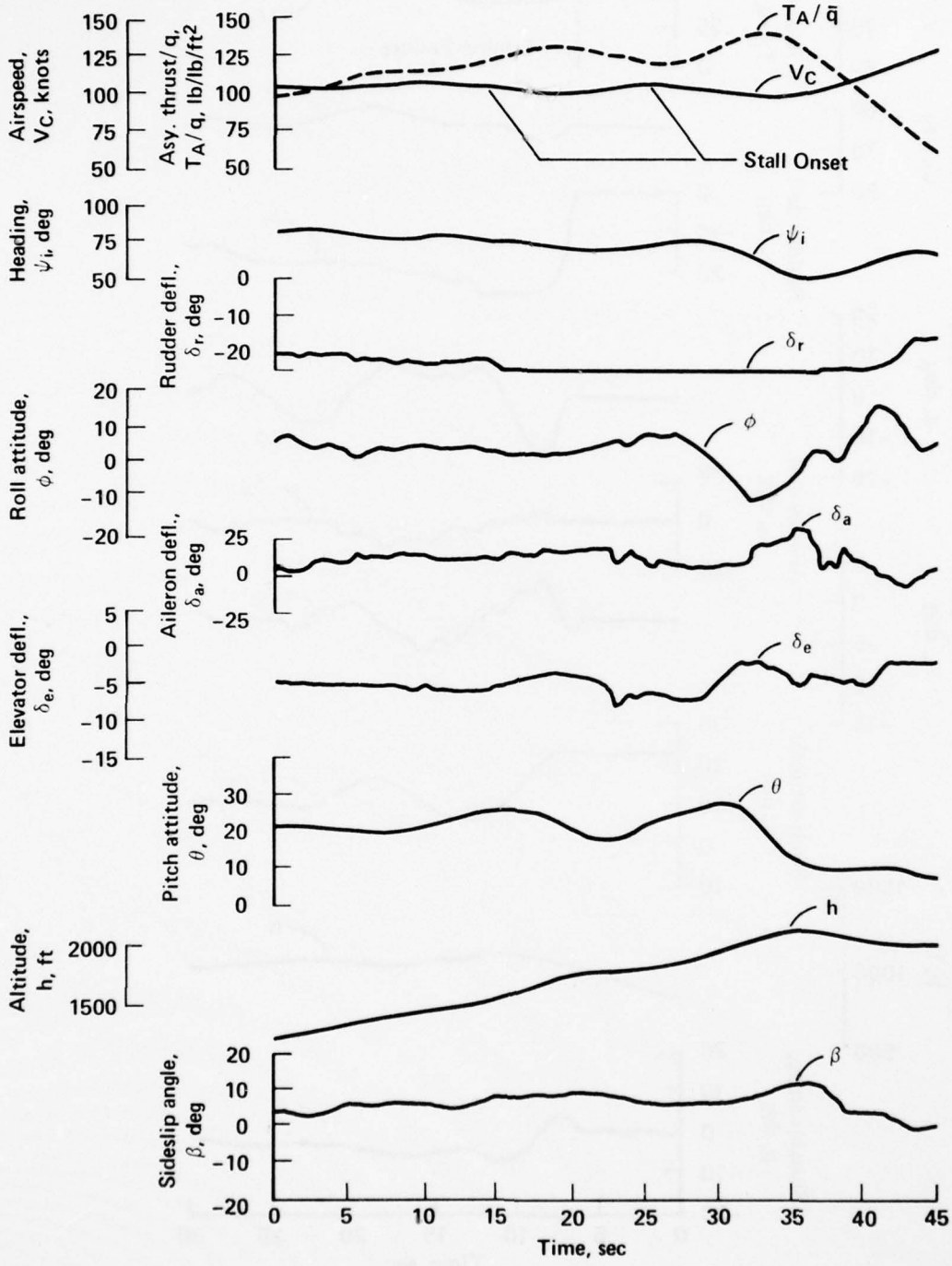

Figure 21.- Steady state minimum control speed test; Model 75B, GW 20,000 lb, cg .325 $\bar{c}$.

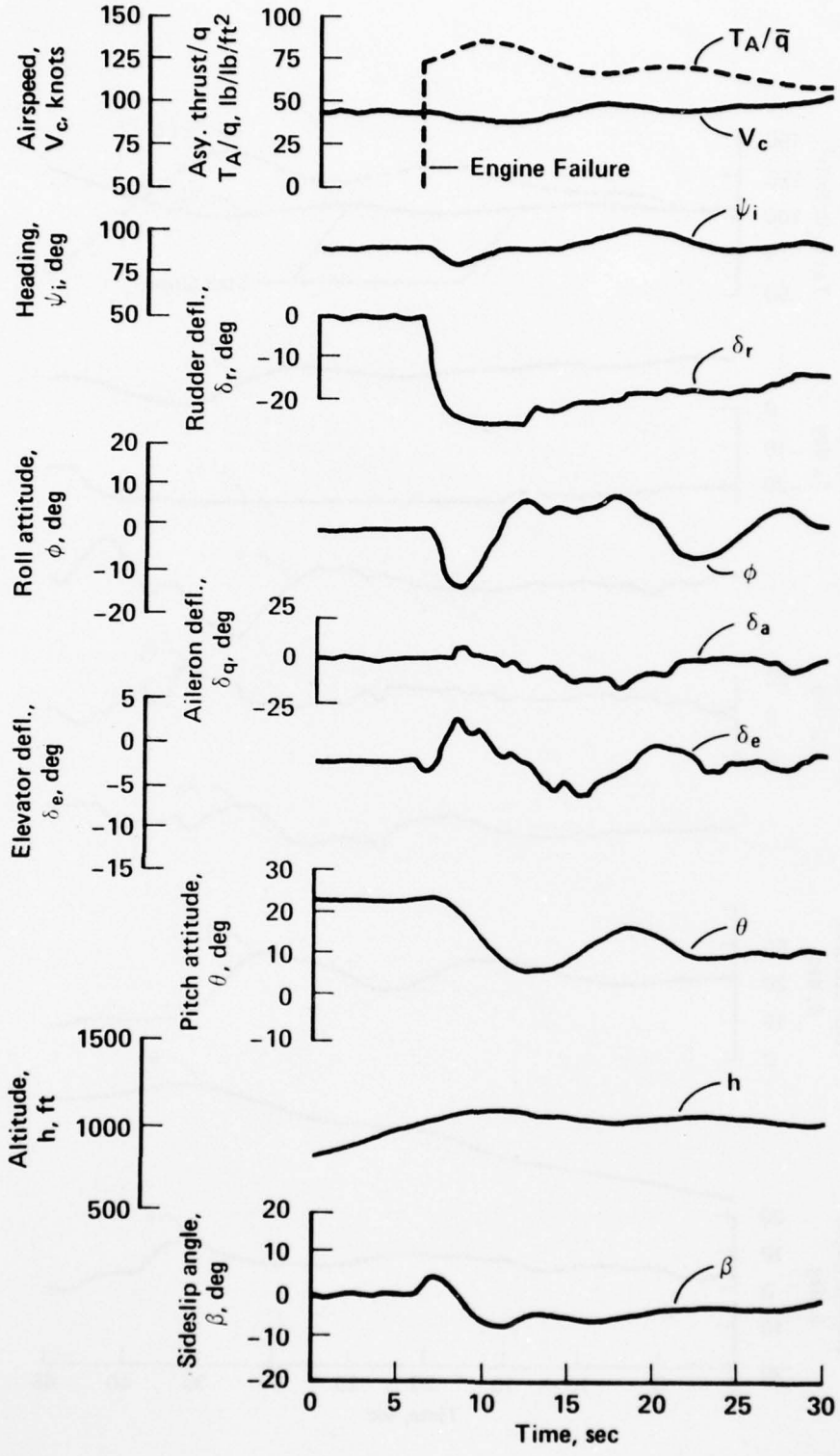

Figure 22.- Failure of left engine at 2260 lb thrust during takeoff climb; Model 75A, GW 15 000 lb, cg .37 $\bar{c}$.

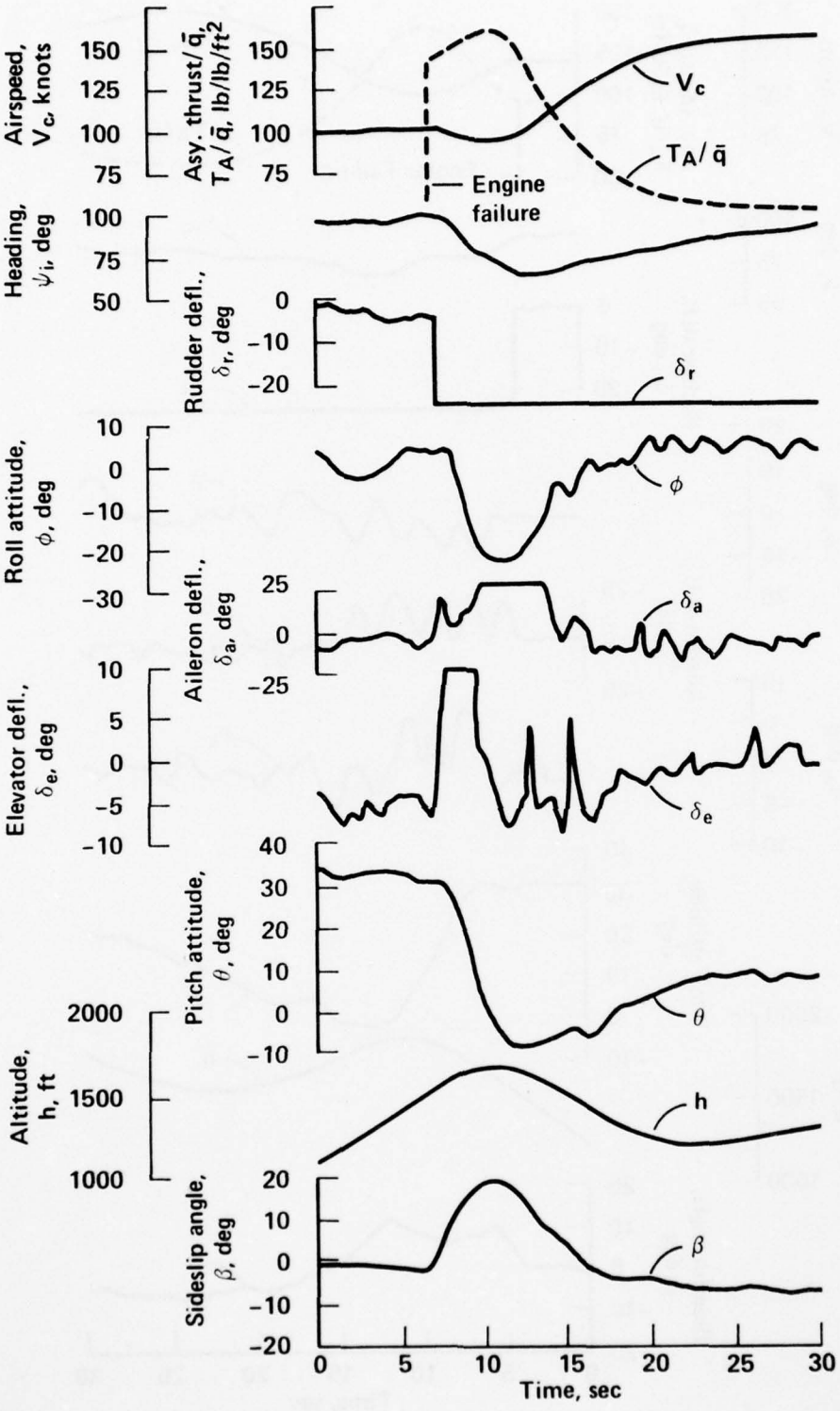

Figure 23.- Failure of left engine at 4940 lb thrust during takeoff climb; Model 75B, GW 20 000 lb, cg .325 $\bar{c}$.

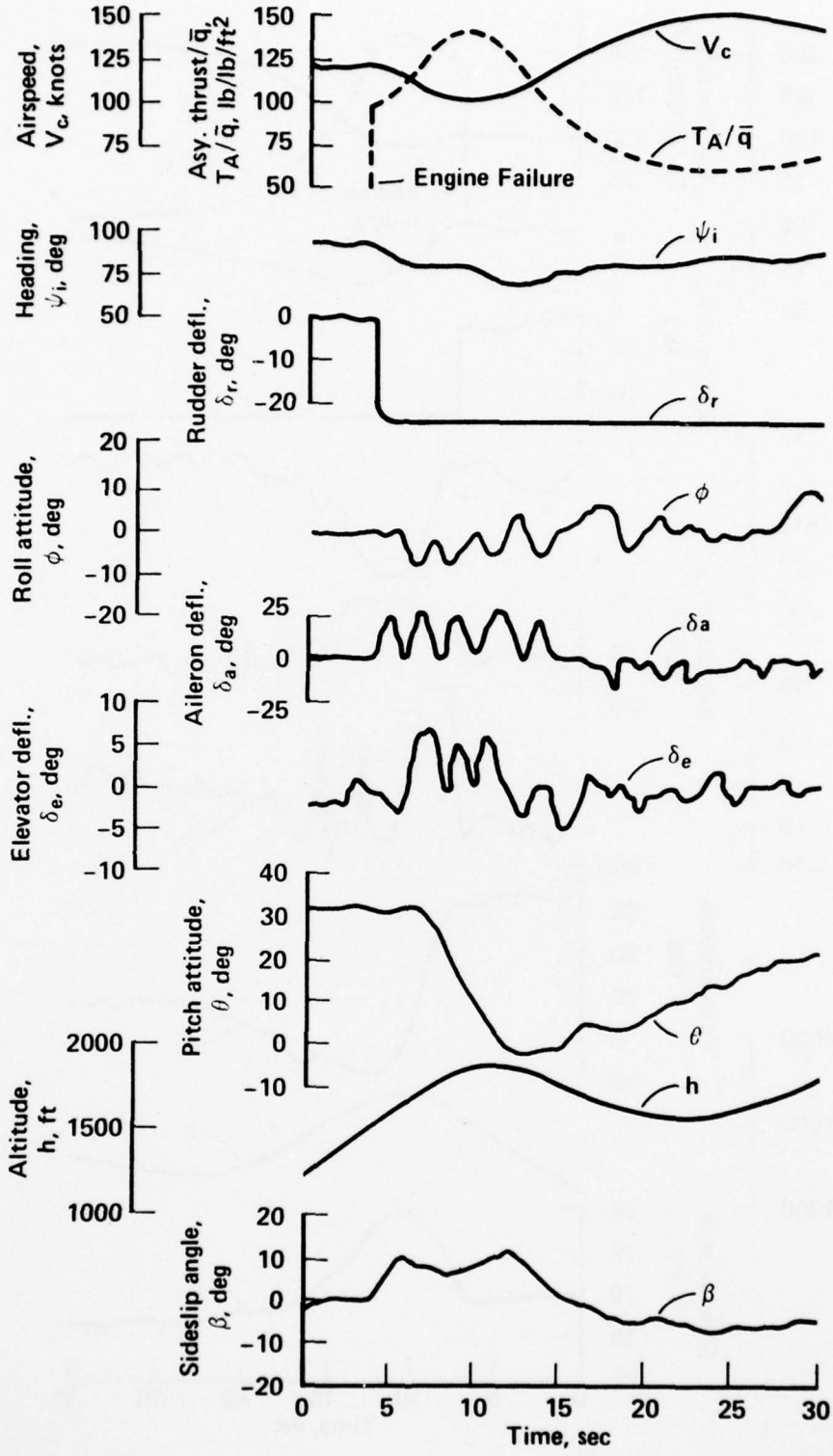

Figure 24.- Failure of left engine at 4805 lb, during takeoff climb, Model 75B, GW 20 000 lb, cg .325 $\bar{c}$.

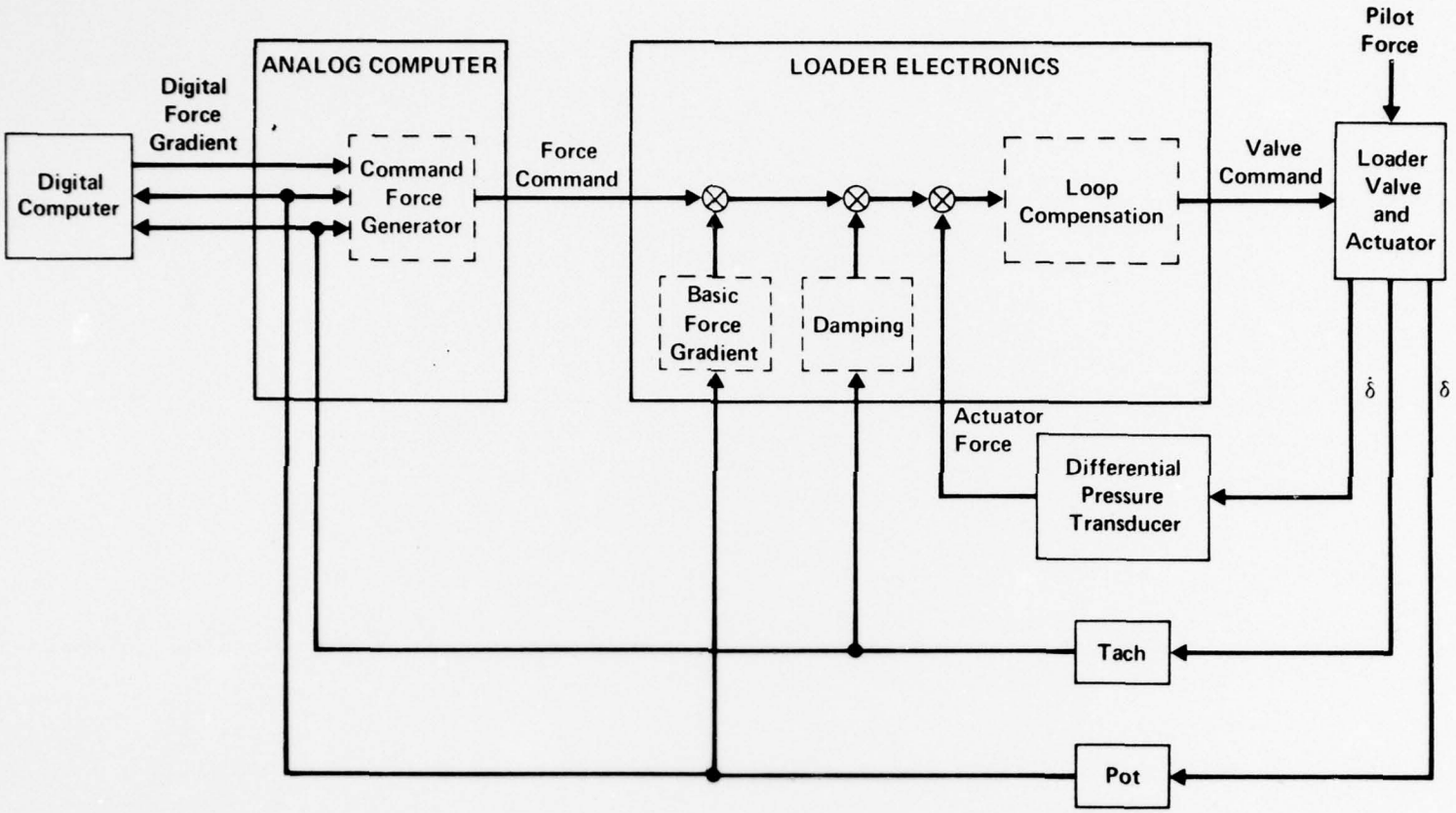

Figure 25.- Block diagram of control loader system, typical single axis interconnection.